

Connector Response of a Grid Pattern Multibody Very Large Floating Structure Subject to Wave Loading

Haico van der Werf
23 – 09 – 2022
Master's Thesis



TNO

 **TU Delft**

The front cover shows a rendering for a grid type very large floating structure in waves by Novacavi [1].

Thesis for the degree of MSc in Marine Technology in the specialisation of
Ship and Offshore Structures

Connector Response of a Grid Pattern Multibody VLFS Subject to Wave Loading

By

H.P. van der Werf

Performed at

TNO

This thesis MT.21/22.051.M is classified as confidential in accordance with the
general conditions for projects performed by the TU Delft.

at the Delft University of Technology
23 September 2022

Company supervisors

Responsible supervisor: Ir. M. G. Hoogeland

Daily Supervisor(s): Dr. Ir. N. P. M. Werter

TU Delft Supervisor

Daily supervisor: Dr. A. Grammatikopoulos

Thesis exam committee

Chair/Responsible Professor: Dr. C. L. Walters

Staff Member: Dr. A. Grammatikopoulos

Staff Member: Dr. J. O. Colomes Gene

Company Member: Ir. M. G. Hoogeland

Company Member: Dr. Ir. N. P. M. Werter

Author Details

Study number: 5394856

Preface

This thesis on the “Connector Response of a Grid Pattern Multibody Very Large Floating Structure Subject to Wave Loading” presents the work performed to obtain a Master’s degree in Maritime Technology specialising in the field of Ship and Offshore Structures at the Delft University of Technology and is in collaboration with TNO. The work has been supervised by Carey Walters (TU Delft), Apostolos Grammatikopoulos (TU Delft), Martijn Hoogeland (TNO), and Noud Werter (TNO).

My intention was to perform some work to contribute towards the energy transition from carbon based fuels to renewable sources. I would initially like to thank Carey and Apostolos who helped focus such a broad objective into something more focussed. This led me to the world of fluid structure interaction and offshore floating solar. I am also grateful to Carey for providing an introduction to Martijn and Noud which began my experience with TNO.

I would like to give special thanks to Apostolos, Martijn and Noud for keeping constant contact throughout my thesis to help improve all aspects of the research. I would also like to give special mention and thanks to Johan Tuitman (TNO) for providing the numerical model used in this thesis and then patiently and humorously explaining this to me. I would also like to thank the structural dynamics team at TNO for giving me interesting insights, useful advice and very importantly a sense of a work community after what felt like a very isolated period of study during the Covid pandemic.

I wanted to also thank all of my family and friends who were able to help me during some challenging times. This support allowed me to keep perspective and stay focussed. They made me feel at home when living in a new country.

H.P. van der Werf
Delft, September 23, 2022

Contents

Preface.....	i
Abstract.....	vi
Nomenclature.....	vii
1. Introduction.....	1
1.1. Introducing Very Large Floating Structures.....	1
1.2. OFPV Connector Design Problem Statement.....	2
1.3. Research Approach.....	3
2. Literature Summary.....	5
2.1. Hydroelastic Behaviour and Modelling Techniques.....	5
2.1.1. Linear Modelling.....	5
2.1.2. Nonlinear Modelling.....	7
2.2. Novel Design Concepts.....	8
2.3. Behaviour of a Joint VLFS.....	9
2.3.1. Connector Types.....	10
2.3.2. Connectors Characteristics.....	12
2.3.3. Connector Stresses and Deformations.....	13
2.3.4. Novel Approaches and Challenges.....	13
2.4. Research Gaps.....	15
2.5. Gaps For Future Research.....	16
3. Modelling Approaches.....	17
3.1. Principles of Joint Design.....	17
3.2. Overview of Computational Model.....	18
3.3. Modelling Assumptions.....	19
3.4. Legacy Numerical Model.....	22
3.4.1. Linear Waves.....	22
3.4.2. Wave Spectrum.....	23
3.4.3. Potential Flow Theory.....	24
3.4.4. Frequency Domain.....	25
3.4.5. Time Domain.....	27
3.4.6. Spring Mass Damper Model.....	30
3.5. Expanded Numerical Model.....	30
4. Verification and Validation.....	33
4.1. Verification.....	33

4.1.1.	Mesh Convergence Study	33
4.1.2.	Motions of Single Floater	34
4.1.3.	Analytical Single Floater	35
4.1.4.	Semi-Analytical Serially Connected	36
4.1.5.	Added Mass and Damping	37
4.1.6.	JONSWAP Spectrum.....	38
4.1.7.	Repeatability Irregular Waves.....	40
4.2.	Validation	41
4.2.1.	Serially Connected VLFS.....	41
4.2.2.	Grid Connected VLFS.....	44
5.	Design and Wave Characteristics	47
5.1.	Case 1 – Three Floater Model.....	47
5.2.	Case 2 – 3x3 Grid Model	48
5.3.	Case 3 – 4x4 Grid Model	49
5.4.	Connectors.....	49
6.	Results	51
6.1.	Case 1 – Three Floater Model.....	51
6.1.1.	Mooring Sensitivity Study	51
6.1.2.	Effect of Connector Stiffness in Sea States	53
6.1.3.	Effect of Varying Connector Stiffness DOF	56
6.1.4.	Effect of Damping	60
6.1.5.	Distribution of Loading.....	61
6.1.6.	Frequency Response Functions	63
6.2.	Case 2 – 3x3 Grid Model	64
6.2.1.	Effect of Wave Heading	65
6.2.2.	Effect of Sea State.....	66
6.2.3.	Effect of Connector Stiffness	67
6.2.4.	Grid Distribution of Loading	68
6.2.5.	Grid Frequency Response Functions	72
6.3.	Case 3 – 4x4 Grid Model	74
6.3.1.	Grid Distribution of Loads	74
6.3.2.	Grid Frequency Response Function	77
6.4.	Discussion of Assumptions	79
6.5.	Practical OFPV Design	80
7.	Conclusions and Recommendations.....	81

7.1. Conclusions.....	81
7.2. Recommendations	82
Bibliography	84
Appendix A – Grid Model Results	91
Sea State and Wave Heading.....	92
Varying Stiffness in Heave and Pitch.....	95

Abstract

The energy transition requires us to explore all options for generating non-fossil energy. Companies are starting to invest in technologies such as offshore floating PV systems (OFPV) to avoid congested urban population centres. OFPV structures are likely to consist of many small, simple, flexibly connected floaters. The entire structure must be able to survive extreme offshore conditions. The OFPV response in various sea states is heavily influenced by the connector design.

In this thesis, a 3D boundary element based numerical model is used which was developed by Tuitman [2]. The model is expanded to output the forces and moments experienced by the compliant connectors which have linear stiffness in 6 degrees of freedom. After successful verification and validation, three case studies are presented which are a three floater serially connected model and a 3x3 and 4x4 grid connected model. Various sea states and wave headings are analysed to show the effect on dynamic behaviour of a compliant connector. The time domain-based approach is used to capture nonlinear Froude-Krylov and hydrostatic forces. The remaining hydrodynamic terms are linearised by solving in the frequency domain. The connector response is linearised by using a finite stiffness matrix but the forces are solved in the time domain to include the effects from the nonlinear hydrostatic terms.

The results show that the resonant response of the structure and connectors is critical in determining the floater motions and loads in the connectors. Additionally, the stiffness of the connector influences the natural frequencies of the structure. The forces and moments in the connectors of the grid are much more varied than the serially connected structure because of the complex interaction of the floater hydrodynamics and connector resonance. The floater motions and connector response becomes less evenly distributed for oblique seas and when sea states match the natural frequency of the structure. The grid experiences bending in multiple directions which results in large connector loads at some locations on the structure. When expanding to a larger 4x4 grid there is a different distribution of connector loading than the 3x3 grid because of the extra degrees of freedom. The aft connectors experience lower loads than connectors facing the waves due to a shielding effect.

Nomenclature

a	Coefficient for connector model
$a_{i,j}$	Added mass matrix relative to VLFS
a_n	Significant wave amplitude in frequency domain
a_{pitch}	Added mass pitch
a_{heave}	Added mass heave
A_c	Cross section of connector
$A_{i,j}$	Infinite frequency added mass matrix
$b_{i,j}$	Damping matrix relative to VLFS
b_c	Connector damping value
$B_{i,j}$	Infinite frequency damping matrix
B_c	Connector damping matrix
$C_{i,j}$	Hydrostatic restoring matrix
C_c	Connector stiffness matrix
E	Young's modulus
E_s	Total system energy
f_y	Connector force for stiffness calculation
f_c	Connector excitation frequency
f_i	Displacement dependent forces
F	Connector force in x, y or z
F_c	Force in connector
F_i	Frequency dependent forces
g	Gravitational acceleration (9.81 m/s)
\hat{h}	Complex wave amplitude
h_i	Hydrodynamic mesh size
H	Water depth
H_s	Significant wave height
I	Inertia of object
J	Polar moment of inertia
k	Wave number
k_{axial}	Connector axial stiffness
k_c	Connector stiffness
$K_{i,j}$	Retardation function
L	Connector loads (force or moment)
L_c	Length of connector
m_c	Moment in connector
m_0	First order spectral moment
M	Connector moment in x, y, or z
$M_{i,j}$	Mass matrix
M_c	Connector mass matrix
n	Normal direction to reference surface
n_g	Number of grid cases in uncertainty analysis
N	Number of samples
N_{freq}	Number of wave frequencies
p	Velocity between two points
P	Fluid pressure

R	Distance to a body fixed origin
s	Standard deviation
S	Uncertainty function
S_B	Wetted surface area
$S(\eta)$	Spectral value for wave spectrum
t	Time
T	Kinetic energy
T_p	Wave spectrum peak period
u_i	Connector displacement
v_z	Wave radial velocity
v	Connector vertical displacement for stiffness calculation
V	Potential energy
V_c	Connector shear force for stiffness calculation
V_n	Normal velocity potential
x_w	Distance in the wave direction
x_j	Displacement in DOF 'j'
\dot{x}_j	Velocity in DOF 'j'
\ddot{x}_j	Acceleration in DOF 'j'
X_{val}	Generic data value
X, Y, Z	Coordinates relative to the global reference system
x, y, z	Coordinates relative to the local reference system
Z_{CI}	Value based on confidence interval
α_θ	Uncertainty constant
β	Safety factor for uncertainty analysis
ε	Wave phase angle
ε_θ	Uncertainty error estimate
γ	Peak enhancement factor for JONSWAP wave spectrum
γ_θ	Order of hydrodynamic mesh convergence
θ_i	Rotational displacement or velocity
θ_n	Random phase angle for ocean wave
η_n	Wave amplitude in time domain
λ_d	Damping constant of proportionality
μ_d	Damping constant of proportionality
ρ	Density of water
σ_{ow}	Standard width value for JONSWAP wave spectrum
τ	Cummins retardation value
ξ_c	Connector damping ratio
ξ_a	Wave elevation
ϕ	Wave velocity potential
ϕ_c	Rotation of connector for stiffness calculation
ω	Wave frequency
ω_p	Circular frequency at spectral peak
$\omega_{n,i}$	Wave natural frequency in DOF 'i'

1. Introduction

1.1. Introducing Very Large Floating Structures

Recent international agreements, such as the Glasgow Climate Agreement [3] are pushing the energy industry to expand the use of renewable sources to meet high decarbonization goals. In order to achieve this, there is a growing interest in expanding current energy production facilities offshore due to the increasing space limitations associated with human expansion and limited land around population centres. One innovative solution being proposed is to construct floating solar islands, Offshore Floating PV (OFPV). To practically contribute to the energy transition these islands are likely to become VLFSs (Very Large Floating Structures).

A VLFS is a structure which is not built-up from the seafloor but rather floats so that it can be disconnected and transported away. The size is so large that assuming the body is one rigid structure is not always valid [4]. A VLFS can be used for many purposes, such as: airports, bridges, accommodation, attraction parks, military bases, supply or storage facilities, food production facilities and energy hubs, which have all gained more attention in the past 20-30 years. Some concept sketches are shown in Figure 1. Broadly speaking, a VLFS can be mat-like which is flexible, has a shallow draft, and is usually a constant thickness or it can be constructed by connecting larger, modular structures. The second type is referred to as joint VLFS in this report. The joint VLFS are usually more elaborate structures which can sustain higher environmental loads and are typically intended to be installed offshore. The connectors are more important in the structural response of the joint type VLFS compared to mat-like structures [5].



Figure 1, Concepts for VLFS [6] (clockwise from top left): offshore fuelling station, military base and/or floating runway, floating city, aquaculture, floating hotel, solar islands.

VLFSs have advantages over land reclamation in that they can be floated to the intended area as required [5]; they can be cost effective when in deeper water [7]; they can have a smaller impact on the marine ecosystem [8]; and are more immune to seismic shocks which can be important in some regions such as in Japan [8]. The joint type VLFS are able to be built in sections and then joined on site or brought to a larger construction yard to be assembled. There is the additional benefit that they can be disconnected and removed from the area for maintenance or decommissioning. An OFPV could be installed between offshore wind installations and utilize some of its infrastructure such as power transmission stations or seabed mooring locations.

A few large research programs such as the TRAM Megafloat aircraft runway in Japan, USA MOB (Mobile Offshore Base), and Chinese MOB projects have all led to significant advances in understanding the dynamic behaviour of these specific types of structures [4]. In contrast, projects relating to floating solar have seen some interest, but there is limited amount of publicly available research. Floating solar structures can behave differently to the MOB or runway designs because the motions of the floaters are not as restricted. Generally, an OFPV system must be easy and low-cost to build and install while surviving harsh ocean conditions. Consequently, they are designed to be simple and lightweight. Usually consisting of many individual floaters, there are numerous connectors and optimizing the design saves costs for the entire system. An efficient design must include reliability, hence the design life should account equally for longevity and the ultimate strength.

1.2. OFPV Connector Design Problem Statement

Offshore Floating PV (OPFV) is seeing increased importance for connector design which is why this thesis identifies, analyses and reports on the challenges faced. In offshore conditions, a structure might experience high sea states but also wave frequencies which are close to its natural excitation frequency leading to large motions and connector loads. A design challenge is that there are usually competing requirements between connectors needing sufficient stiffness to avoid certain issues (contact for instance) but then also keeping connector forces and moments low. It is proposed that a compliant connection may be able to meet these requirements by providing stiffness in each degree of freedom. There is a more detailed explanation of a compliant connector in Section 2.3.

In the context of this thesis there are two types of structural responses which are relevant for an OFPV; a static response which occurs slowly over time and a dynamic response. The static responses are dependent on the location and magnitude of the load but not how (quickly) the load might be applied. Therefore, they are inertia independent. However, for the dynamic case the response is dependent on how the load is applied in terms of frequency and speed such that inertial characteristics must be considered. Both of these response types may need to be considered when considering an OFPV system design because of the wide range of sea states that can be encountered during its lifetime.

An OFPV is likely to be constructed using smaller floating modules which are mechanically connected in a grid pattern. There are very few publicly available research papers related to grid-like connected floating structures. In this thesis a pre-existing 3D-BEM numerical model was expanded to output the forces and moments

at the connectors caused by irregular waves. A serially connector structure is modelled and then compared to the response of a grid of floaters. Furthermore, multiple sea states are investigated which provide results that are representative of conditions at the Hollandse Kust Noord site in the Netherlands. This area is being considered for the development of offshore renewable energy.

1.3. Research Approach

The problem statement described above highlights the need to investigate the connector response for a grid-like VLFS. This Section presents a research question which is answered within the scope of this master's thesis. The research focuses on the multibody interaction of rigid floaters with connectors that have compliance in multiple degrees of freedom. The primary research question is:

“How do compliant connectors on a multibody VLFS connected in a grid-like pattern respond when subjected to wave loading?”

Given the context of the research question, the following sub-questions can be generated:

- A. *How does wave direction and frequency affect the connector response for grid-like VLFS?*
- B. *What is the connector response in irregular waves?*
- C. *How does connector compliance affect the motions of a VLFS and what are forces and moments at the connectors?*
- D. *How does connector damping affect its loads and the motions of the floaters?*
- E. *How does the distribution of connector forces and moments vary from a 3x3 to a 4x4 grid?*

The research sub-questions are selected based on the research gaps found in the literature review which are presented in Chapter 2. It is the ambition of this thesis that by answering the research question, there will be a greater understanding of the interaction between compliant connectors and floaters on a large multi-body floating structure in offshore conditions.

A numerical tool is used which was developed by Tuitman [2] and is described in Chapter 3. The tool is a 3D-BEM which calculates the hydrodynamic terms and then performs a time domain simulation to solve an equation of motion for a multi-body structure. The time domain is used because the nonlinear Froude-Krylov and hydrostatic forces are captured. In this thesis the model is expanded to extract the connector forces and moments.

The methodology is verified and validated in Chapter 4. Verification activities include a mesh convergence study, comparing frequency and time domain added mass and damping terms, wave spectrum definition, a numerical comparison with a single floater, and a 2D semi-analytical comparison. The numerical code was validated by Tuitman [2] using an experimental test case with 12 serially connected box shaped floaters. In this thesis, additional validation is performed on the motion response of the same 12 floater model and also a calculation of the vertical bending moment using the

same experimental results by Remy et al. [9]. A comparison is also made with the numerical results for a 3x3 grid VLFS presented by Michailides and Angelides [10].

In Chapter 5 the inputs are described for three cases, Case 1 being for a serially connected three floater structure, Case 2 is a 3x3 grid, and Case 3 is a 4x4 grid of connected floaters. The results and discussions for the cases and also a mooring sensitivity study are presented in Chapter 6. The VLFSs are modelled with rigid floaters joined by flexible connectors that are compliant in all degrees of freedom. Simple mooring lines which have a constant stiffness are used to keep the structures in position. The Hollandse Kust Noord site is used as a basis for the wave conditions being analysed. Various parametric studies show the effect of modifying connector stiffness, sea states, and wave headings on the floater motions and connector loads. The distribution of loading for all of the connectors is also presented. In addition, the vertical bending response functions are shown all of the cases. Finally, Chapter 7 outlines the main findings of this thesis, draws conclusions and provides recommendations for future scientific work.

2. Literature Summary

2.1. Hydroelastic Behaviour and Modelling Techniques

This Section describes the background and numerical modelling techniques of a VLFS used by previous researchers. There has been a distinction in literature between pontoon and semi-submersible structures [5]. The pontoon type is a box-like structure with relatively low manufacturing and maintenance costs. There are usually many buoyant compartments which are floating on the sea surface. These structures are commonly deployed in sheltered waters [5], but some preliminary concepts are intended to be deployed offshore [11]. The semi-submersible VLFS are usually more elaborately constructed and can be used either in sheltered or open waters. There is a buoyant compartment(s) connected using columns, piles, or truss bracing.

Early research into VLFSs found that the response of such a large structure can be best predicted using hydroelastic theory. This is true for both semi-submersible types [12], [4], and pontoon types [13], [14]. Hydroelasticity is the study of the elastic behaviour of a structure in a fluid and was pioneered by Bishop and Price [15] who researched the harmonic response of ships using 2D elastic beam theories and potential flow hydrodynamic solvers. Before this, a marine structure was idealized as a rigid body which was found to be invalid when the natural frequency of the structure aligns with the wave excitation frequencies. The theory of hydroelasticity was initially expanded to multi-hull ships by Price and Wu [16] and then arbitrary shapes [17] by solving using 3D-FEM (Finite Element Method) which opened up the analysis method to determine the motions and loads experienced on a VLFS.

The US Navy performed research on VLFS for the purpose of Mobile Offshore Bases (MOBs). There was a partnership between the USA (MOB concept) and Japan (Mega float aircraft runway concept) where many joint research projects progressed research in the fields of numerical simulation and environmental compliance [5]. More recently the MOB concept has been resurrected by Chinese research groups who are interested in expanding numerical models to capture novel connector concepts, structural and hydrodynamic nonlinearity, and improving experimental validation techniques in various water depths and bathymetries [18]. A MOB is particularly relevant for this research it is intended to be deployed offshore and designed to have multiple interconnected modules. However, a MOB is design is much more complex and the relative displacements must be much smaller than an OFPV. There is no research made publicly available which explore a grid like joint type OFPV.

2.1.1. Linear Modelling

Researchers commonly use linearised methods to investigate the hydroelastic response of a VLFS. The fluid and structural response can be linearised to reduce the computation time of already very large simulations. The hydroelastic response of a VLFS was initially determined using hybrid models which combined 2D hydromechanics with a 3D plate response [19]. The hybrid analytical-numerical solution can be relatively quick to solve but is limited to specific cases. The numerical solutions became more prominent when Struova [20] used 3D BEM (Boundary Element Method) model the fluid and FEM (Finite Element Method) to model the

structure. These models are more accurate when solving for more complicated situations that are discussed in this thesis.

Initially the hydroelastic effect was captured using hybrid analytical methods based on elastic plate theories and numerical methods such as strip theory or BEM. The Kirchhoff plate theory is suited to structures with small length to depth ratios and assumes the VLFS is vibrating on the water surface with free edges [14]. As the structural depth increases, it was found that Mindlin first-order shear deformation theory is preferable because it also captures the effects of shear deformation [21]. There is some literature which idealized the VLFS to be a 2D Timoshenko beam if the length to depth ratio becomes small [4].

The most common method of fluid analysis when calculating the hydrodynamic response of a floating structure is to use potential flow theory because of the low computational effort for high accuracy in many cases. It is assumed that the fluid is ideal, incompressible, inviscid and irrotational. The wave steepness is assumed to be the mean value of its random probability distribution and only the vertical component of the wave is considered. The analysis can be carried out in the frequency or time domain. The main advantage of using potential flow code is the relatively fast computational time.

Solving in the frequency domain response using linear wave theory is convenient because it allows superposition of incoming regular waves to form a wave spectrum with significantly less computational effort than solving in the time-domain. The wave spectrum can be used to calculate the loading response spectrum. Irregular waves can cause peak stresses or deflections due to the uneven loading along the structure [22]. However, by solving in the frequency domain requires linearising the hydromechanical response which can be inaccurate in certain cases outlined in Section 2.1.2.

There are three common approaches used to analyse the hydroelastic problem for VLFS: the direct method, modal expansion method, and lumped mass method. These methods combine hydroelastic and structural dynamic theories together to determine the overall structural response in the frequency domain.

The direct method requires developing and directly solving an equation which captures both the hydromechanical and structural components. The hydromechanics are solved from the velocity potentials and the structure using a finite difference scheme [23]. There have been variations of the direct method such as proposed by Ohkusu & Namba [24] where pure hydromechanics is used by assuming the structure is part of the fluid domain but with different characteristics to water. In this way, the solution could be obtained using only a boundary element method which could also provide results for shallow water. The direct method can be more accurate because all of the physics is solved in one equation but then is more complicated because the equation of motion must be developed independent of commercial hydrodynamic or structural solvers.

The modal expansion method separates the analysis into the hydrodynamic part and a dynamic plate response. The deflection of the plate is calculated for different modes. There have been several models used over time such as free-free beam modes, vibration of a free plate [25], Green's functions [26] and B-spline functions [14]. The radiation forces due to wave action is then calculated for each mode with unit

amplitudes. The Galerkin method is used to determine the amplitude of motion of the vibrating plate for the given wave environment. The final deformation is a summation of the principal modes. The solution is accurate but can lose accuracy if all the principal mode shapes are not captured, in other words if the mass participation is too low [27].

Another method of solving the hydroelasticity problem for modular constructions is proposed by Lu et al. [28]. The hydrodynamic coefficients are initially calculated assuming that the floaters are rigid bodies to determine the 6 DOF motions at the modules centre of gravity. The modules are then connected with a mass-less equivalent beam with finite stiffness. The assumption is that the structure is a Euler-Bernoulli such that the forces acting on the beam ends can be related to the displacement. The dynamic response can be determined by solving a multibody motion equation. Complicated geometries can be modelled by extending this approach using FEM to describe the beam element [29].

It should be mentioned that the fluid-structure interaction for large ice structures can be equally applied to describe the response of a VLFS [30]. The pioneering work of Meylan & Squires [25], and [31], and [32] on researching ice floes has led to the advancement of 3D hydroelastic analyses of structures in waves. This has led to the development of analytical methods of predicting floater responses when thickness varies along the length.

2.1.2. Nonlinear Modelling

There are also nonlinearities present in the hydrodynamic and structural calculations that might be significant and these are discussed in this Section. Nonlinearities are impossible to capture in the frequency domain which assumes linearity by definition. The displacement dependent terms then must be solved in the time domain. The time domain response can be solved using the direct time integration method which incorporates both the fluid and structural responses [33]. A time integration strategy is used in this thesis which is based on a Runge-Kutta method, but this will be explained in later Chapters.

The structural dynamics can be solved in the time domain when solving for impacts, when the geometry is discontinuous, or there is nonlinear deformation. It was reported that geometry nonlinearities can occur when secondary structures become discontinuous such as when stiffeners don't align [34]. This can lead to unexpectedly high stresses because some part of the structure is taking more load than is realistic. Impact loads (such as aircraft landings or green water loads) are nonlinear because they occur very quickly resulting in strong inertia driven structural responses [33]. For some nonlinear cases such as for impacts, the hydrodynamics are solved in the frequency domain and converted to the time domain using a transfer function to solve the structural part [35].

It is possible that VLFSs can be deployed in all depths of water, namely infinite, finite, and shallow water. The early studies were performed assuming deep water [12]. However, it is found that shallow water can have a substantial impact on the structural response because of reflected waves from the seafloor [36]. Furthermore, the nonlinearity associated with the hydrodynamics increases significantly as water depth decreased due to the viscous effects.

It is perhaps logical to expect that nonlinear effects occurring at shallow water are also be influenced by the bathymetry and underwater shapes or obstructions. The impact of uneven bathymetry on a VLFS response is demonstrated analytically by Athanassoulis & Belibassakis [37]. This was later verified using numerical simulations in the time domain [38]. The presence of an underwater object alters the hydrodynamic response of the VLFS due to the changes in the pressure distribution away from the floating object.

There are relatively few research papers where viscous effects are modelled using advanced techniques such as the finite volume method with RANS solvers. This is because of high computational time when many wave frequencies need to be investigated. Fluid viscosity becomes dominant in the calculation of the hydrodynamic damping term especially due to the sharp corners on a barge or due to viscous losses at the gap between two floating bodies [39].

Fluid nonlinearity can also be captured using potential flow theory if the equation of motion is solved in the time domain. Research has shown that the elastic response of waves alters the wave radiation force such that a more flexible structure exhibits a more nonlinear the response [40]. The wave radiation can also become nonlinear in response to the interaction of multiple floaters which is referred to as gap resonance. This increases the hydrodynamic forces as the gap distance decreases [41].

2.2. Novel Design Concepts

Novel designs of a VLFS have been proposed which aim to reduce motions or loads of the structure and some of these concepts are discussed in this Section. The plan shape of the VLFS was traditionally conceived to have a rectangular shape. This structure may suit a floating airport or MOB concepts but there are applications such as OFPV where other shapes may be more suitable. The most studied alternative geometries are circular [42], [32] followed by L, X or T plan shapes [43]. It was concluded that if the wave direction is unknown, these shapes may reduce the resulting floater motions because obliquely loaded structures experiencing greater loads particularly in the connections but this is discussed in further Chapters.

The displacement of a VLFS can either be dampened by means of either installing anti-motion structures or by reducing wave loads by installing breakwaters. In many cases, it might be necessary to reduce deflections for functionality (e.g., runways), safety, maintenance, practicality or to avoid damage. There have been design proposals with underwater plates oriented either vertically [44] or horizontally [45] which can dissipate some wave energy before it reaches the main structure. The same is true for designs with perforated edges [46], additional connected structures [44], [47] or moonpools [48].

An alternative approach is to construct a nearby breakwater that minimizes structural deformations of the VLFS [49]. The motion reduction of a floating breakwater was investigated by Tay et al. [50] who was interested in this effect on the motions of two floating floaters. A breakwater dissipates the energy of the waves onto an alternative structure. A breakwater would only be able to be installed close to shore and in relatively shallow water.

Another concept being developed is using inflatable floaters which compress when the structure deforms from an incoming wave. The compression adds to the

restoring coefficient term in the equation of motion which can reduce structural stresses and deformations [51], [27]. Similarly, the incorporation of air pockets or ‘gill cells’ into sections of the structure is shown to effectively reduce deformations [52]. This concept is beneficial for OFPV because it floats with the main structure and so water depth is not as important.

2.3. Behaviour of a Joint VLFS

The focus of this discussion will now shift towards a joint VLFS which is closer to what is envisaged for the future OFPV systems in the Netherlands [53]. The multibody hydrodynamic interaction of a joint VLFS requires an understanding of the connections between floating modules. An example of possible configurations is shown in Figure 2. Increasing the connector stiffness generally results in higher stresses but lower motions. Thus, there is a dilemma for designers who want to simultaneously reduce motions and stresses.

A joint VLFS has traditionally been categorized as one of four cases:

- Rigid module, rigid connection
- Rigid module, flexible connection
- Flexible module, rigid connection
- Flexible module, flexible connection

A connectors can be rigid, free, or compliant. If the connector is rigid it does not allow any movement, if there is zero stiffness it is free, and if there is a finite stiffness then the connector is compliant. Generally a kinematic joint is defined free or compliant in limited (usually one) DOF and then rigid in others. A common example is a hinged connection. An OFPV might benefit from a connector with compliance in many DOF because of the direction of movement of the floaters in waves.

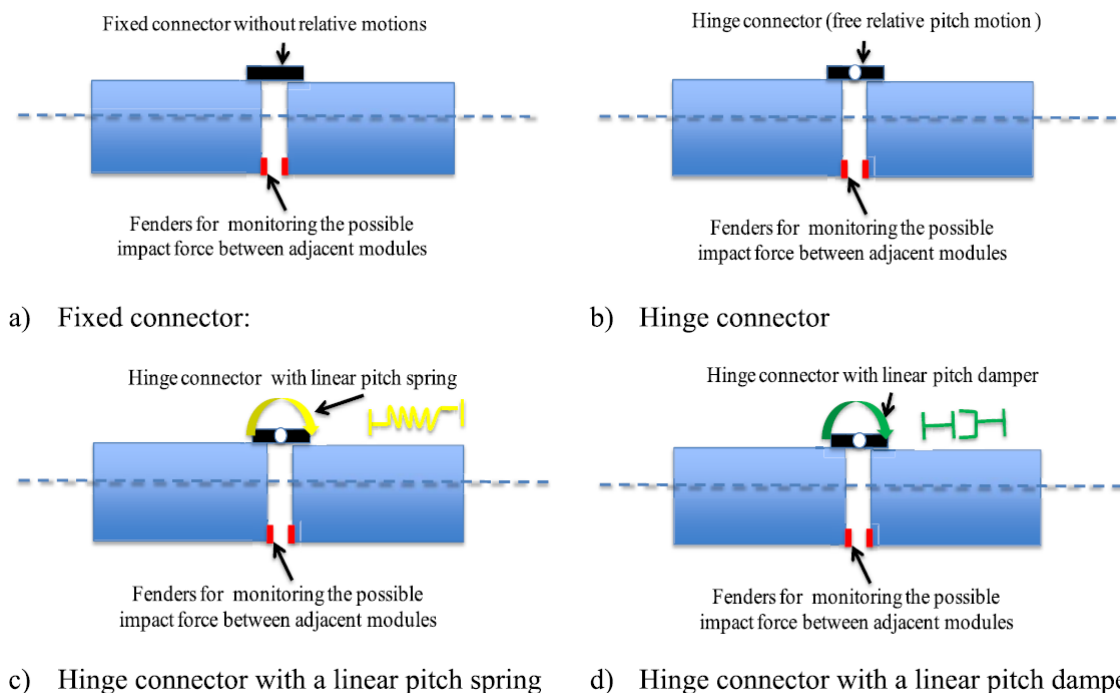


Figure 2, Example of different types of articulated connections [54].

A connectors can be rigid, free, or flexible. If the connector is rigid it doesn't allow any movement, if there is zero stiffness it is free, and compliant if there is a finite stiffness. Generally an articulating joint is defined as one which is free in limited (usually one) DOF whereas, for an OFPV it might be beneficial to include compliance in many DOF because of the direction of movement of the floaters in waves.

The concept of a compliant connector was first developed by NASA [55] and later adopted by Derstine and Brown [56] for a MOB. This design (shown in Figure 3) would allow small deformations in some degrees of freedom but larger deformations in others. This reduced connector loads compared to a pure kinematic hinge joint.

The stiffness characteristics can be used to influence the floater motions and connector forces. One extreme case is that the floater is flexible, and connectors are rigid which reduces stresses globally in the floater but causes extremely high connector stresses which is undesirable [57]. The other extreme is to make the connector flexible or even free and the floater rigid. This may cause very high floater displacements and cause excessive connector deformations. Alternatively, the connection is free but if there is oblique loading this could cause high stresses due to bending in two perpendicular directions. The compliant connector which is made flexible in all DOF is beneficial because it doesn't create rigidity in any connector DOF.

2.3.1. Connector Types

Various connector types and connection methods are described in this Section. Firstly, the connectors can be placed at an upper and lower location of the cross-section so that the floaters behave more like one continuous structure. This can be beneficial for designs which must be made relatively stiff and reduces the relative motion between floaters. The more common design is to have connectors only at an upper location and use fenders to prevent damage if there is contact (Figure 2). It is also shown that the number and location (in the horizontal plane) of connectors can have an effect on the motion response of the structure [58].

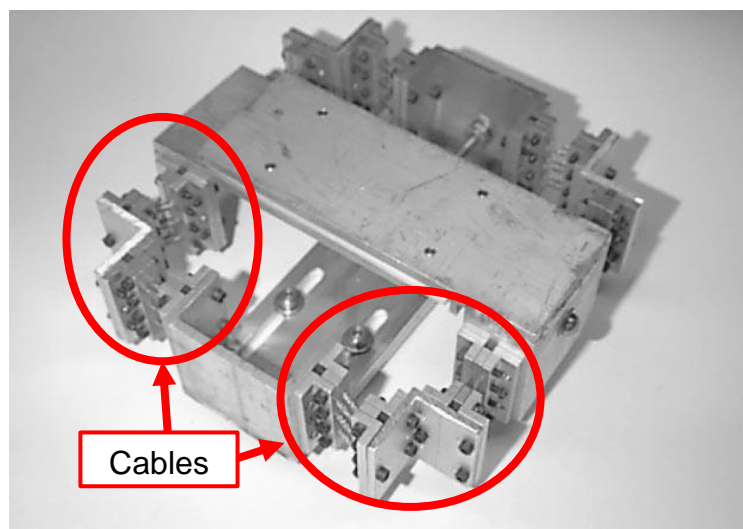


Figure 3, Example of 6 DOF compliant connector [56].

The connector can be designed as articulating or compliant as explained at the beginning of this Chapter. The articulating type can be modelled using a discretized stiffness matrix [28] or a stiffness value in a single DOF which means the stiffness is linearly interpolated relative to two nodes and doesn't explicitly account for bending. The compliant connector needs to be modelled using a discretized stiffness matrix. The compliant connector relies on cables with known stiffness and damping characteristics.

Early analyses of the flexible (elastic) floaters with flexibly articulated connected structures were performed by determining the flexural modes on an individual section assuming the others are rigid and calculating piecewise along the structure [59], [60]. Here, the connection stiffness plays an important role in the overall response because it influences how loads transfer between floaters. The hydroelastic response of the floater could be mimicked by modifying the stiffness of a connectors [61]. This gave cause for many researchers to model the floater as rigid and only change the flexibility of the connectors thus simplifying the problem considerably [62], [63], [64]. Increasing the number of floaters is favourable to reducing the global loads and motions [65].

The hinge joint has been widely investigated for joint VLFs where most designs are serially connected. The behaviour of hinged floating structures was investigated analytically by Newman [66], [67], [68]. The use of a hinged connection effectively reduces stresses if the predominant wave direction is known. It was also noted that increasing the number of floaters in a serially connected pattern increases the loads in the connectors. The disadvantage of a hinge design is that the motion in the free DOF or the stresses in the rigid DOFs can become excessive in offshore conditions.

A compliant connector design can simultaneously reduce loads and the relative displacement between floating modules if well designed. There is a greater versatility in this type of connector because the stiffness can be controlled in each DOF. The first compliant connectors were numerically modelled by idealizing as line connections [58]. However, in reality introducing compliance can be done by, amongst others, springs [56], rubber and cable [69], air cushion and cable [70], or hydraulic, fender and elastomer bearing [71] combinations. A compliant connector makes it more difficult to accurately predict the system behaviour because of the complex interaction with the connectors and the floater response.

The compliant connector can also be developed from a commercial off-the-shelf (COTS) solution. The most common example would be a fender with cable connectors. Similarly, the use of a semi-flexible rubber or even hydraulics as they are used in crane fall arrest systems might be a solution if the floaters are connected with cross connections. There are no examples of COTS solutions employed on VLFs with flexible compliant connections.

The connectors of an OFPV system are critical elements of the structural design regarding both ultimate strength and fatigue life. A greater understanding of the connector response allows a better estimate of loads which influences safety margins and design standards. Increasing the knowledge of the margin between loads and

structural limits of a connector improves the design, lead to reduced costs for maintenance, and provides greater confidence to the industry for investment.

2.3.2. Connectors Characteristics

Important connector characteristics such as, the stiffness, damping and DOFs, are discussed in this Section. These variables play an important role in the overall response of the structure because they influence the floater motions and connector loads [4]. Initial designs of a VLFS with rigid connections led to excessive forces developing at the connectors which are significantly reduced when there is a flexibility introduced [21]. Further studies showed that the motions of the floaters and the forces at the connectors are influenced by varying the stiffness of the connectors [62].

It can be difficult to numerically model the structure's motion responses because the complex multi-body interaction results in convergence issues. The convergence issues were shown to be a result of strong geometrical nonlinearity, even if the material remains elastic, due to the large connector displacements compared to those of the floaters [72]. This was termed the 'amplitude of death' because it would result in an unstable (resonant) system response in certain sea states. This nonlinearity was particularly prominent for compliant connectors because the stiffness in one DOF is shown to affect motions in all other DOFs.

Damping is also an important design characteristic of a connector which has been largely ignored by many researchers. Damping can reduce connector loads if the response is driven by structural dynamics and inertial influences are large. Riggs et al. [73] first researched structural damping on the connectors of a VLFS assuming that it was a percentage of critical damping. Karperaki et al. [74] proposed that Rayleigh damping can be modelled using a spring-mass damper system as shown in Figure 4.

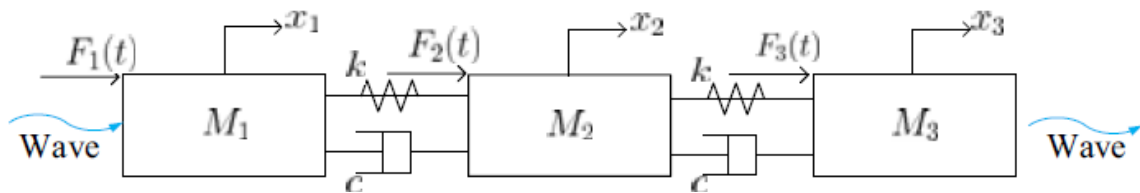


Figure 4, spring-mass damper system modelling connectors of 3 module VLFS [75]

The damping is proportional to the linear combination of the mass and stiffness matrices (equation 2-1) but varies with the response frequency (equation 2-2).

$$b_c = \mu_d \cdot M_c + \lambda_d \cdot C_c \quad 2-1$$

$$\xi_c = \pi \left(\frac{\mu_d}{f_c} + \mu_d \cdot f_c \right) \quad 2-2$$

Where B_c is the damping matrix, and M_c , C_c are the mass and stiffness matrices respectively and μ_d and λ_d are constants of proportionality. Also, the damping ratio is expressed as ξ_c and f_c is the excitation frequency. Karperaki et al. [74] deduced that the effect of damping diminishes as the stiffness of the connector increases. It is also

shown that the effect of damping is only significant at frequencies where the incident (Froude-Krylov) wave dominates because this is close to structural resonance [75].

2.3.3. Connector Stresses and Deformations

The stress or deformation of a connector can be predicted if a design already exists. However, VLFSs are mostly concept designs and researchers are more concerned with the loads generated in a fictitious connector. The study performed by Newman was perhaps the first to investigate the shear and bending stresses developed in simple hinged connectors of a VLFS because of hydroelastic behaviour [76]. The results showed that a hinged connector decreased the internal loads on the flexible floater but did develop extremely high stresses in directions out of the main bending direction of the hinge.

It was shown by Kim et al. [77] that there are nonlinearities associated with the large deformation of the connectors and that they have a meaningful impact on the structural response. A time-domain analysis was required to solve the stresses of the connector of a two floater VLFS in regular waves. Results also showed that bending forces dominated the structural response. Loukogeorgaki et al. [78] conducted experiments to investigate the internal forces in the connectors of a three-module floating breakwater. The results showed the dependency between the connector loads and wave frequency.

2.3.4. Novel Approaches and Challenges

There has been some recent progress in the evaluation and design of novel connections for the MOB concept. A compound connection is one where there are multiple connectors used to satisfy different design requirements. These types of connectors might use a combination of compliant connectors and/or various articulated joints and offer more flexibility to designers. An example was proposed by Shi et al. [79] where the submersible modules are flexibly connected while the deck is separated from the main structure and hinged. Lu et al. [80] extended this concept such that the main deck sits on inflatable rubber cushions as shown in Figure 5.

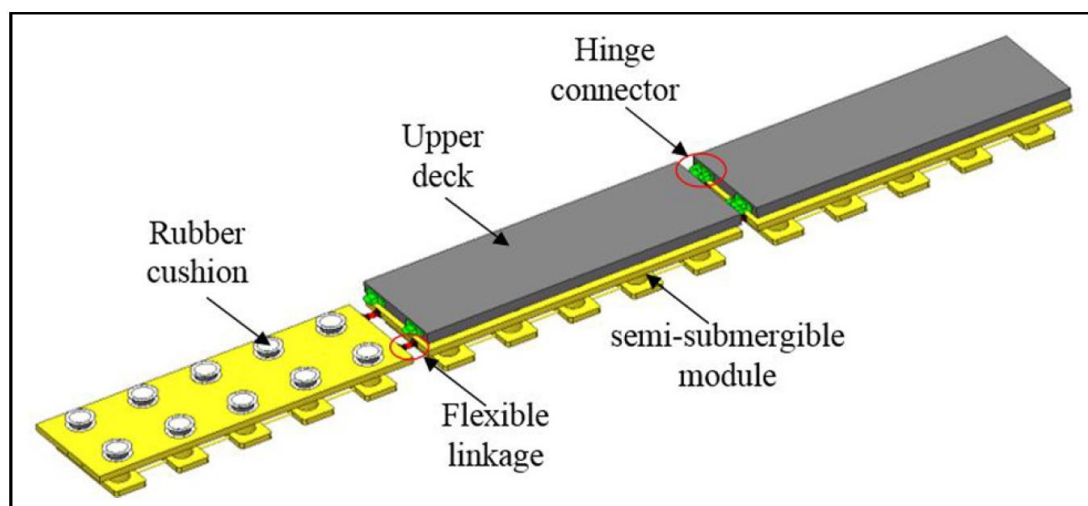


Figure 5, Design of MOB using multiple connection types [80].

There is a challenge to design a compound joint which can be used for experimental studies. Shi et al. [63] used a compound connection of 8 linear springs connected to 2 central ball joints to model a hinge joint with varying linear stiffness (Figure 6). This design can be used to determine the effect of increasing linear stiffness in 3 directions on the loads and motions of a floating platform. The results show that increasing stiffness to limit the relative motion between floaters resulted in high connector loads.

Most of the studies are performed in regular waves acting in head or beam seas. However, when considering a 3D problem there are torsional effects which must be considered in oblique or irregular seas [81]. Further complicating the issue is that experimental results are difficult to obtain to validate analytical or numerical simulations because of challenges when scaling, especially when trying to capture nonlinear effects due to large deformations [82].

Uneven loading due to irregular waves creates peak stresses at certain connector locations across the structure. The effect of oblique seas increases connection stresses to such an extent that dynamic positioning has been proposed to optimize the VLFs heading relative to the waves [64]. Simple connector models (like a 2D hinge) can fail to accurately capture the complex 3D interaction in oblique loading.



Figure 6, Combination model representing a hinged joint between two floating modules [63].

The connection of multiple floating elements in a grid was first considered by Ochi and Malakar [83] using simple hinged connections. Michailides et al. [84] performed studies on grid-connected structures and aimed to optimize the shape and stiffness of semi-rigid articulating connectors in oblique seas (Figure 7). In these studies, the floaters are modelled as stiff and the connectors have linear and rotational stiffness in one DOF. An interesting development is the use of genomic algorithms to find the optimum stiffness of the connectors in such complex multi-body structures [10], [85].

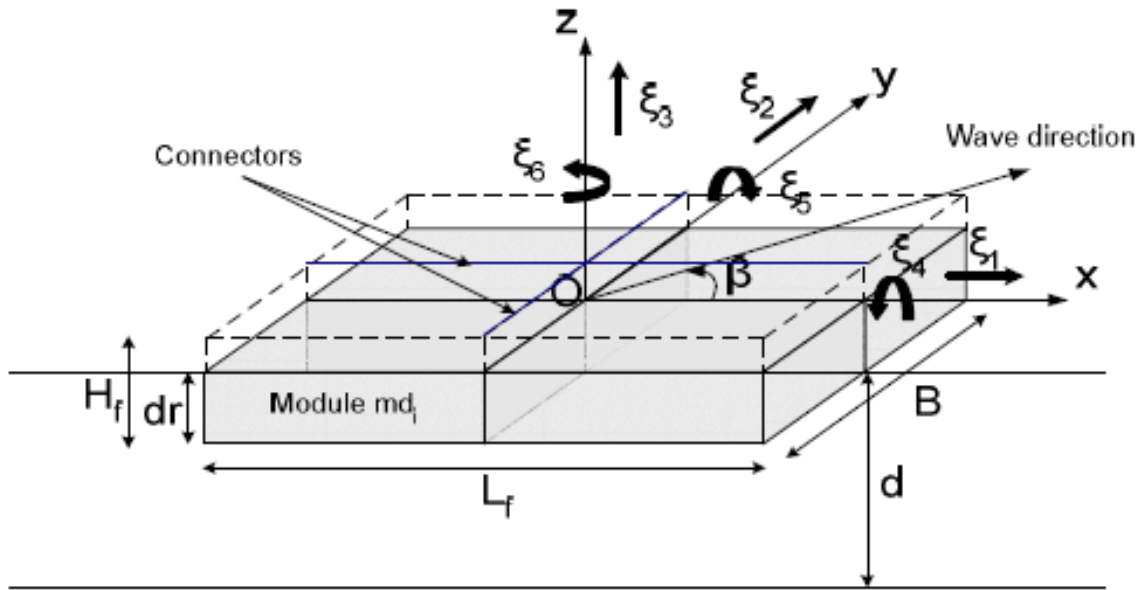


Figure 7, Multi module mat like VLFS [84].

2.4. Research Gaps

The literature study has identified some research gaps which can be addressed within the context of this thesis. There has been a wide range of research performed to determine the motion and structural response of a VLFS. An extensive range of studies have related to problems specific to the MOB or floating airport concepts. However, there is less publicly available research performed for an OFPV system because they are a relatively new concept but one that is gaining in popularity. These systems have less stringent requirements on relative motions between floaters so might see more flexibility in the connectors to reduce their loads.

The numerical model used in this thesis assumes a rigid module, flexible connector model first proposed by Riggs et. al. [61] thus, assuming the floater behaves like a rigid body. As presented in the previous Section, there has been significant amount of research using this model for a serially connected joint type VLFS. The grid type floating structure is almost non-existent in the literature with the only example with a 3x3 grid [84]. However, this model uses hinged connectors and also linearises all of the hydrodynamics terms while this thesis considers 6 DOF compliant connectors and nonlinear Froude-Krylov and hydrostatic forces. Using nonlinear hydrodynamic forces provides more accurate results close to the resonant response of the structure.

The connector model that is proposed in this thesis is based on linear beam elements. It can be used to determine the maximum and significant wave loads at the connectors. A linear beam element connector model with compliance in 6 DOF has been published on other serially connected structures [28] but not for a grid structure. Furthermore, a discussion of the distribution of the forces and moments across the structure has been investigated in this thesis which has not been found in other research papers.

The hydrodynamic problem is often solved exclusively in the frequency domain because of faster solve times. There are very few examples of time domain being used to capture nonlinearities with the wave excitation forces. Mostly, these are used to capture effects associated shallow water or bathymetry [38], [46]. The numerical model used in this thesis solves the equation of motion in the time domain to capture the nonlinear Froude-Krylov and hydrostatic wave forces.

2.5. Gaps For Future Research

The topics which have been identified as research gaps but are not covered within the scope of this thesis are discussed in this Section. Shallow water affects the response of a VLFS but there is limited research covering this topic for a grid structure. The radiation force and added mass are primarily affected by the shallow water and they become nonlinear as the depth decreases. A deep water assumption is also made in this thesis but it would benefit the scientific understanding if more research was performed for shallow water.

The connector models used by other researchers are generally simplified to linear spring constants in a limited number of degrees of freedom. The connector response would differ if the stiffness would be nonlinear. There is also a different response if the stiffness changes in tension or compression which would be the case for fenders. Nonlinear damping might be relevant if a piston type attachment would be incorporated into the connector design. Furthermore, there are few compliant connector designs presented in research and fewer still which address the stresses and strains in the connectors.

Numerical studies found in literature have always assumed the floaters are box shaped barge, pontoon or semi-submersible structures. However, there are few studies involving other floater designs such as triangular or hexagonal plan shapes. The company Solar Duck developed a triangular offshore floating concept which may reduce some incompatible connector loads in irregular and multi-directional seas [86] but results are not publicly available. While alternative geometries have not been studied, it is a recommendation for future work.

There is a lot of research for semi-submersible (MOB) structures but for OFPV structures a box shaped barge is always assumed. The response of a semi-submersible will be very different to a box shaped structure because of the differences in waterplane area and mass distribution. Alternative floater designs should be further researched as these are not investigated in this thesis.

There have been very limited physical experiments performed which record the motions or forces associated with multiple connected floating bodies. Several experimental studies present a serially connected MOB type structure [65] or one with box shaped barges by Remy et. al. [9]. However, no experimental work is found that has a grid shaped VLFS and especially the loads which are generated at the connectors. These can be used to validate the numerical models.

3. Modelling Approaches

3.1. Principles of Joint Design

The OFPV that is used as the basis of this thesis is one that is modular consisting of simple floaters joined with connectors. This Section elaborates on the basics of joint design that can be used for the model. A kinematic connection (joint) connects two or more components together and constrains motion in one or more DOF. Alternatively, the compliant connection can be used which is flexible in multiple DOF and offers greater versatility for a structure with complex multi-body interaction.

A kinematic connection can be made to offer translational freedom such as a slider and/or rotational freedom such as a ball and socket, hinge, or pin. The simplest modelling technique is to assume the joint is either rigid or free in one or more prescribed DOFs. different types of connections are shown in Figure 8 and can be categorized as:

- Hinge/revolute allows one rotational DOF and is rigid in others.
- Prismatic (sliding/roller) joint allows one translational DOF and is rigid in others.
- Ball and socket joint allows rotational DOFs but has rigid linear constraints.
- Fixed (welded or bolted) is rigid in all DOF.

A compliant connector is a special case where there is a finite stiffness in all DOF but is usually made more or less stiff in certain DOFs depending on the loading conditions. Compliant connectors are springs/cables usually paired with rubber which allow movement in multiple DOF. The connector model can be made more complex and accurate by including finite stiffness or damping to one or more DOF.

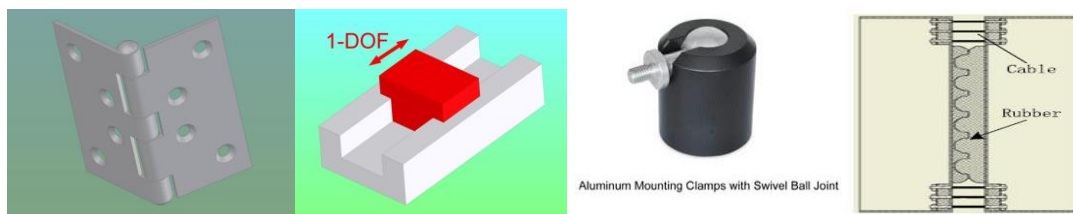


Figure 8, Joint types (from left); hinge, prismatic, ball and socket [87], and compliant [56].

The stiffness of a connector can be caused by its material properties, geometry, or from springs. For a beam connection, increasing the length while keeping a constant cross section will decrease the bending stiffness. Nonlinear stiffness can be experienced when certain materials, such as steel, exceeds its elastic limit. There is a release of energy from the system which means that it does not return to its initial position after the load is removed. Some materials such as rubber have a nonlinear stiffness while remaining within their elastic limits.

The stiffness of a joint can be caused by springs which can behave linearly or nonlinearly. While many joints might be modelled as springs, this paragraph refers to connectors that are partially or fully comprised of physical springs. Linear springs have a constant deformation for each unit of force applied which is not the case for nonlinear

springs. A compliant connector design is reliant on springs or cables to provide stiffness in various DOFs [56].

Another characteristic of a connection is that it can have damping which is caused by friction between contact surfaces, the inherent structural properties, or because of energy losses such as viscous losses. Frictional damping is the most common in joints and occurs when there is microslip between non-smooth contact surfaces. The response becomes nonlinear if the surfaces are non-uniform. The damping of a cable connector is also nonlinear due to the rubbing of the individual wire strands [55].

Then there is the damping contribution which originates from the structure itself and is referred to as structural (or material) damping. This type of damping is dependent on the geometry, material properties, stress and internal forces, number of cycles, and temperature [88]. In the case of connections, this has a lesser effect on the total damping than the frictional damping [88].

Finally damping can be caused by kinetic energy dissipating to a fluid through viscous effects or radiation [89]. This viscous damping is commonly studied in maritime applications because it reduces the motions of a structure in water but has many applications in connection design such as a dashpot system. Fluid-related viscous damping can be relevant to VLFS if the joint has a large contact area with the ocean and velocities are high. Damping is commonly modelled with a spring-mass damper system as described in Section 2.3.

There is often a problem with having a detailed FEM model of the connector because of the relative scale compared to the VLFS. This can result in simulations which take excessively long to solve. Alternatively, the model can be simplified and can be used to obtain the forces and moments which can be inputs to a more detailed sub-model. The approach taken in this thesis is to simplify the connectors such that they are defined by a linear beam element connecting two nodes and then solving an equation of motion to obtain the relevant forces and moments. Further analysis of stresses would require connector design but this is considered out of scope for this thesis.

3.2. Overview of Computational Model

This Section provides an overview of the numerical tool used in this thesis and certain concepts will be expanded in later subsections. A legacy model that is developed by Tuitman [2] is the basis of the numerical tool. The calculation flow is shown in Figure 9. In this thesis the model is expanded to obtain the forces and moments of the connectors.

Initially a hydrodynamic mesh is generated using the program GMSH, then the hydrodynamic coefficients such as the added mass, radiation damping, and the diffraction and radiation wave excitation forces are calculated in the frequency domain using the boundary element program PRECAL. The influence of all hydrodynamically meshed structures is considered in the calculation of these wave forces.

The program HETIME is developed by Tuitman [2] and converts the hydrodynamic terms calculated in the frequency domain to the time domain using the Cummins equation. These terms are linearised by initially performing these calculations in the

frequency domain. The Froude-Krylov (incident wave) and hydrostatic forces are then calculated based on the time-dependent position of the floaters to capture nonlinearities. Finally, an equation of motion is solved using the hydrodynamic terms and user defined linearised constraint terms for mooring lines and connectors. The solution to the equation of motion gives the motions, forces and moments for the floaters and connectors.

The connectors are modelled with a beam element connecting two nodes on two bodies. The connector stiffness is defined using a linearised stiffness matrix and this is multiplied by the displacement between nodes to obtain the forces and moments. The mooring lines are modelled using a spring mass damper element with a constant linear stiffness and damping.

The incoming waves are defined as regular or irregular. If irregular waves are used, a JONSWAP sea-spectrum is generated using wave peak period, significant wave height, a wave spreading coefficient (γ), and a randomized wave frequency as inputs. The connector forces and moments are calculated from the stiffness and relative displacement of nodes. The ability to extract these connector loads and present their distribution across the structure is novel to this thesis.

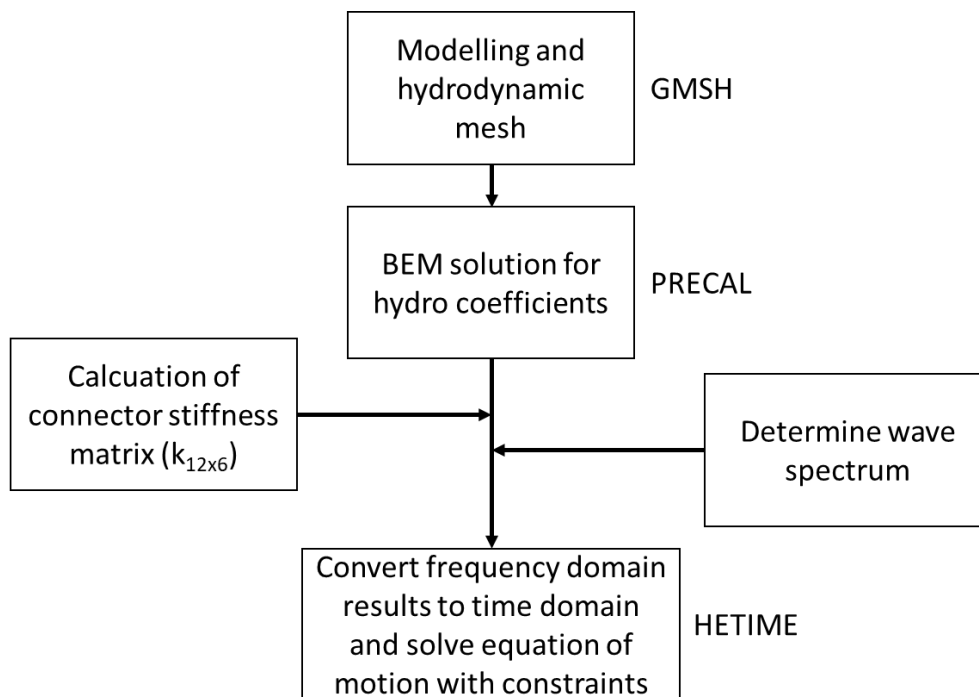


Figure 9, Overview of calculation flow used in this thesis.

3.3. Modelling Assumptions

There are certain important assumptions made for this numerical model that are relevant to mention specifically in this Section. The assumptions that are discussed are use of a potential flow 3D-BEM, wave linearisation, solving the equation of motion in the time-domain, floaters are rigid bodies, linearised connectors and connector stiffness, floater dimensions, and the mooring arrangement.

A potential flow based method has been used to determine the frequency dependent hydrodynamic coefficients and wave excitation forces. While an analytical description of the flow around the floaters can also be accurate for very simple structures the complex fluid interaction around multiple floaters means that more advanced methods are needed. A comparison has been made between the natural frequency calculated using an analytical model and the BEM method in Section 4.1.3.

The potential flow method isn't able to model the viscous damping, gap resonance, and shallow water effects. The sharp corners on a box shaped floater cause turbulence and flow separation which increases hydrodynamic damping. The floater motions (particularly roll and pitch) could be overpredicted close to resonance.

Another effect which is strongly influenced by viscosity is gap resonance where a large amount of fluid energy is dissipated through turbulence caused by viscosity. Therefore, an inviscid solution would have higher wave forces at gaps between floaters than a viscous solution. The viscous effect becomes smaller as the gap becomes larger.

Shallow water can also affect the hydrodynamic radiation force which becomes nonlinear because the wave energy is not distributed evenly away from the structure. In this thesis a deep water assumption is made. More advanced computational fluid dynamics such as the finite volume method are more accurate in this situation because they can model viscous effects but then the computational time increases significantly.

The hydrodynamic coefficients and the wave diffraction and radiation potentials are all linearised whereas the incident wave (Froude-Krylov) potential and hydrostatic pressure are both solved in the time domain hence, nonlinearities are able to be captured. The nonlinear effects might increase at wave frequencies close to resonance. The wave diffraction and radiation terms are linearized to improve the solution times but would ideally also be solved in the time domain.

The hydrodynamic potentials are solved with all meshed bodies considered boundaries to the fluid domain because of the no-penetration boundary condition (which will be described in Section 3.4.4). What is not included is the connector (or mooring line) influence on the dynamic pressure terms. This might result in some inaccuracies because of the interaction of the radiation potentials which are caused by the motions of the connected floating bodies.

Using numerical methods requires the geometry to be discretised to a hydrodynamic mesh which results in some uncertainty. The mesh size is primarily determined by the highest frequency being considered and a general rule of thumb is to use 1/6 times the shortest wavelength [90]. The mesh should also sufficiently represent the geometry however for a simple box this is often not limiting. A mesh convergence study should be conducted to identify a mesh size with suitably low uncertainty.

The waves generated in the numerical model are linearised such that the effects of wave steepness, shallow water, and wave breaking are all ignored. Nonlinear waves are important in engineering due to rogue waves which are extremely large, rare, and unpredictable but can result in significant loading on the structure. There is also a nonlinearity associated with shallow water due to the reflection of waves from the

seabed. This creates much steeper and larger waves which can exacerbate the motions and connector loads. These waves have not been modelled in this thesis.

It might also be important to consider the wave breaking on a structure. Wave breaking is nonlinear and can cause green water loading which can be important for both fatigue and ultimate strength. By linearising the waves, both of these phenomenon are ignored. This is because the solution times would be extremely large and the current thesis is investigating floater motions and connector loads more generally. Once the defining load cases are defined then it would be recommended to investigate these nonlinear waves in more detail.

Other wave related assumptions are for the sea states and use of long-crested waves. The sea state is assumed to follow of JONSWAP spectrum which is appropriate for the Hollandse Kust Noord site. This thesis investigates long-crested waves because the wave energy would be more concentrated towards a certain wave heading. Therefore, it is assumed that the wave loading would be more extreme and the worst case for design. By assuming there is no wave-spreading it is also easier to interpret which wave headings contribute more to the structural response.

The equation of motion is solved in the time-domain rather than the frequency domain. There is quite a large computational penalty for choosing to solve in the time-domain. This is justified because the multi-body interaction is displacement dependent and not frequency dependent. The irregular waves are generated with a randomised wave height and frequency meaning the structure is hydrodynamically excited in random phases. This type of excitation leads to certain resonant responses which are not fully captured in the frequency domain. To account for this nonlinearity, the Froude-Krylov and hydrostatic terms are solved in the time domain. This allows a better prediction of the hydrodynamic interaction when motions are large and there are rapid changes to the waterplane area which can occur close to resonance.

The next assumptions are related to the floaters being rigid bodies and their dimensions. A rigid body assumption might be significant because it means that the wave load is directly transferred through the connectors. If there is elasticity in the floaters, some of the wave energy would be transferred to the structure to deform its shape. However, it is assumed that because stiffness of the connector is much lower than the floaters, there will be no impact on the results.

The floater dimensions are initially estimated from similar OFPV concepts being tested in The Netherlands [53]. The box shape is initially selected because of the availability of data which could be used for verification and validation. There are some concepts such as the SolarDuck, Swimsol, and OceanSun designs [53] which have non-rectangular floaters but these shapes are not investigated in this thesis.

For the case studies used in this thesis a square plan shape floater is chosen because the OFPV is expected to be deployed in seas with waves coming from multiple directions and it will not be able to weathervane. This makes the square the most versatile to changes in wave heading compared to other sized rectangles. As mentioned, the sharp corner of the box floater may result in an underprediction of hydrodynamic damping because viscous effects are not captured.

The connectors are also an integral part of this thesis so how they are defined and how the connector forces and moments are calculated has important implications to the results. The connectors have been modelled assuming linear stiffness and damping. It has been mentioned that it might be appropriate to define nonlinear stiffness and damping curves but this would need to be validated through experiments. However, the design of the connector should first be known which requires knowledge of the forces and moments that it might experience. There is also the assumption that the material will behave elastically. This is valid for certain materials such as steel assuming the yield stress is not exceeded but for rubber this is usually not the case.

The connectors are modelled using linear beam elements assuming a cubic shaping function. In this way, the forces and moments are calculated using the relative displacement between two nodes (one connected to either floater) and the pre-defined stiffness matrix. Linearising the beam element means that higher order effects are ignored. These become more significant when deformations are large. The beam element also assumes a cubic shaping function which is the exact solution for coupled shear and bending. However, there may be more than two DOFs per node which might mean another shaping function could be more appropriate.

The mooring design has been assumed in this thesis and has the main objective of keeping the structure in position for the simulation. The mooring lines are idealised with linear stiffness and without damping which is unlikely to be realistic. Often, the mooring stiffness is nonlinear due to the materials used and line length. There is also damping due to the rubbing of individual wire strands and viscous effects. Furthermore, the mooring pattern is carefully selected to minimise motions in certain directions. Regardless, the mooring arrangement is considered acceptable because the focus of this thesis is on OFPV connectors and so only relative motions are considered. Also, a mooring sensitivity study has been performed in Section 6.1.1.

3.4. Legacy Numerical Model

3.4.1. Linear Waves

The legacy numerical model assumes linear Airy waves which allows the use of linear superposition. This means it is possible to apply potential theory to describe the seakeeping behaviour of a floating structure in waves. It is assumed that nonlinear hydrodynamic behaviour from viscous damping, shallow water effects and/or body interaction is small [90]. Superposition means that regular, sinusoidal waves with a certain height and phase angle can be combined to form a wave spectrum. The structural response can then be obtained by multiplying by the wave spectrum.

The dispersion relation is satisfied for Airy waves such that for finite water.

$$k \cdot \tanh(kH) = \frac{\omega^2}{g} \quad 3-1$$

The wave number is 'k', the water depth is 'H', the angular frequency is 'ω' and 'g' is the gravitational acceleration. In this thesis, it is assumed there is infinite water depth

so the 'tanh' term becomes equal to 1 and wave potential and velocity (3-2 and 3-3 respectively) can be simplified to.

$$\phi = Re \left(-i \cdot \frac{\omega}{k} \cdot \hat{h} \cdot e^{-k \cdot H} \right) \quad 3-2$$

$$v_z = \frac{d\phi}{dz} \quad 3-3$$

Simplifying the solution by assuming deep water improves the simulation time but it doesn't account for reflected waves from the seabed. This creates a kind of suction effect due to the uneven pressure distribution from the sides of the structure to the seabed. Furthermore, the added mass calculation is lower in shallow water because there simply isn't the fluid there to accelerate. This shifts the natural frequency of the structure to the left. It is recommended that future research is performed which investigates the effect of shallow water of a grid structure.

3.4.2. Wave Spectrum

A body floating in the ocean is subject to a wide range of irregular waves which need to be analysed to determine the motion and structural response. The ocean wave spectra can be characterized as wind dominated, swell dominated or a combination of the two. The energy distribution of both types of waves follow that the wind-dominated waves have greater spreading components both in terms of energy and direction and the wavelength is generally shorter. The swell dominated waves are generally more uni-directional and the energy density is more concentrated. It is shown that short waves adapt more quickly to changes in wind than long waves [90].

In the North Sea, it is appropriate to use JONSWAP spectrum has been used to define the irregular waves. The assumption is that the wind does not have time to fully develop the ocean waves [90]. For this thesis, only the long-crested waves are analysed hence, there will not be an effect of wave spreading. This is chosen because the wave spreading would dissipate the wave energy and the peak response might not become as prominent. The JONSWAP spectrum is defined by the function.

$$S_{\eta} = \frac{320 \cdot H_s^2}{T_p^4} \cdot \omega^{-5} \cdot \exp \left(-\frac{1950}{T_p^4} \cdot \omega^{-4} \right) \gamma^{\exp \left\{ -1 \left(\frac{\omega - \omega_p}{\sigma \sqrt{2}} \right)^2 \right\}} \quad 3-4$$

Where:

$$\gamma = \begin{cases} 5 & \text{for } \frac{T_p}{\sqrt{H_s}} \leq 3.6 \\ \exp \left(5.75 - 1.15 \frac{T_p}{\sqrt{H_s}} \right) & \text{for } 3.6 < \frac{T_p}{\sqrt{H_s}} \leq 5 \\ 1 & \text{for } \frac{T_p}{\sqrt{H_s}} > 5 \end{cases}$$

And:

$$\sigma = \begin{cases} 0.07 \text{ for } \omega \leq \frac{2\pi}{T_p} \\ 0.09 \text{ for } \omega > \frac{2\pi}{T_p} \end{cases}$$

The significant wave height is given as ' H_s ' and the wave peak period is ' T_p '. The spectral value, ' S_η ' can be used to calculate the wave amplitude using equation 3-5.

$$a_n = \sqrt{2 \cdot S_\eta(\omega) \cdot \Delta\omega} \quad 3-5$$

The wave profile in the time domain is calculated using an inverse Fourier transform from the spectrum in the frequency domain. If only regular waves are considered, then N is equal to 1.

$$\eta_n = \sum_N a_n \cdot \cos(\omega_n t - k_n x_1 + \theta_n) \quad 3-6$$

3.4.3. Potential Flow Theory

This thesis uses potential flow theory and a 3D-BEM to solve for the frequency dependent terms in the equation of motion. The present method assumes that the fluid problem is continuous, inviscid, incompressible, non-rotational and initially uniform. In this way, the solution is linearized such that the fluid velocity can be described using potential theory assuming mass conservation such that the Laplace equation is used to solve for the velocity potential (φ) shown in equation 3-7.

$$\Delta\varphi = 0 \quad 3-7$$

A BEM is powerful because it has reasonably fast computational times and provide a good accuracy. Comparing to analytical methods which are faster but more limited in situations where they are accurate. Conversely more advanced computational fluid dynamic methods (such as finite volume) can capture more physical phenomenon than BEM but are computationally more expensive.

Potential flow is less accurate when viscous effects are dominant in the flow because viscosity is not modelled. For motion analysis of a VLFS a BEM might underestimate hydrodynamic damping leading to an overestimation of the motion response close to resonance. Additionally, there is no mechanism to model wave-breaking which can result in unrealistically high waves forming if pressure becomes very low. This can occur if there is a very narrow gap between the floaters. In this case, a lot of wave energy would realistically be dissipated through viscosity and vorticity but this is not captured using potential flow.

3.4.4. Frequency Domain

Initially the hydrodynamic coefficients are calculated in the frequency domain using the 3D-BEM described by Tuitman [2]. This requires generating a hydrodynamic mesh which is reasonably consistent and small enough to capture frequencies up to 3 rad/s. The maximum panel size needed to achieve a stable hydrodynamic solution is proportional to the wavelength [2]. The mesh requires integrating over the entire wetted surface and must be defined up to the still water free surface boundary.

In this thesis the floaters are assumed to behave like rigid bodies. This simplifies the solution considerably because the motions are not coupled to the deformation of the floaters. The work by Riggs et. al. showed that for a joint type MOB which is serially connected, the elasticity of the floater can be represented in the stiffness of the connector [61]. The floater structure is usually made very stiff either by using certain materials such as concrete or by reinforcing steel structures. This means that the connectors are often so much more flexible that assuming the floater is a rigid body is considered valid. A significant proportion of the incoming wave force is transferred between the floaters through the connectors which means they might experience greater loads than if there were flexibility in the floater as well.

The hydrodynamic coefficients describe the fluid motion around the floater and are needed to solve the equation of motion. These coefficients are computed in the frequency domain to reduce the simulation time, however this means that nonlinear hydrodynamic effects are not captured using this method. The added mass and hydrodynamic damping are frequency-dependent while the spring stiffness (restoring coefficient) is frequency-independent.

The wave potentials which are used to determine the wave excitation force can be divided into an incident, diffracted and radiated component such that:

$$\varphi = \varphi_I + \varphi_D - i\omega \sum_{j=1}^N \vec{\xi}_a \cdot \varphi_{R_j} \quad 3-8$$

Where φ is the total velocity potential, φ_I is the incident potential, φ_D is the diffracted potential, ω is the wave frequency, N is the number of degrees of freedom, ξ_a is the wave elevation, and φ_R is the radiated potential.

The incident potential is displacement dependent is calculated using equation 3-9.

$$\varphi_I = -\frac{i\xi_a g}{\omega} e^{k(z-ix_w)} \quad 3-9$$

Where k is the wave number, z is the vertical position of the node, x_w is the distance in the wave direction.

The diffracted and radiation velocity potentials are calculated by solving the Laplace problem (from equation 3-7) using the following boundary conditions.

$$\left\{ \begin{array}{ll} \Delta\varphi = 0 & \text{In the fluid,} \\ -k\varphi + \frac{\partial\varphi}{\partial z} = 0 & z = 0, \\ \frac{\partial\varphi}{\partial\vec{n}} = V_n & \text{On } S_b, \\ \lim \left[\sqrt{kR} \left(\frac{\partial\varphi}{\partial R} - ik\varphi \right) \right] = 0 & R \rightarrow \infty \end{array} \right. \quad 3-10$$

Where, V_n is the normal velocity potential, k is the wave number, z is the vertical distance from the still water line, S_b is the wetted surface, n is a normal vector to the surface, R is the distance to a body fixed origin.

The first boundary condition ensures conservation of mass and no fluid can escape from the domain. The second linearises the free surface such that no fluid can detach from the domain (i.e., no wave breaking) because the pressure of the free surface is zero which is equal to the ambient pressure. The third condition assumes no fluid enters the floating body. The final condition ensures that the diffraction and radiation potentials will become equal to zero away from the body. The boundary value problem is solved numerically at the centre of the mesh elements using pulsating Green's source functions.

To obtain the frequency dependent forces the pressure can be obtained from the potentials using the linearized Bernoulli equation shown in equation 3-11.

$$P = i\omega\rho\varphi \quad 3-11$$

Where the pressure (P) is calculated for the respective potentials. Here ρ is the water density which is assumed constant. The frequency dependent force is then obtained by integrating the pressure over the wetted surface. The frequency dependent Froude-Krylov (incident wave) force (F_I) and diffraction force (F_D) are calculated using equation 3-12 and equation 3-13 respectively.

$$F_{I,i} = \iint_{S_B} P_I \vec{h}_I \vec{n} dS \quad 3-12$$

$$F_{D,i} = \iint_{S_B} P_D \vec{h}_I \vec{n} dS \quad 3-13$$

The frequency dependent radiation force is described using added mass and damping coefficients as shown in equation 3-14.

$$\omega_e A_{ij} + i\omega_e B_{ij} = \iint_{S_B} P_{R_j} \vec{h}_I \vec{n} dS \quad 3-14$$

Where, P_{R_j} is the radiation pressure, h_I is the wave amplitude vector, n is a vector normal to the surface, and A and B are the frequency dependent hydrodynamic added mass and damping terms (respectively).

The equation of motion for every (i^{th}) DOF can then be obtained in the frequency domain using equation 3-15.

$$\vec{F}_{I,i} + \vec{F}_{D,i} = (M_{i,j} + A_{i,j}) \cdot \ddot{\vec{x}}_i + B_{i,j} \cdot \dot{\vec{x}}_i + C_{i,j} \cdot \vec{x}_i \quad 3-15$$

Where \ddot{x}_i is the acceleration, \dot{x}_i is the velocity, and x_i is the displacement of the body.

3.4.5. Time Domain

The hydrodynamic terms should be calculated in the time domain rather than the frequency domain. The process of obtaining the time domain results is discussed in this Section.

Starting with the incident wave force which is also known as the Froude-Krylov force. This force is due to the pressure of the undisturbed incoming waves. Both the Froude-Krylov and the hydrostatic wave force are solved exclusively in the time domain to make them displacement dependent. Figure 10 shows how the terms are calculated. The pressure cannot be solved using the linearized equation from equation 3-11 but rather using the following conditions for the incident wave pressure.

$$\left\{ \begin{array}{ll} P_{FK} = \sum_{i=1}^{N_{freq}} \rho g \zeta_i(t, x_w, \omega) e^{k(\omega_i)z} & z < \min(0, \zeta_{tot}(t, x_w)) \\ P_{FK} = \rho g \zeta_{tot}(t, x_w) \left(1 - \frac{z}{\zeta_{tot}(t, x_w)}\right) & z \geq 0 \text{ and } z < \zeta_{tot}(t, x_w) \\ P_{FK} = 0 & z \geq \zeta_{tot}(t, x_w) \end{array} \right. \quad 3-16$$

The pressure is now dependent on the wave position in space and time. The Froude-Krylov force must be linearly interpolated above the still water line because the wave potential has not been defined yet.

The nonlinear hydrostatic pressure is also calculated based on the wave position.

$$\left\{ \begin{array}{ll} P_{HS} = -\rho g z & z < \min(0, \zeta_{tot}(t, x_w)) \\ P_{HS} = 0 & z \geq 0 \text{ or } z \geq \zeta_{tot}(t, x_w) \end{array} \right. \quad 3-17$$

These terms are combined into one force term (f_i) as shown in equation 3-18.

$$f_{i,i} = \iint_{S_B} (P_{FK} + P_{HS}) \vec{h}_i \vec{n} dS \quad 3-18$$

The incident wave force has been calculated in the time domain so that it is displacement dependent rather than frequency dependent. This allows non-linear effects associated with large rigid body mode displacements (e.g., pitch or heave motions) to be captured more accurately.

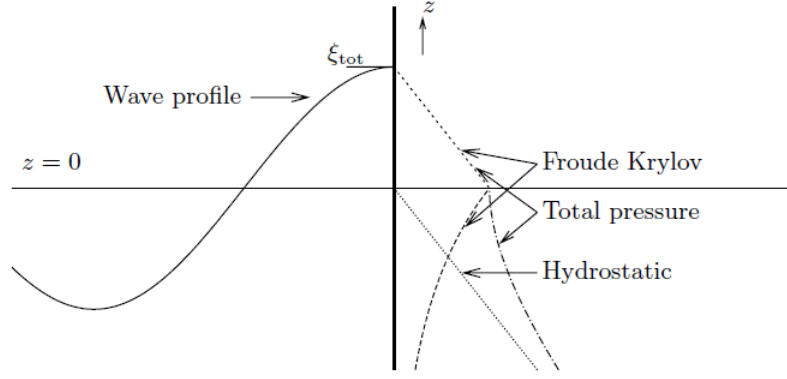


Figure 10, Incident (Froude-Krylov) pressure [2].

The diffraction force is then calculated using the frequency dependent result ($F_{D,i}$) shown in equation 3-12. The time dependent diffraction force ($f_{D,i}$) is calculated in the time domain using equation 3-19.

$$\vec{f}_D = \sum_{i=1}^{N_{freq}} \zeta_a(\omega_i) \cdot \vec{F}_D(i) \cdot \cos(\omega_i t + \varepsilon) \quad 3-19$$

Where ε is the phase angle of the incoming wave from the frequency domain calculation.

Finally, the radiation force is calculated in the time domain using the Cummins equation which is derived from impulse theory [91]. First the radiation force is calculated using equation 3-20.

$$\vec{f}_{R,i} = B_{i,j}(\omega_\infty) \cdot \vec{\xi}_a(t) + \int_{-\infty}^t K_{i,j}(t - \tau) \cdot \vec{\xi} d\tau \quad 3-20$$

Here a retardation function (K_i) is introduced which accounts for the response delay of an impulse load over time. This allows the conversion of the added mass and damping terms as shown in equation 3-21.

$$K_{i,j}(\tau) = \frac{2}{\pi} \cdot \int_0^\infty b_{i,j}(\omega) \cdot \cos(\omega\tau) \cdot d\omega \quad 3-21$$

The added mass term becomes.

$$A_{i,j} = a_{i,j}(\omega_\infty) + \frac{1}{\omega_\infty} \cdot \int_0^\infty K_{i,j}(\tau) \cdot \sin(\omega\tau) \cdot d\tau \quad 3-22$$

However, given that the expression can be valid for infinite frequencies, the expression can be simplified to.

$$A_{i,j} = a_{i,j}(\omega_\infty) \quad 3-23$$

Careful attention should be paid using the Cummins equation because the result will only be valid if the coefficients are calculated at frequencies sufficiently high that the response functions tend to zero. For this this analysis that frequency is 5 rad/s. This requires a small panel size in the hydrodynamic mesh which might result in extremely large computations computational time if the VLFS becomes very large, such as when there are many floaters.

The computational time might increase significantly if the hydrodynamic problem is solved at such high frequencies. To solve this problem the calculations are performed to a sufficiently high frequency (in this case 3 rad/s) and interpolated to an even higher frequency using a function with the general form $\frac{a}{\omega^b} + c$ for higher frequencies [2].

$$\vec{f}_i = \vec{f}_{I,i} + \vec{f}_{\text{grav}} + \vec{f}_{\text{beam},i} + \vec{f}_{R,i} + \vec{f}_{D,i} \quad 3-24$$

Thus, having obtained the hydrodynamic terms in the time domain, the general equation of motion can be expressed as.

$$\sum_{j=1}^6 \{(M_{i,j} + A_{i,j}) \cdot \ddot{\vec{x}}_j(t) + b_{i,j}(\omega_\infty) \cdot \dot{\vec{x}}_j(t) + \dots \dots \int_0^\infty K_{i,j}(t - \tau) \cdot \dot{\vec{x}}_j d\tau + C_{i,j} \cdot \vec{x}_j(t)\} = \vec{f}_i(t) \quad 3-25$$

Here, the damping coefficient at infinite frequency cannot be obtained using 3D-BEM; hence, the value at the maximum calculated frequency is used. The frequency independent terms such as the mass (M) and stiffness matrices (C) remain constant. Also, the term (f_i) represents by the following force terms.

$$\vec{f}_i = \vec{f}_{I,i} + \vec{f}_{\text{grav}} + \vec{f}_{\text{beam},i} + \vec{f}_{R,i} + \vec{f}_{D,i} \quad 3-26$$

Where F_i is the total force in DOF 'i', $f_{I,i}$ is the Froude-Krylov and hydrostatic force combined, f_{grav} is the gravitational force, f_{beam} is force in the beam element, $f_{R,i}$ is the radiation force, and $f_{D,i}$ is the diffraction force.

The equation of motion is solved in the time domain such that the Froude-Krylov, hydrostatic, and beam forces are solved exclusively in the time domain and can capture any nonlinearities in the hydrodynamics or structural interaction. The displacement and its differential terms are solved using a 4th order Runge-Kutta numerical time-integration scheme as described in [2]. The integration method uses an explicit integration scheme. This means that the solution becomes unstable if the time-step is too large. The maximum value for a stable time-step is dependent on the maximum frequency and stiffness being analysed.

Ideally the radiation and diffraction forces would be solved in the time domain like the Froude-Krylov force. However, this would become too computationally demanding and is currently not implemented in this solution. Instead, these forces are converted to the time domain using the Cummins equation (radiation force) and equation 3-19 (diffraction force). There might be some nonlinearities which are not captured using

this assumption, especially with the radiation potentials which would be affected by the connector and other floaters position in space. If the model would be in shallow water, the radiation force also becomes more nonlinear.

3.4.6. Spring Mass Damper Model

Another model which is used in the legacy model is a spring mass damper connecting two nodes. This is expressed in equation 3-27 and can represent mooring lines which for this thesis have zero damping (i.e., b_s is equal to zero). Alternatively, this can also be used to apply linear damping to the connectors between the floaters and in this case the stiffness is equal to zero because the beam element represents this (i.e., k_s equals zero). The total force in the element is determined based on the relative position and velocities of two pre-defined nodes as shown in equation 3-27. These nodes can be attached to two bodies or to a single body and a position in space.

$$f_{sd0} = k_s(|\Delta p| - L_c) + b_s(\Delta \dot{p}) \cdot s_n \quad 3-27$$

Here k_c represents the linearized connector stiffness, Δp is the relative displacement and $\Delta \dot{p}$ is the relative velocities between two points, L_c is the original length and s_n is a unit vector in the direction of the element. For both the damping model for the connectors and for the mooring line model, the force is linearised and defined by two nodes connecting either two bodies or a body with a point in space.

In reality the mooring lines might exhibit nonlinear behaviour both in stiffness and damping. The use of a linear damping model for modelling mooring lines has the potential to lead to inaccuracies in the overall motions. However, considering the thesis is focussed on the connector forces and moments and relative floater motions rather than global results this model should be acceptable.

3.5. Expanded Numerical Model

The legacy numerical model is able to model the connectors using linear beam elements. This thesis expands the model by developing a method of calculating the linear stiffness matrix based on Euler-Bernoulli beam equations. Additionally, the forces and moments of the connector are output for post-processing.

The connectors for the numerical model are modelled as beam elements with a prescribed stiffness matrix. This matrix is initially calculated based on the Euler-Bernoulli beam equations. There is an axial component as well as a coupled vertical bending with vertical shear and a coupled horizontal bending with horizontal shear. The axial force component is calculated using equation 3-28.

$$k_{axial} = \frac{A_c E}{L_c} \quad 3-28$$

The coupled bending stiffness is first calculated assuming that the beam deformation follows a cubic function as shown in Figure 11. This model can be used for both the coupled vertical and horizontal bending and shear coupling.

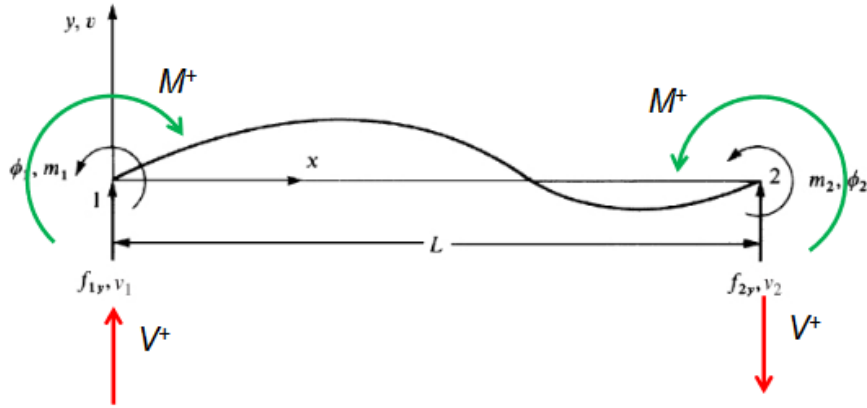


Figure 11, Vertical and horizontal coupled shear and bending.

It is assumed that there is a coupling between the shear and bending components for the vertical and horizontal bending. Using this model, the transverse displacement is described by a cubic shape function as shown in equation 3-29. The cubic shape function is the exact solution for the four DOF. The actual deformed shape is unknown without experimental testing so some coupled terms might not be accounted for using this idealised model. In this case, the actual connector design would need to be known and physical testing could be performed to obtain the exact response.

$$v = a_1x^3 + a_2x^2 + a_3x + a_4 \quad 3-29$$

Then the equations for bending and shear are applied as follows.

$$m_c(x) = EI \left(\frac{d^2v}{dx^2} \right) \quad 3-30$$

$$V_c(x) = EI \left(\frac{d^3v}{dx^3} \right) \quad 3-31$$

And then the stiffness can be solved using the equation.

$$\begin{Bmatrix} f_{1y} \\ m_1 \\ f_{2y} \\ m_2 \end{Bmatrix} = k_c \begin{Bmatrix} v_1 \\ \phi_{c1} \\ v_2 \\ \phi_{c2} \end{Bmatrix} \quad 3-32$$

And the stiffness matrix becomes.

$$k_c = \frac{EI_c}{L_c} \begin{bmatrix} 12 & 6L_c & -12 & 6L_c \\ 6L_c & 4L_c^2 & -6L_c & 2L_c^2 \\ -12 & -6L_c & 12 & -6L_c \\ 6L_c & 2L_c^2 & -6L_c & 4L_c^2 \end{bmatrix} \quad 3-33$$

The connector is then modelled using a beam element in the hydrodynamic software by assuming linearity between two nodes connected to each body. The relative displacement of the two nodes and the prescribed linear stiffness is used to calculate the forces and moments in the connector using equation 3-34.

$$\{f_{beam}\} = k_c * \{\vec{u}_i\} \quad 3-34$$

Where f_{beam} is the force or moment, k_c is the stiffness and u_i is the deformation in a prescribed DOF. Assuming beam linearity vastly improves the calculation speed and allows the solution to be solved in the equation of motion. If a nonlinear element was used, the stiffness could be nonlinear and solve accurately but then at a greater computational cost and also the response curve would need to be known before running the simulation. This could be done using experiments or a very precise parametric FEM analysis.

The beam element assumes a cubic shape function to describe the deformation between both nodes. This assumed shape might lead to some inaccuracy in the results of the connector forces and moments if the actual deformed shape is very different. However, in most cases this would also be nonlinear and could not be captured using a linear beam element. The cubic shaping function is the same as in equation 3-29.

The connector loads are calculated in the time domain along with the equation of motions. For this reason, the current numerical model doesn't allow the determination of the mode shapes of the entire connected structure. Additionally, the response functions must be calculated by solving the simulation with regular waves of a certain frequency and then manually creating the plot of the frequency response.

4. Verification and Validation

4.1. Verification

The numerical model has been verified to ensure the solution is being solved correctly. There are various types of verification exercises performed such as a mesh convergence study, added mass and damping impulse conversion study, and irregular sea state confidence study. Furthermore, semi-analytical comparisons are made for the natural frequency of a single floater and a 2D three floater model in vertical bending using a Lagrangian approach. Finally, motion RAOs on a single floating floater were compared to a numerical study performed by Newman [13].

4.1.1. Mesh Convergence Study

A mesh convergence study was performed to determine the mesh size for the numerical computations. A single box shaped floater with the dimensions 15x15x1m (L x B x T) is used for this study. There are no mooring lines or connectors in the model. A 100 second simulation is performed in regular waves with a height of 1.0m, and a wave period of 2.0 seconds. This wave period requires the smallest mesh size to solve the hydrodynamic terms. The mesh sizes analysed are 2.00, 1.00, 0.80 and 0.35m. A floater with the mesh size of 1.00m is shown in Figure 12. The grid is generated such the horizontal (x and y) directions have the specified size but the height (i.e., in z-direction) has half of this size.

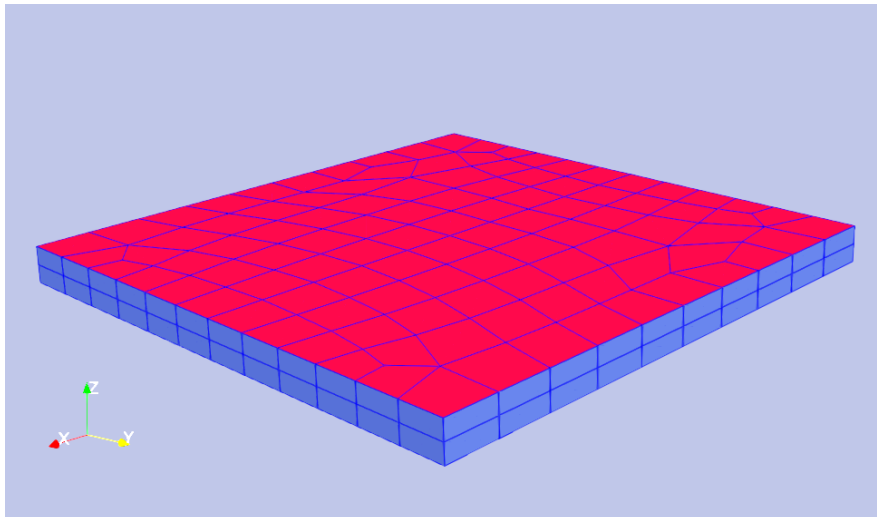


Figure 12, 15x15x1m single floater hydrodynamic mesh with size of 1.00m.

The peak pitch motions are compared in the uncertainty analysis. The least squares method with weighted residuals is used following the procedure proposed by Eca and Hoekstra [92]. The uncertainty estimate is given by equation 4-1.

$$U_{\theta} = \beta \cdot \epsilon_{\theta} \quad 4-1$$

Where α is a safety factor calculated based on the trend of the results, and ϵ_θ is the error estimate which uses a Richardson extrapolation as shown in equation 4-2.

$$\epsilon_\theta = \theta_i - \theta_0 = \alpha_\theta h_i^{\gamma_\theta} \quad 4-2$$

Where, θ_i is the calculated value, θ_0 is an approximation of the exact solution, α_θ is a constant to be calculated, h_i is the mesh unit size, and γ_θ is the order of grid convergence which can be calculated if unknown. The coefficients can be calculated by minimizing a least squares function (S) shown in equation 4-3. The approximate solution is found using a nonlinear partial differential equation solver.

$$S(\theta_0, \alpha_\theta, p) = \sqrt{\sum_{i=1}^{n_g} (\theta_i - (\theta_0 + \alpha_\theta h_i^p))^2} \quad 4-3$$

Where n_g is the number of grids studied (must be at least 4 grids). The minimum of S can be found by setting its derivative with respect to the coefficient terms equal to zero. The standard deviation is then calculated using equation 4-4.

$$\sigma_U = \frac{S(\theta_0, \alpha_\theta, p)}{n_g - 3} \quad 4-4$$

The factor of safety in the uncertainty estimate is calculated based equation 4-5.

$$\begin{aligned} \text{For } \sigma_U < \theta_i - \theta_{i-1} & \quad \beta = 1.25 \\ \text{For } \sigma_U > \theta_i - \theta_{i-1} & \quad \beta = 3.00 \end{aligned} \quad 4-5$$

The results of the uncertainty study are shown in Table 1. The uncertainty value means that the calculated motion is within a margin of plus or minus the uncertainty. A mesh size of 1.00m is used because the uncertainty is within 5% of the calculated value which is recommended by the Eca and Hoekstra [92].

Table 1, Uncertainty study on mesh size.

	ms = 2.00m	ms = 1.00m	ms = 0.80m	ms = 0.35m
Ratio grid size / Finest grid	5.71	2.50	2.00	1.00
Pitch motion (deg)	0.285	0.260	0.256	0.252
Uncertainty	0.045	0.013	0.012	0.003

4.1.2. Motions of Single Floater

The numerical results for a single box shaped floater are compared against the numerical results obtained by Newman [13] and is used to verify the motion response. The floater has the length, breadth and draft dimensions of 80m x 10m x 5m respectively. Regular wave periods of 5- 12 seconds were analysed for head seas to obtain the response amplitude operators (RAOs) in the frequency domain.

The motion RAO for a single box shaped barge in waves is compared with the results of Newman [13]. The heave and pitch motion RAOs are shown in Figure 13. There is almost perfect agreement between the results. This is expected considering that both use a boundary element method with similar assumptions. There is a slight discrepancy at low wave periods (i.e., high frequencies). It is expected that for the simple box shape in using potential flow theory the results would match.

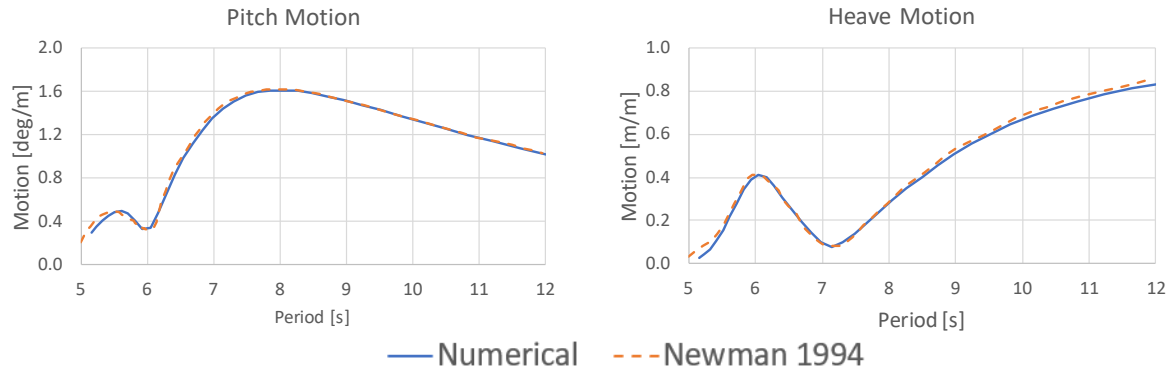


Figure 13, Motion RAOs for pitch (left) and heave (right) comparing the numerical result from this thesis (solid line) against the numerical result obtained by Newman [13] (dashed line).

4.1.3. Analytical Single Floater

Various types of 2D analytical and semi-analytical validation were also performed to compare with the results obtained using the numerical model. The first is a simple calculation of the natural frequencies of a single free box shaped floater. There were two cases investigated, a narrow (dimensions 60m x 10m x 10m) and a wider floater (dimensions 60m x 15m x 10m). The results for the simple box shape are expected to be reasonably similar.

The pitch natural frequency is calculated using equation 4-6 and the heave natural frequency using equation 4-7.

$$\omega_{n,pitch} = \sqrt{\frac{\rho g A_{WL}}{m + a_{pitch}}} \quad 4-6$$

$$\omega_{n,heave} = \sqrt{\frac{\rho g \nabla \cdot GM_L}{m + a_{heave}}} \quad 4-7$$

Where ω_n is the analytical natural frequency, ρ is the fluid density, g is gravitational acceleration, A_{WL} is the waterline area, ∇ is the volumetric displacement, GM_L is the longitudinal metacentric height, m is the mass of the floater, and a is the added mass. For pitch, this is calculated using the numerical tool making this calculation semi-analytical. For heave, the added mass can be estimated using equation 4-8.

$$a_{heave} = \rho C_A \frac{\pi}{4} a^2 b \quad 4-8$$

Where C_A is the coefficient of added mass which is determined based on the dimensions of the floater [93]. Then the terms a and b are the length and breadth of

the floater respectively. For pitch, the added mass is taken from the numerical model because this depends on the instantaneous angular position of the structure which is frequency dependent and not a constant term like it is for heave.

A comparison of the heave and pitch motions for the analytical and numerical results are shown in Table 2. The results are obtained for regular head waves. There is a smaller difference between the numerical and analytical results for the narrow floater (3% for heave and 4% pitch) than for the wider floater (12% and 16% for pitch). Generally the analytical calculation predicts a lower natural frequency than the numerical model.

The difference in the natural frequency increases for the wider barge. This could be a result of the added mass being calculated in the numerical model being more accurate than the analytical approximation. The added mass calculated analytically is approximately 10% higher than numerically (at the natural frequency) for both floaters. Increasing the added mass will reduce the natural frequency.

Table 2, Analytical and numerical heave and pitch motion for a narrow and wider box shaped floater.

	Narrow Floater			Wider Floater		
	Analytical	Numerical	Difference	Analytical	Numerical	Difference
Heave	0.86 rad/s	0.90 rad/s	4%	0.80 rad/s	0.88 rad/s	12%
Pitch	0.98 rad/s	0.97 rad/s	3%	0.83 rad/s	0.97 rad/s	16%

4.1.4. Semi-Analytical Serially Connected

A semi-analytical comparison was made with the natural frequency of the three floater model with flexible hinges. Using a Lagrangian energy-based method the problem can be simplified to 2D and 3 DOF (i.e., one per floater which can rotate in pitch). The kinetic (T) and potential energy (V) are calculated using equations 4-9 and 4-10 respectively.

$$T = \sum_{i=1}^n \frac{1}{2} J_i \dot{\theta}_i^2 \quad 4-9$$

$$V = \sum_{i=1}^n \frac{1}{2} k_i \theta_i^2 + \frac{1}{2} k_1 + \frac{1}{2} k_2 \quad 4-10$$

Such that the total system energy E_s is.

$$E_s(t) = T + V \quad 4-11$$

Then finding the natural frequencies can be achieved by assuming harmonic motion and solving the eigenvalue problem.

$$-\omega^2 [J] + [K] \cdot \theta = 0 \quad 4-12$$

The floater mass and inertia are taken from the inputs to the three floater model and are 230.6 tonnes and $2.66e8 \text{ kg/m}^2$ respectively. The added mass for the pitch motion is $6.86e6 \text{ N}$ which is obtained using BEM at the calculated natural frequency. This means there are some iterative steps required to obtain the added mass which makes this method semi-analytical. The spring stiffness is $6.96e6 \text{ N/m}$ which is the vertical bending stiffness for the medium sized connector. The natural frequency of the first bending mode is equal to 1.02 rad/s .

4.1.5. Added Mass and Damping

This Section provides verification that the added mass and damping terms are appropriately converted from the frequency to the time domain. The added mass and damping are part of the solution for the equation of motion and also used to calculate the wave radiation force. The conversion requires that the maximum frequency is sufficiently high so that the impulse function is able to converge to zero. This means that enough of the impulse response has been captured that the response at the highest frequency can be assumed to be the response at an infinite frequency. A comparison is made for the added mass and damping obtained for the centre floater of the grid model. The exact details of this model are described in Chapter 5. The floaters are all equally sized ($15\text{m} \times 15\text{m} \times 1\text{m}$) and equally spaced (2.0m).

The impulse response functions are shown for the cross diagonal terms for heave and pitch of the centre floater in Figure 14. The result shows that the impulse function is converging to zero which means the frequency range is sufficient for the calculation. The result in Figure 15 then compares the frequency domain results for added mass and damping for heave (33 33) and pitch (35 35). The result confirms that the terms are indeed matching. There is minor instability observed for the pitch plot which is caused by the hydrodynamic interaction of the floaters. The trends and peaks generally correlate well so this technique is considered to be acceptable.

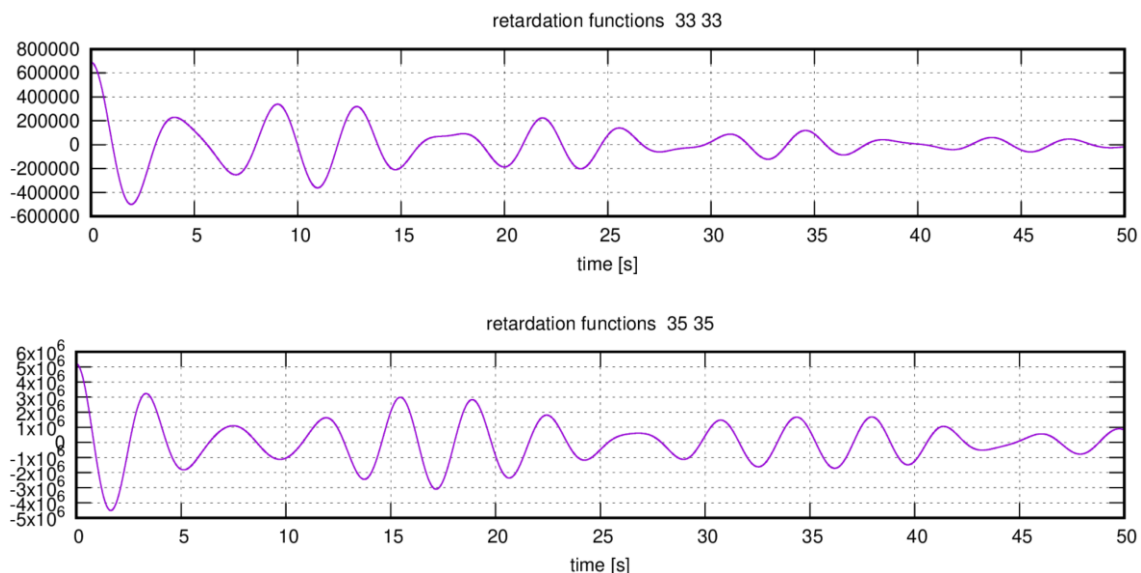


Figure 14, Impulse functions for the center floater in heave (upper) and pitch (lower).

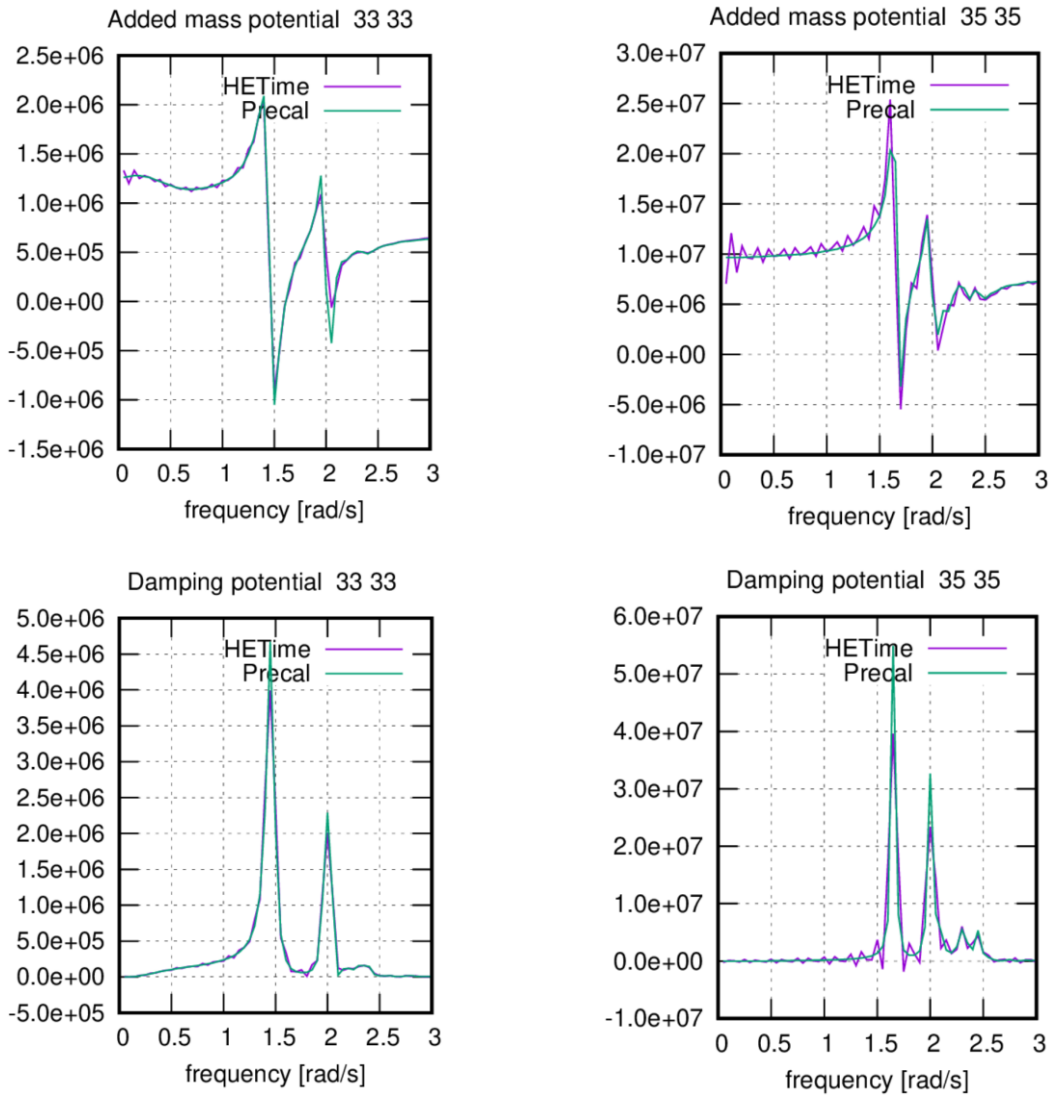


Figure 15, Added mass and damping for the frequency domain (Precal) and time domain (HETime) calculation for heave (33 33) and pitch (35 35) of the center floater of the grid model.

4.1.6. JONSWAP Spectrum

The irregular wave train used for studying the effect of different sea states is generated using a JONSWAP spectrum. The input parameters that define the spectrum are the significant wave height, pitch peak period and wave peakedness. A wave train is generated using a randomly distributed random wave frequency as input. A sample of the time varying wave elevation is shown in Figure 16 for SS-A (Hs 3.5m, Tp 5.0sec) and SS-D (Hs 7.6, Tp 11.8sec). The wave heights and frequencies generated over the time-period follow a JONSWAP normal distribution. The wave height is smaller and occur at a higher frequency for SS-A than SS-D which follows the inputs.

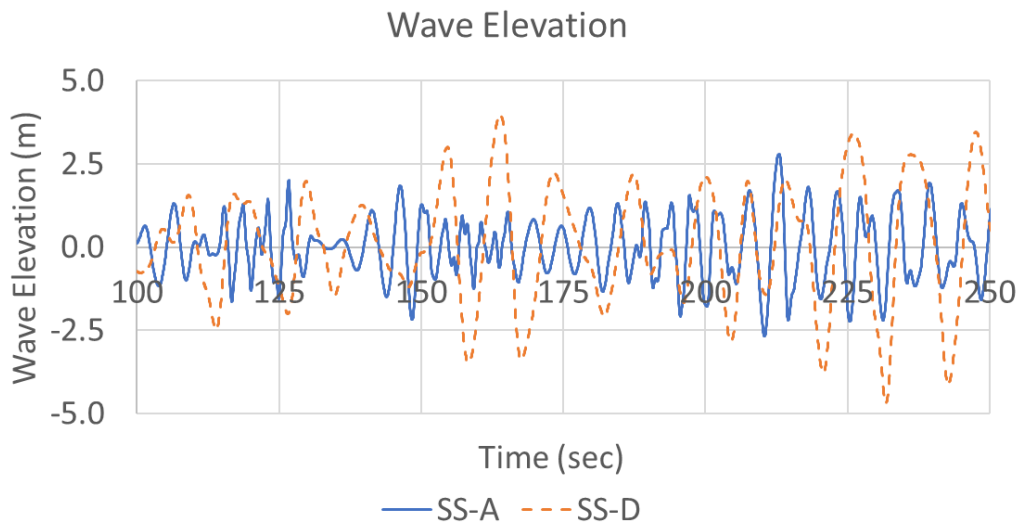


Figure 16, Wave elevation for SS-A (solid line) and SS-D (dashed line).

A Fast Fourier Transform (FFT) is used to convert this to the frequency domain and the result is compared to the theoretically calculated wave distribution. An example is shown in Figure 17 for SS-D showing the time-trace (lower) and then upper plot shows the FFT conversion compared to the theoretical distribution. The result shows that while the peak period is accurately captured by the FFT, the peak value is about 30% lower. This is because the wave energy is distributed at the higher and lower sides of the wave spectrum.

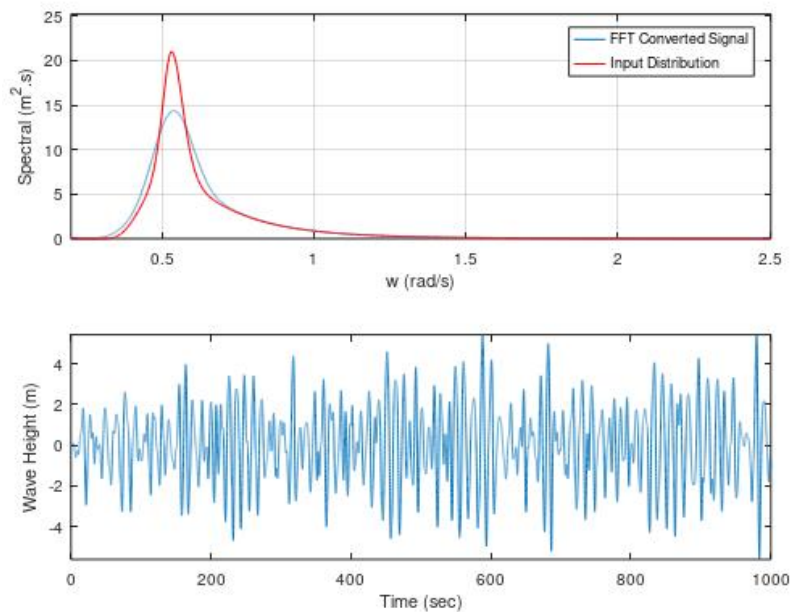


Figure 17, JONSWAP wave spectrum for sea state D showing time-trace of generated spectrum with random wave frequencies over 1000 seconds (lower) and FFT conversion of time signal to frequency domain (blue solid line) and the wave distribution (red solid line).

The significant wave height (H_s) can also be calculated with the area under the measured FFT curve (m_0) using equation 4-13.

$$H_s = 4\sqrt{m_0} \quad 4-13$$

The calculated value of H_s is 7.65m rather than the required value of 7.6m. Alternatively, the significant wave height can also be determined using the RMS (Root Mean Squared) of the time-signal as shown in equation 4-14. Using this method the value of H_s is 7.52m. The difference in the two results shows that there is some error when converting the time signal to the frequency domain using the FFT. The error could reduce when increasing the number of bins when performing the FFT, or alternatively the RMS of the time-signal can be used.

$$H_s = 4 * rms(X_{val}) \quad 4-14$$

For this thesis when the results are presented as significant values they are taken as the RMS of the time-trace. The difference in the FFT converted signal and the input distribution is only 1.1% which is considered acceptable.

4.1.7. Repeatability Irregular Waves

A repeatability study has been performed for the grid model in SS-C which is described in Chapter 5. The purpose of this study was to ensure the results for the motions and connector loads for irregular waves would be consistent within a predefined criteria. The irregular waves are generated using a random phase angle which also determines the distribution of wave amplitudes (see Section 3.4.2). There is some variability in the waves for the same sea state in different runs. To achieve a better match with the theoretical distribution the number of wave components in the wave spectrum can be increased.

The confidence can be calculated to give a percentage likelihood that the actual value is within a certain range. A common confidence interval used is 95% likelihood, that is 95% of the results are within the calculated range. The confidence band is calculated using equation 4-15.

$$\bar{X}_{val} \pm Z_{CI} \frac{s}{\sqrt{N}} \quad 4-15$$

Where \bar{X} is the averaged value, Z is the value based on the confidence interval, s is the standard deviation, and N is the number of samples. For this study, a 95% confidence interval is used which gives a Z value of 1.950 and the number of samples taken is 4. A grid model has been used which is described in Chapter 5 with head seas in SS-C (H_s 5.6 and T_p 10.0) and medium stiffness connectors.

The results for the confidence study are shown for relative motions in Table 3 and connector forces and moments in Table 4. The relative motions are shown so Y represents floaters connected forward and aft while X represents floaters connected side by side. There are also separate connectors that join the floaters forward and aft (Y) and side by side (X). These are separated because they experience different motions and loads.

There are some values which are small and perhaps show a larger confidence band than is important to consider. For example, there is large confidence band for yaw motion which means there is a lower confidence in the average value. However, the actual yaw motion is small to this might not be so important for the results. The more significant motions are heave and pitch and the more significant forces and moments are in vertical shear and bending. For these motions and loads, there is a higher confidence in the average value. Therefore, the simulation time of 1000 seconds and 300 wave components is considered acceptable for this thesis.

Table 3, Significant motions and confidence band of grid-connected structure in SS-C (Hs 5.6, Tp 10.0). The percentage of the confidence level over the average value is shown below the values. Y represents floaters connected forward and aft while X represents floaters connected side by side (see Figure 40).

		ux	uy	uz	rx	ry	rz
Y	Value with confidence	2.57 ± 0.12	0.31 ± 0.05	0.78 ± 0.03	2.70 ± 0.14	0.28 ± 0.07	0.40 ± 0.14
	% confidence over value	4.5%	17.2%	3.2%	5.3%	27.0%	35.0%
X	Value with confidence	0.65 ± 0.07	2.70 ± 0.07	5.01 ± 0.03	0.09 ± 0.01	42.57 ± 0.42	1.63 ± 0.22
	% confidence over value	10.9%	2.7%	0.6%	11.9%	1.0%	13.2%

Table 4, Significant connector forces and moments and confidence band of grid-connected structure in SS-C (Hs 5.6, Tp 10.0). The percentage of the confidence level over the average value is shown below the values. Y represents floaters connected forward and aft while X represents floaters connected side by side (see Figure 40).

		Fx	Fy	Fz	Mx	My	Mz
Y	Value with confidence	741 ± 21	180 ± 22	483 ± 8	108 ± 7	1052 ± 70	117 ± 32
	% confidence over value	2.9%	12.1%	1.7%	6.1%	6.7%	27.2%
X	Value with confidence	766 ± 101	185 ± 38	481 ± 16	87 ± 13	3715 ± 193	68 ± 16
	% confidence over value	13.1%	20.8%	3.3%	15.1%	5.2%	24.1%

4.2. Validation

There are two validation cases used to ensure that the 3D-BEM numerical model accurately captures the physics associated with the motions and connector loads of a multiple-body floating structure with box shaped floaters. The first validation case compares numerical results with an experiment conducted by Remy et al. [9] on a 12 floater model connected by two beams. The second case compares to a numerical analysis of a 3x3 grid structure which was presented by Michailides and Angelides [10].

4.2.1. Serially Connected VLFS

The first validation case compares numerical results of this thesis with model scale experiments conducted by Remy et al. [9]. There are 12 rigid box barges connected by two beams running along the length of the model. The beams had a square cross section 10x10mm. The floater motions were tracked using an optical tracking

technique of 6 groups of 3 infrared LEDs attached to locations along the structure. The connector forces and moments have been determined from the relative displacement of the floaters. In the experiment the motion responses are derived from the irregular wave time trace at various wave headings.

For this thesis the response functions are generated for head (180 degrees) and beam (90 degrees) wave headings using regular waves at multiple wave periods between 0.8- 1.8 seconds. In the numerical case, the connectors are modelled separately between the floaters rather than as two long beams as used in the experiment. This allows the connector forces and moments to be extracted as a direct output. The stiffness of the beams in the numerical model are shown in Table 5.

Table 5, Stiffness matrix for connectors of the numerical model.

	x (N/m)	y (N/m)	z (N/m)	rx (N.m/rad)	ry (N.m/rad)	rz (N.m/rad)
X	0	0	0	0	0	0
Y	0	9.35E+04	0	0	0	9.58E+03
Z	0	0	9.35E+04	0	-9.58E+03	0
Rx	0	0	0	0	0	0
Ry	0	0	-9.58E+03	0	1.31E+03	0
Rz	0	9.58E+03	0	0	0	1.31E+03
X	0	0	0	0	0	0
Y	0	-9.35E+04	0	0	0	-9.58E+03
Z	0	0	-9.35E+04	0	9.58E+03	0
RX	0	0	0	0	0	0
RY	0	0	-9.58E+03	0	6.54E+02	0
RZ	0	9.58E+03	0	0	0	6.54E+02

Table 6, Physical properties of floater in experiment by Remy et al. [9].

Length	190 mm
Breadth	600 mm
Depth	250 mm
Draft	120 mm
Floater gap	15 mm

The results in Figure 18 show the motion response functions for the experimental and numerical analyses. The heave, roll and pitch motions are shown. In general, there is a good correlation between the numerical prediction and experimental result. The trends are captured using the numerical model, especially for the roll natural frequency in beam seas. There are some differences in the pitch result, especially the first pitch excitation mode is not captured numerically. The numerical result is also much smoother across the frequencies.

There is some uncertainty in both the experimental and numerical results which could lead to some of the observed discrepancies. The experimentally obtained RAOs are retrieved from time signals, using the input wave spectrum. Such process is prone to disturbances being picked up. The numerical results have inherent uncertainty due to discretization errors and calculating the hydrodynamics using an inviscid solver. The RAOs are retrieved from response signals calculated using a numerical wave spectrum, hence without disturbances. Nonlinear effects associated with the wave radiation force and viscosity are not included, generally resulting in smooth curves.

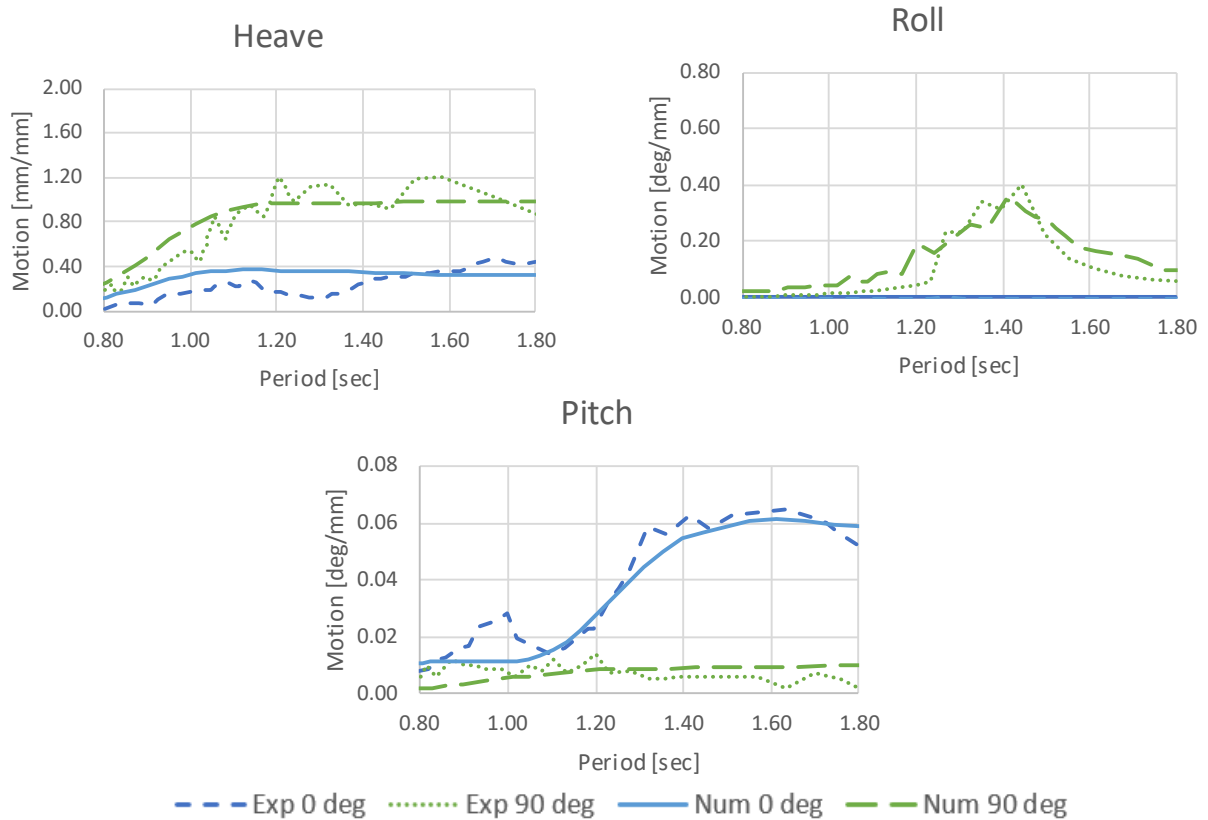


Figure 18, Motion RAOs for heave, roll and pitch with experimental results for head waves (medium dashed line) and beam waves (dotted line) and numerical results for head waves (solid line) and beam waves (longer dashed line).

The numerical and experimental results have also been compared for the bending moment as shown in Figure 19. The results are calculated for the highest bending moment which is at the centre of the 12 floaters (amidships of the entire structure). For the numerical result the bending moment in the ‘numerical beam’ case is taken at the connectors joining the centre two floaters whereas, for the ‘numerical pitch’ and the experimental cases the pitch displacement of the forward and aft floaters are used to derive the bending moment assuming a simply supported Euler beam.

$$\theta_{pitch} = \pm \frac{F_c L_c^2}{16EI} \quad @x = 0 = L \quad 4-16$$

$$M_{c,max} = \frac{F_c L_c}{4} \quad @x = \frac{L}{2} \quad 4-17$$

The numerical results align well with the experiment however, for wave periods between 1.1 and 1.6 seconds the numerical result taken at the connector is up to 40% lower than calculated in the experiment. The results indicate that the magnitude of the bending moment varies depending on how the measurement is taken because the difference between the numerical result calculating bending based on floater motions is 5% at the peak value. This is then within the numerical uncertainty of the mesh size.

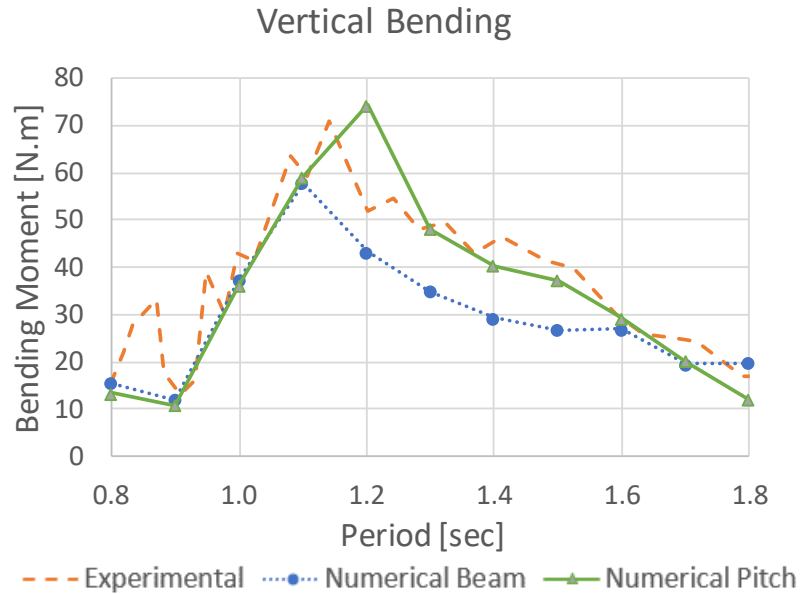


Figure 19, Forced response for vertical bending moment at centre of structure. Results numerically calculated based on bending at beams (dotted line circles), numerical calculated from pitch displacement (solid line dots), and experimental calculated from pitch displacement (dashed line).

4.2.2. Grid Connected VLFS

The second validation case compares the floater motions and connector forces for a 3x3 grid with the result obtained by Michailides and Angelides [10]. In this numerical model the floaters are flexible and the modal superposition method is used to combine the elastic response with the hydrodynamic response. Initially the dry and wet eigenmodes and eigenfrequencies are calculated before a boundary element method is used to compute the hydrodynamic coefficients and pressures. Finally, the two solutions are combined and solved with the connector constraints using FEM.

The grid layout is similar to that shown in Figure 23 with the floater dimensions shown in Table 7. Response functions are generated using regular waves at various frequencies between 0.5- 4.5 rad/s. There are two rotational connector stiffnesses analysed; 1e3 N.m/rad and 1e5 N.m/rad. The ratio of floater to connector stiffness is 50 for the low stiffness case and 5000 for the stiffer connector case. The translational DOF have stiffnesses of 1e7 N/m.

The model by Michailides and Angelides does not have any gaps between the floaters. However, the numerical tool used in this thesis must have a connector length to generate a beam element. It was decided to keep the floaters the same size but increase the overall VLFS footprint. This is because the floater geometry has a larger influence on the motion response at resonance and on the hydrodynamic terms than the overall VLFS size. Furthermore, the dimensions of the structure do not become significantly greater (10% in width and 2% in length). Finally, a gap size of 0.3m has been selected which doesn't have a large influence on the results but also avoids gap resonance which could result in unrealistically high motions.

Table 7, Physical properties of floaters in paper by Michailides and Angelides [10].

Length	10.0 m
Breadth	2.0 m
Depth	1.22 m
Draft	0.66 m
Floater gap	0.0 m (0.3 m in this thesis)

The numerical results are generated by obtaining the motions and connector forces and moments at certain regular wave frequencies which are solved in the time domain. The floater with the maximum peak motion is used to make the comparison as stated in the paper however, position of this floater in the grid is not mentioned. The numerical result has been calculated assuming the stiff hinged connector stiffness from Michailides and Angelides.

The resulting response function for pitch motion is shown in Figure 20. The results calculated in this thesis for the peak pitch motion are approximately 22% higher for the stiff connector and 14% higher for the soft connector compared to the results by Michailides and Angelides. The peak motion is also shifted towards a slightly lower frequency. The maximum pitch motion occurs on floater number 6 which is located on the aft corner.

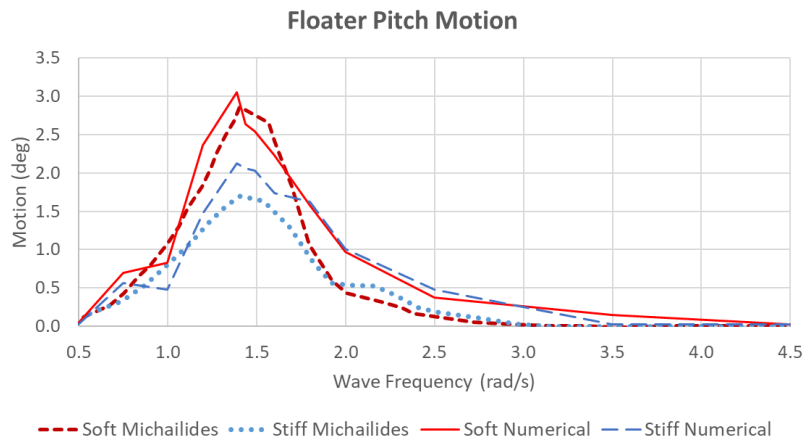


Figure 20, Numerical result of floater maximum pitch motion for 3x3 grid using soft (solid line) and stiff hinged connectors (long dashed line) with results obtained by Michailides and Angelides [10] for soft (short dashed line) and stiff (dotted line) hinged connectors.

The connector forces and moments have also been calculated and compared with the numerical result by Michailides and Angelides [10]. The results in Figure 21 show that the axial force and bending moments are higher in this thesis. The connector shear force is similar when the connector stiffness is high but then varies significantly for the lower stiffness case.

All results are taken for the maximum force or moment which occurs on a beam located in the aft corner. The results from this thesis show that the peak forces and moments occur at the pitch natural frequency whereas the results Michailides show a shift to a higher frequency. The value for the stiff connector shear force is significantly higher (approximately 300%) however, the shear force and bending moment are more similar at 26% and 45% respectively.

There are some differences in the results of the grid structure which are caused by the gap between the floaters. The hydrodynamic forces which are occurring in the gap are caused by the high pressure region developing. The potential flow code results in higher incident wave forces due to the wave resonance. Additionally, there would normally be greater hydrodynamic damping caused by turbulence which would also reduce the motions and connector loads. Both of these phenomenon might explain why the floater motions are found to be larger in this thesis.

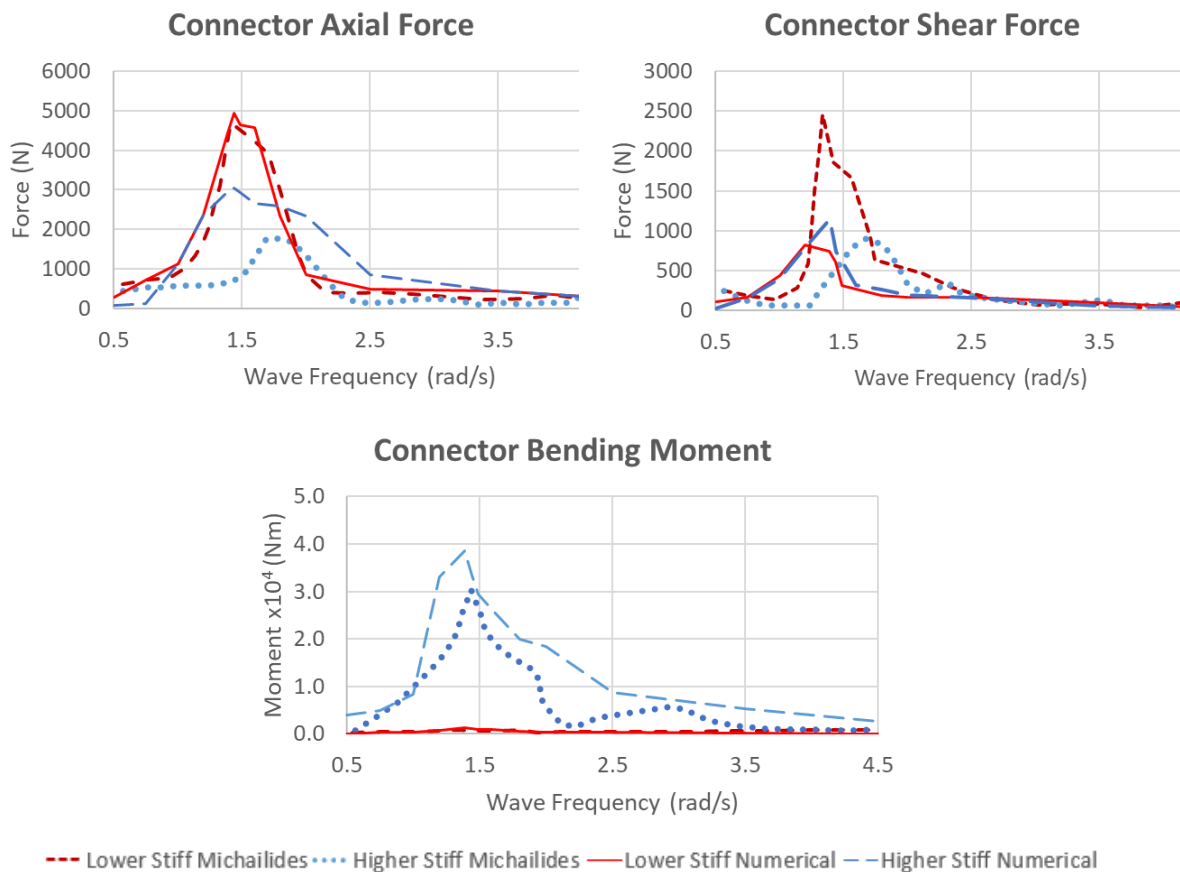


Figure 21, Connector axial force (top left), horizontal shear force (top right) and vertical bending moment (bottom) for grid model comparing calculated numerical result (dashed line) with result obtained from Michailides and Angelides [10] using stiff hinged connections (solid line).

There are some discrepancies in the calculated connector forces and moments. The forces being greater could be because of the distance between the floaters. The gap between the floater is likely to lead to higher connector forces and moments because of the lever arm that develops between connected floaters. While there is a discrepancy in the magnitude of the loads, the peaks and trends are usually captured.

5. Design and Wave Characteristics

The three case studies are used to explore the effect of connectors on an OFPV and the inputs to both of these models are described in this Chapter. The first case study is for a three floater model which is serially connected. The second and third are for a 3x3 grid and 4x4 grid of floaters respectively. The physical dimensions and parameters of the floaters and the environmental boundary conditions are described further.

5.1. Case 1 – Three Floater Model

The three floater model is an OFPV which consists of three serially connected identical box shaped floaters as shown in Figure 22. The floater size is indicative based on pilot offshore floating solar projects. The floater dimensions and properties are given in Table 8. The distance between floaters will have an influence on the hydrodynamics. It is important to avoid making the gap too small because the gap resonance might artificially increase the magnitude of the results. The length of the connector is accounted for in the calculation of the stiffness matrix.

A water density of 1025 kg/m^3 is used for the fluid domain. The hydrodynamic mesh was generated with a mesh size of 1.0 m using the open-source program GMSH. The mesh size has been determined through a grid refinement study as described in Section 4.1.1.

There are 4 mooring lines attached to the forward and aft floater. The purpose of the mooring lines is to prevent the structure from drifting away but should avoid interfering with the motion of the structure. This will avoid the structure from responding to wave headings which are outside of the case being analysed. A constant stiffness value of $1e4 \text{ N/m}$ was selected based on a mooring sensitivity study performed in Section 6.1.1. Using a linear mooring stiffness is considered appropriate because its influence on the relative floater motions is minimal. If the overall motions were to be investigated, a more accurate mooring model should be used. The mooring lines are fixed to some arbitrary location at sea level approximately 200 m away from the structure.

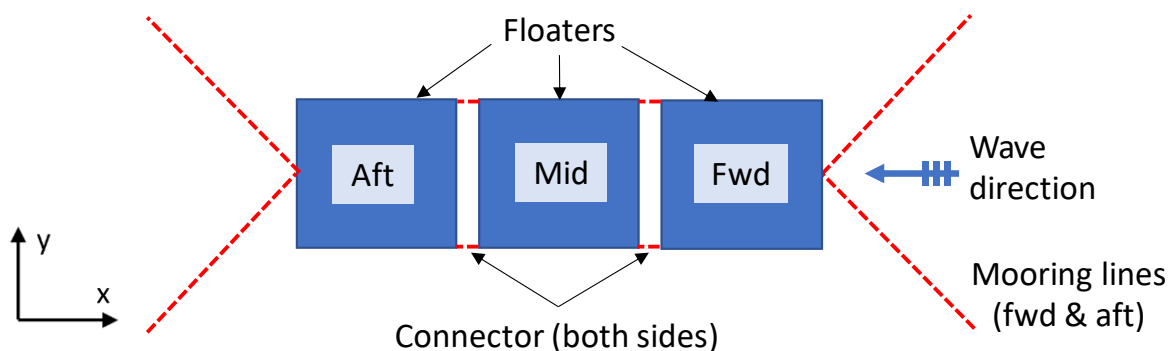


Figure 22, Three floater OFPV arrangement (plan view). NOT TO SCALE.

Table 8, Physical properties of single floater.

Length	15.0 m
Breadth	15.0 m
Depth	2.0 m
Draft	1.0 m
Floater gap	2.0 m
Ixx	8.65e6 kg.m ²
Iyy	4.34e6 kg.m ²
Izz	4.34e6 kg.m ²

5.2. Case 2 – 3x3 Grid Model

The 3x3 grid structure is modelled with the same individual floaters as the three floater model with the dimensions and physical properties given in Table 8. The plan shape is shown in Figure 23. Where there is a floater adjacent to another, two connectors are used to restrain them. The structure is moored at locations surrounding the structure, there are 2 lines per side and also two lines at every corner. The mooring line stiffness is $1e4$ N/m, the same as for the three floater model. The mooring line length is approximately 200m and attached at the still waterline away from the structure.

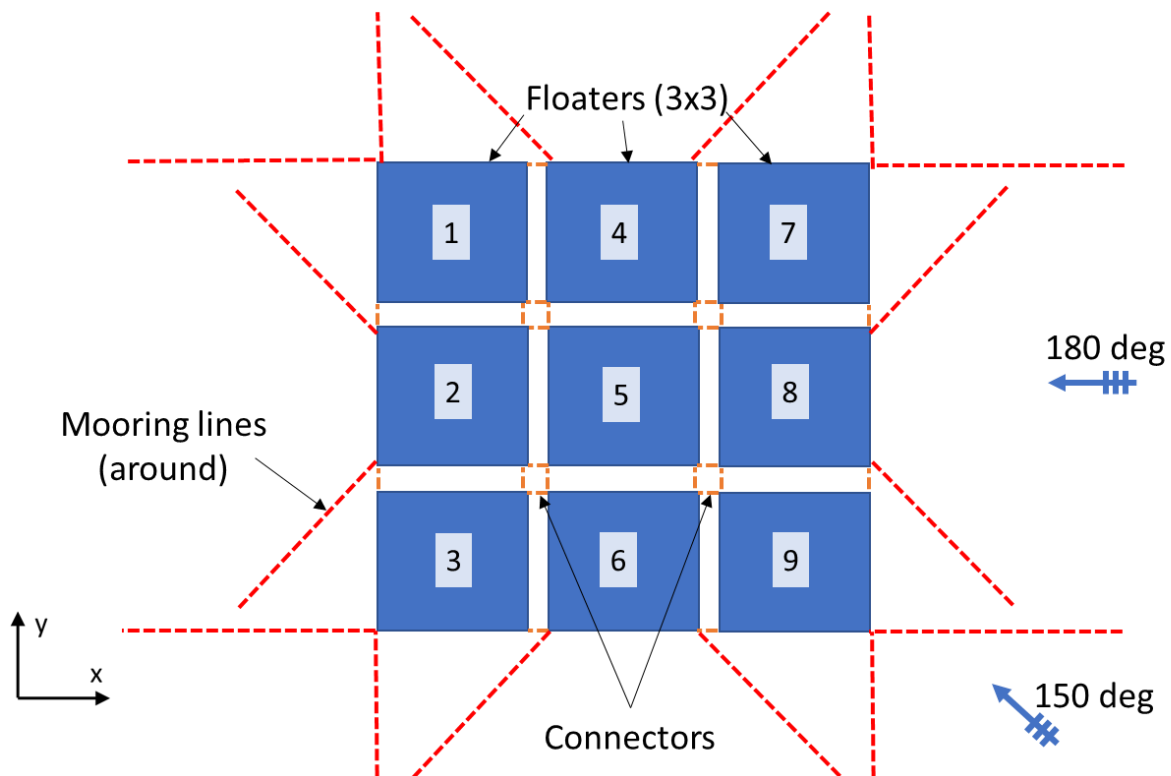


Figure 23, The 3x3 grid model OFFPV arrangement (plan view). NOT TO SCALE.

5.3. Case 3 – 4x4 Grid Model

The 4x4 grid structure is modelled very similar to the 3x3 grid model because the floaters have the same properties as presented in Table 8. The plan shape is shown in Figure 23. Where there is a floater adjacent to another, two connectors are used to restrain them. The structure is moored at locations surrounding the structure, there are 2 lines per side and also two lines at every corner. The mooring line stiffness is slightly higher in the larger grid and is $4e4$ N/m. The mooring line length is approximately 200m and attached at the still waterline away from the structure.

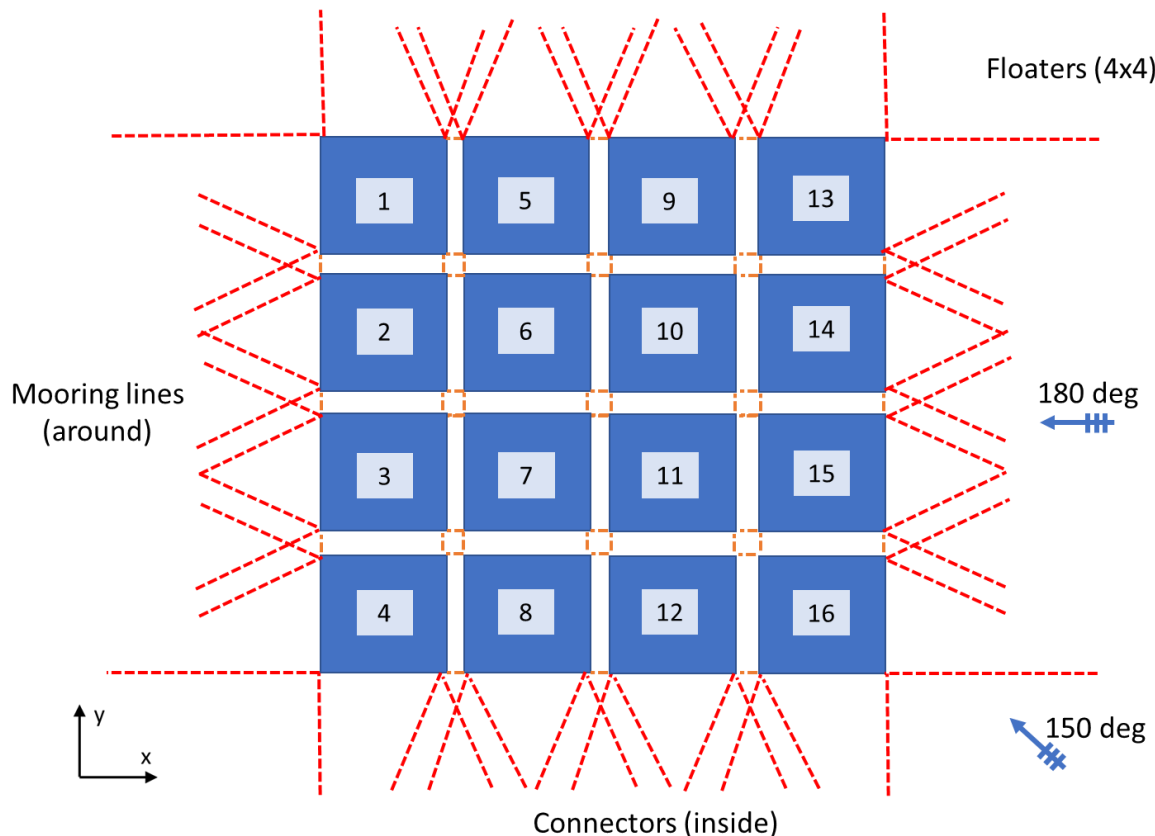


Figure 24, The 4x4 grid model OFPV arrangement (plan view). NOT TO SCALE.

5.4. Connectors

The connectors are idealized as extremely large solid circular beams, having axial and bending stiffness. There are two connectors between each of the floaters at the waterline and there is a span of 2m to cover the gap. Stiffness values are derived from equations for Euler beams in bending and compression or tension for an arbitrary solid steel rod of diameter 180, 260, and 300mm. The stiffness of the compliant connectors is defined assuming a 12x6 stiffness matrix as shown in Table 9 for a medium (nominal) stiffness connector.

The analysis is performed initially using data for the 1- and 100-year extreme wave conditions in the Hollandse Kust Noord location, which has been selected for offshore energy development by the Dutch Government. The significant wave height (H_s), wave peak period (T_p), and gamma have been obtained online [94]. In addition to the

two initial sea states, two are selected which approximately match the pitch natural frequency for the three floater model (SS-A) and the grid model (SS-B). These sea states are shown in Table 10.

Table 9, Stiffness matrix for nominal stiffness (260mm diameter solid steel rod) compliant connectors.

	x (N/m)	y (N/m)	z (N/m)	rx (N.m/rad)	ry (N.m/rad)	rz (N.m/rad)
X	1.33E+09	0	0	0	0	0
Y	0	6.73E+07	0	0	0	6.73E+07
Z	0	0	6.73E+07	0	6.73E+07	0
Rx	0	0	0	6.73E+07	0	0
Ry	0	0	6.73E+07	0	8.97E+07	0
Rz	0	6.73E+07	0	0	0	8.97E+07
X	-1.33E+09	0	0	0	0	0
Y	0	-6.73E+07	0	0	0	-6.73E+07
Z	0	0	-6.73E+07	0	-6.73E+07	0
RX	0	0	0	-6.73E+07	0	0
RY	0	0	6.73E+07	0	4.49E+07	0
RZ	0	6.73E+07	0	0	0	4.49E+07

The VLFS headings are 90 (beam seas), 120 (beam oblique), 150 (bow oblique) and 180 degrees (head seas). For the grid model, only the wave headings 150 and 180 degrees were analysed due to symmetry. A time trace representing the sea state has been generated using the JONSWAP formulation of the spectrum to represent ocean conditions for 1000 seconds, which is approximately one return period for 300 wave components. This value is chosen because it ensures repeatability when analysing the statistical results. A repeatability study was performed in Section 4.1.2 for the grid model in head seas for SS-C.

Table 10, Input JONSWAP irregular wave conditions.

		Three Floater (SS-A)	Grid Model (SS-B)	1 Yr. Extreme (SS-C)	100 Yr. Extreme (SS-D)
Significant wave height (m)	H_s	3.5	4.5	5.6	7.6
Wave peak period (sec)	T_p	5.0	6.3	10.0	11.8
Gamma (-)	γ	3.3	3.3	3.3	3.3

There has been a parametric study performed to determine the effect of damping. The values are selected based on the critical damping value of 1.09e6 Ns/m which is calculated in equation 5-1. The damping constants of 1e3 and 1e5 Ns/m represent approximately 0.1 and 10% of critical damping. The connector stiffness (k_c) is 1.44e9 N/m which is the vertical bending stiffness of the nominal connector.

$$b_c = 2\sqrt{k_c \cdot m_c} \quad 5-1$$

The results by Wang et al. found the appropriate damping ratio for a spring-mass damped system varies with excitation frequency and the damping constants of proportionality [75]. The percentage of critical damping increases with frequency. For the range of sea states being investigated in this thesis, the maximum damping ratio should range from 10- 15% of critical damping. There would be an advantage into researching the effects of different damping ratios and models.

6. Results

6.1. Case 1 – Three Floater Model

The three floater VLFS described in Chapter 5 was numerically modelled, and motions calculated in the time-domain using 3D-BEM. Figure 25 shows the time-varying pitch motion of the middle floater in SS-C and SS-D for the three floater model with nominal connector stiffness.

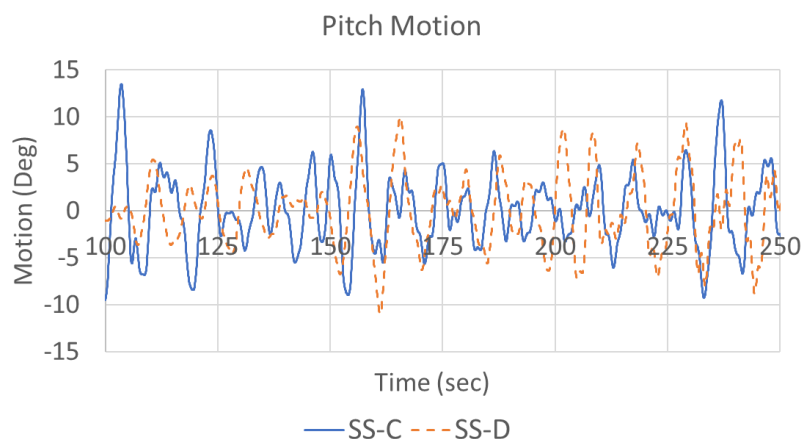


Figure 25, Pitch motion of mid floater through time for SS-C (solid line) and SS-D (dashed line).

6.1.1. Mooring Sensitivity Study

A mooring sensitivity study was performed for the three floater model that is presented in Figure 26. The study is used to determine the ideal mooring stiffness that has the least impact on the 6 DOF motion of the floaters. Results are shown for four mooring stiffnesses ($1e2$ N/m, $1e3$ N/m, $1e4$ N/m, and $1e5$ N/m) and relative motions between adjacent floaters. The results show that the value for the mooring stiffness affects the motions of the floater, particularly in pitch. There is an average of 3% and 8% difference between the pitch motion for the lowest and low mooring stiffness (respectively) while there is a 53% difference to the highest stiffness. There is less than 10% difference from the high mooring stiffness to the lower stiffness for the other motion DOF.

The connector forces and moments are also presented for the three floater model in Figure 27 for the 4 mooring stiffness configurations. Similar to the motion results, the stiffness of the mooring also influences the forces and moments of the connectors. The lowest and low stiffness cases are more similar in heave (1%) than the high (16%) and higher (29%) stiffness result. The vertical bending is also very similar for the lower and low stiffness (3%) compared to the high (7%) and higher stiffness (50%) cases.

The highest stiffness case has much higher connector loads than the other cases. The mooring lines are interacting with the structure which increases the motion for this case. The extremely high mooring line stiffness is undesirable because this will not provide meaningful results for the connector structure interaction.

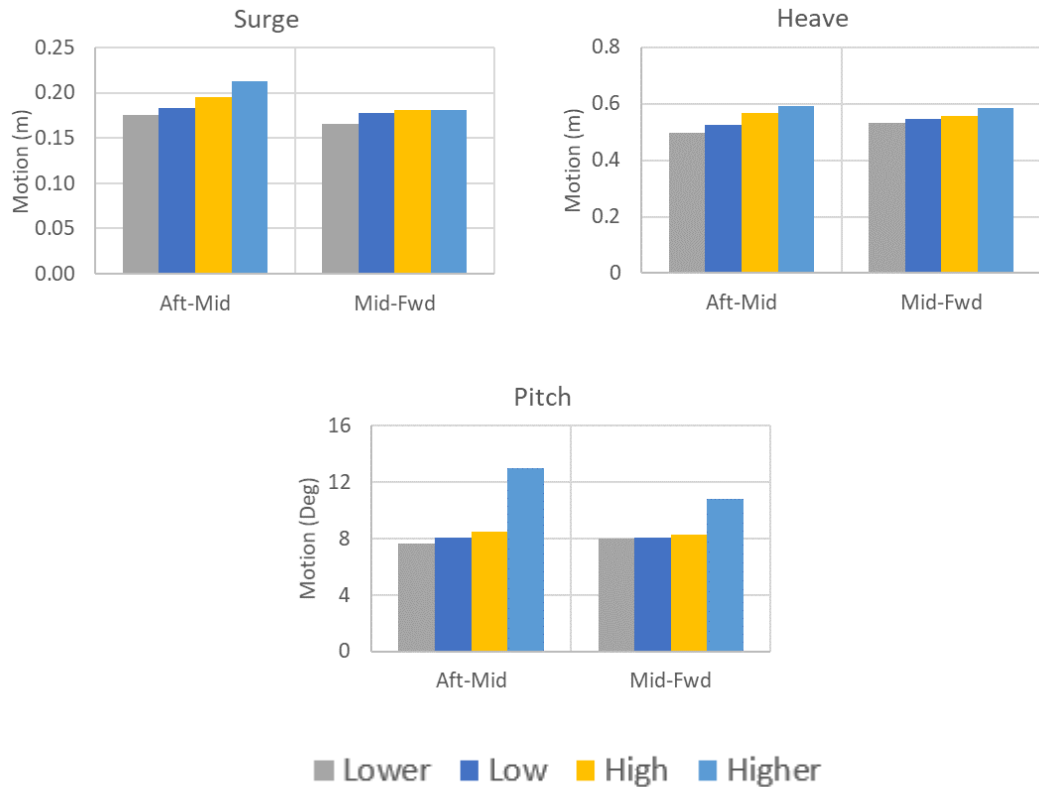


Figure 26, Mooring sensitivity study showing relative significant **motions** in surge, heave for head seas in SS-C (Hs 5.6m, Tp 10.0). Stiffness varies between 1e2 N/m (lower), 1e3 N/m (low), 1e4 N/m (high), 1e5 N/m (higher).

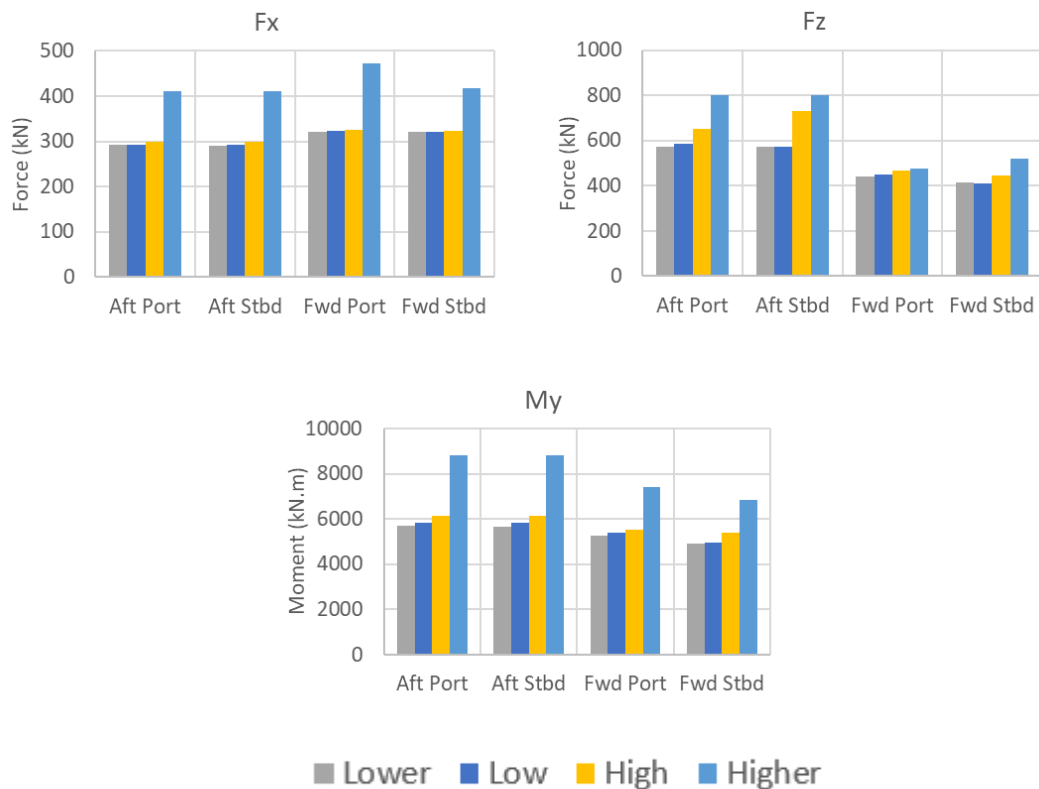


Figure 27, Mooring sensitivity study showing significant connector axial and vertical shear **forces** and bending **moments** for head seas in SS-C (Hs 5.6m, Tp 10.0). Stiffness is 1e2 N/m (lower), 1e3 N/m (low), 1e4 N/m (high), 1e5 N/m (higher).

The mooring lines should also keep the structure in the same position. The global surge motion is presented in Figure 28. A sample of the time-trace is shown. It is clear the lowest mooring case is drifting considerably and is not desirable for the simulation. The lowest mooring stiffness configuration that doesn't result in drift is the high stiffness case ($1e4$ N/m) so this value is used for further calculations.

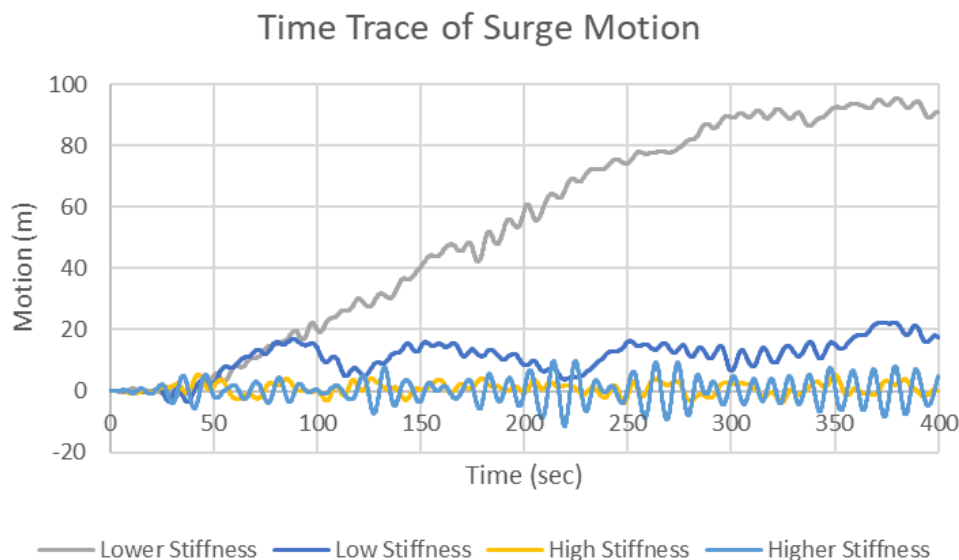


Figure 28, Time trace of the global surge motion of the aft barge in SS-C (H_s 5.6m, T_p 10.0). Four mooring stiffness configurations are shown with values $1e2$ N/m (lower), $1e3$ N/m (low), $1e4$ N/m (high), $1e5$ N/m (higher).

6.1.2. Effect of Connector Stiffness in Sea States

The effect of connector stiffness on the resulting motions and connector loads has been investigated for 3 sea states and 4 wave headings from 90– 180 degrees. The significant values are presented in SS-A, SS-C, SS-D in Figure 29, Figure 30, and Figure 31 respectively. The results are averages and error bars are used to show the maximum and minimum values for the three connector stiffnesses represented by the solid steel rods (180, 260, 300mm diameter). The motions are relative as they are calculated at the position of the connector node.

The maximum relative floater motions are experienced when the stiffness of the connector is the lowest and conversely the motions are lower when the stiffness is greater. The differences in the floater motions are quite large for sway and pitch. Especially in pitch the difference can be up to 60% of the averaged value. The variation in the maximum and minimum results also increases from SS-A to SS-B and SS-C. The magnitude of the motions is generally larger in SS-A and SS-D than SS-B.

The relation between the floater motions and connector forces and moments also presented. The maximum and minimum connector forces vary especially for F_x and F_y depending on the wave heading and sea state. The force in vertical shear (F_z) tends to be higher for stiffer connections and is largest for SS-A. The moment was generally larger for the stiffer connectors and the vertical bending moment is always significantly greater than the other moments and is largest in SS-A. There is very small variation between the connector moments even for the oblique sea headings. There

is much more variability in the connector translational forces between the connector stiffness cases than for the moments. The connector stiffness has a greater effect on the forces and moments in SS-D.

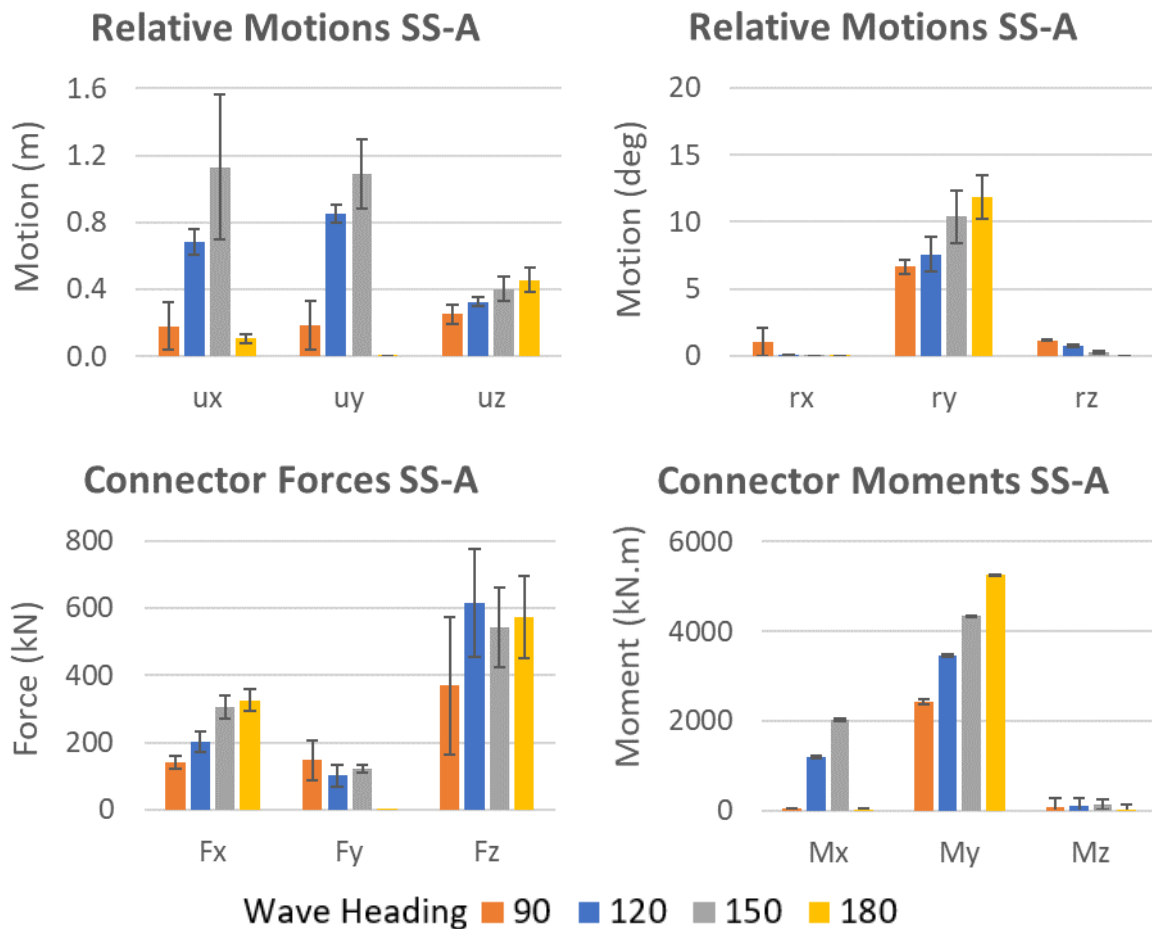


Figure 29, Floater relative motions and connector forces and moments for **SS-A** (H_s 3.5m, T_p 5.0sec) with wave headings (90, 120, 150, and 180 degrees). Connector rod diameter varied from 180-, 260-, and 300-mm and error bars show minimum and maximum values from three stiffness cases. The maximum motions occur with the least stiff connectors and lowest motion has the stiffest. For F_x and F_y the maximum varies without any trends, but F_z is generally maximum for stiff connectors. For the moments the maximum is the stiffest connection and lowest is least stiff.

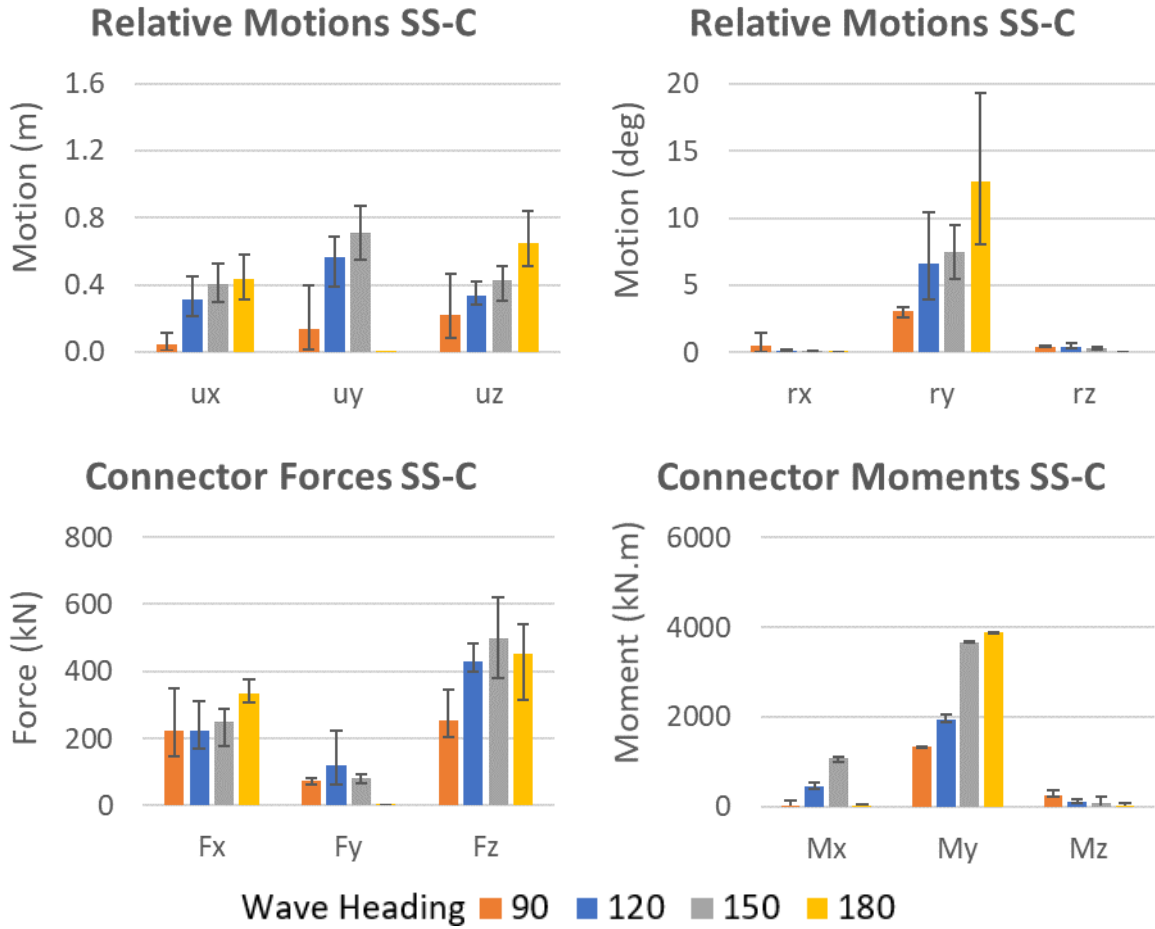


Figure 30, Floater relative motions and connector forces and moments for **SS-C** (H_s 5.6m, T_p 10.0sec) with wave headings (90, 120, 150, and 180 degrees). Connector rod diameter varied from 180-, 260-, and 300-mm and error bars show minimum and maximum values from three stiffness cases. The maximum motions occur with the least stiff connectors and lowest motion has the stiffest. For F_x and F_y the maximum varies without any trends, but F_z is generally maximum for stiff connectors. For the moments the maximum is the stiffest connection and lowest is least stiff.

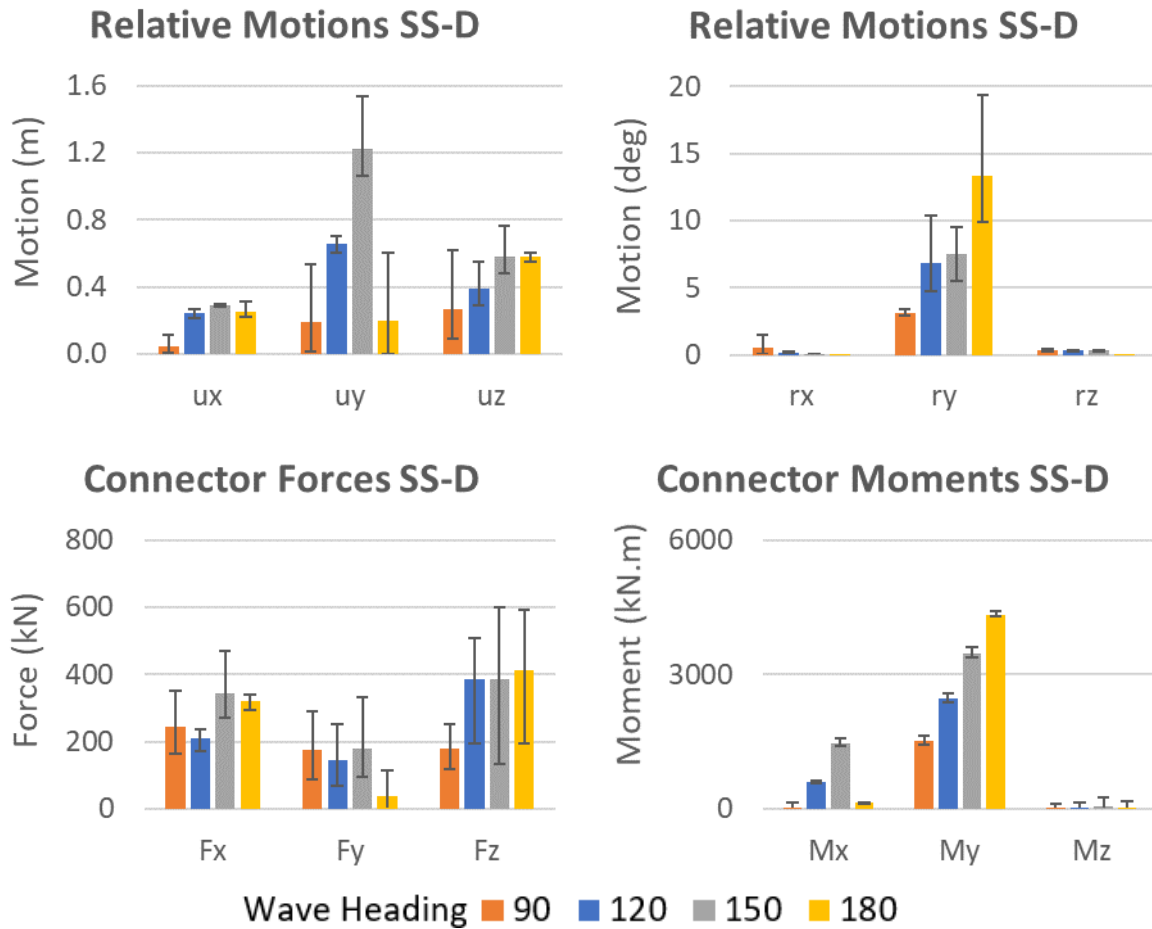


Figure 31, Floater relative motions and connector forces and moments for **SS-D** (H_s 7.6m, T_p 11.8sec) with wave headings (90, 120, 150, and 180 degrees). Connector rod diameter varied from 180-, 260-, and 300-mm and error bars show minimum and maximum values from three stiffness cases. The maximum motions occur with the least stiff connectors and lowest motion has the stiffest. For F_x and F_y the maximum varies without any trends, but F_z is generally maximum for stiff connectors. For the moments the maximum is the stiffest connection and lowest is least stiff.

The results presented show that the sea state has an influence on the motions of the floaters which then also influences the connector forces and moments. The main parameters which are used as inputs to the JONSWAP sea-spectrum are the peak period and wave height. Increasing the wave height can increase the motions of the floater because of the larger excitation force. The peak period is significant because the wave energy distribution is concentrated around a certain wave frequency. The peak period is more important when considering dynamics because certain wave frequencies cause resonance with the structure. This is clearly demonstrated when observing the results at SS-A which has a much smaller wave height but the floater motions and connector loads are generally higher.

6.1.3. Effect of Varying Connector Stiffness DOF

The effect of varying the connector stiffness has been varied individually in the axial, vertical shear and vertical bending directions in SS-C. The individual stiffness has been investigated as a sensitivity into how critical each stiffness DOF is on the floater motions and connector loads. The stiffness is varied by a factor of 5 times small/larger

for every DOF including coupled terms. This means that all the stiffness terms in the vertical or horizontal directions of the matrix are affected. Results are presented as an average of significant values for wave headings of 180, 150, and 120 degrees in Figure 32, Figure 33, and Figure 34 respectively. Error bars show the maximum and minimum value for the three connector stiffnesses modified for each of the three DOF.

The maximum values for motions generally occur for the least stiff connectors and there is a large variation in the results when modifying individual stiffnesses for vertical shear and bending and a lesser variation when modifying axial stiffness. The variation is also greatest for bow oblique waves (i.e., wave heading 150 degrees). Modifying the axial stiffness has a very small effect on the motions. In contrast, varying the vertical shear and vertical bending stiffness has a very large effect on the motions of up to 70%.

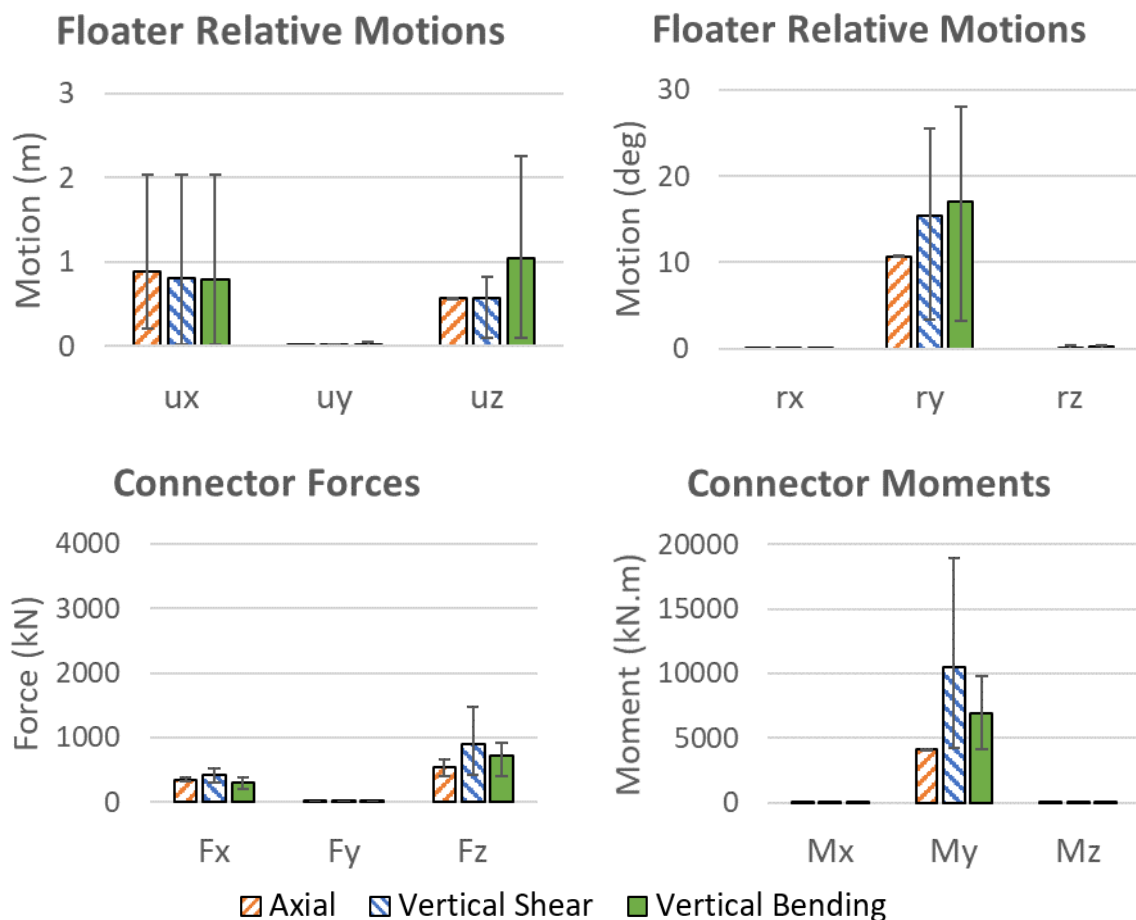


Figure 32, Wave heading **180 degrees** floater relative motions and connector forces and moments for varying individually connector stiffness for DOF (soft, medium, and stiff) in axial, vertical shear and vertical bending. Values are averaged for the three floaters and error bars show maximum and minimum values. For motions the least stiff connector is generally the maximum and most stiff is the minimum. For forces and moments, the maximum is generally the stiffest connector and minimum is the least stiff.

The results shown in Figure 33 for oblique seas shows that modifying vertical bending has the large effect on the surge motion. This seems counterintuitive because there is no axial coupling with the vertical bending stiffness. However, in the oblique seas case this could be caused by the structure experiencing more motion overall with softer connectors.

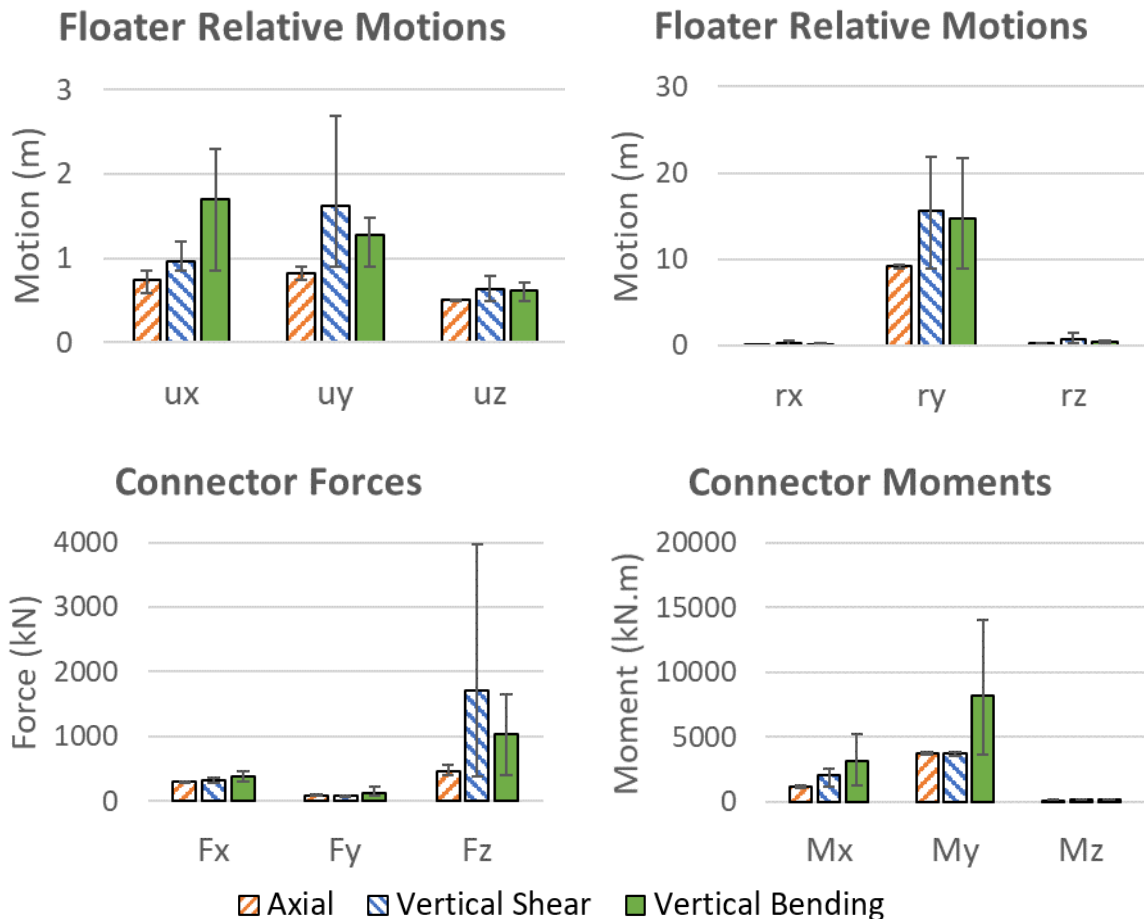


Figure 33, Wave heading **150 degrees** floater relative motions and connector forces and moments for varying individually connector stiffness for DOF (soft, medium, and stiff) in axial, vertical shear and vertical bending. Values are averaged for the three floaters and error bars show maximum and minimum values. For motions the least stiff connector is maximum and most stiff is the minimum. For forces the maximum and minimum varies for different stiffnesses. For moments when varying surge and heave the maximum and minimum varies but when varying pitch, the maximum is for stiff connections and minimum for least stiff.

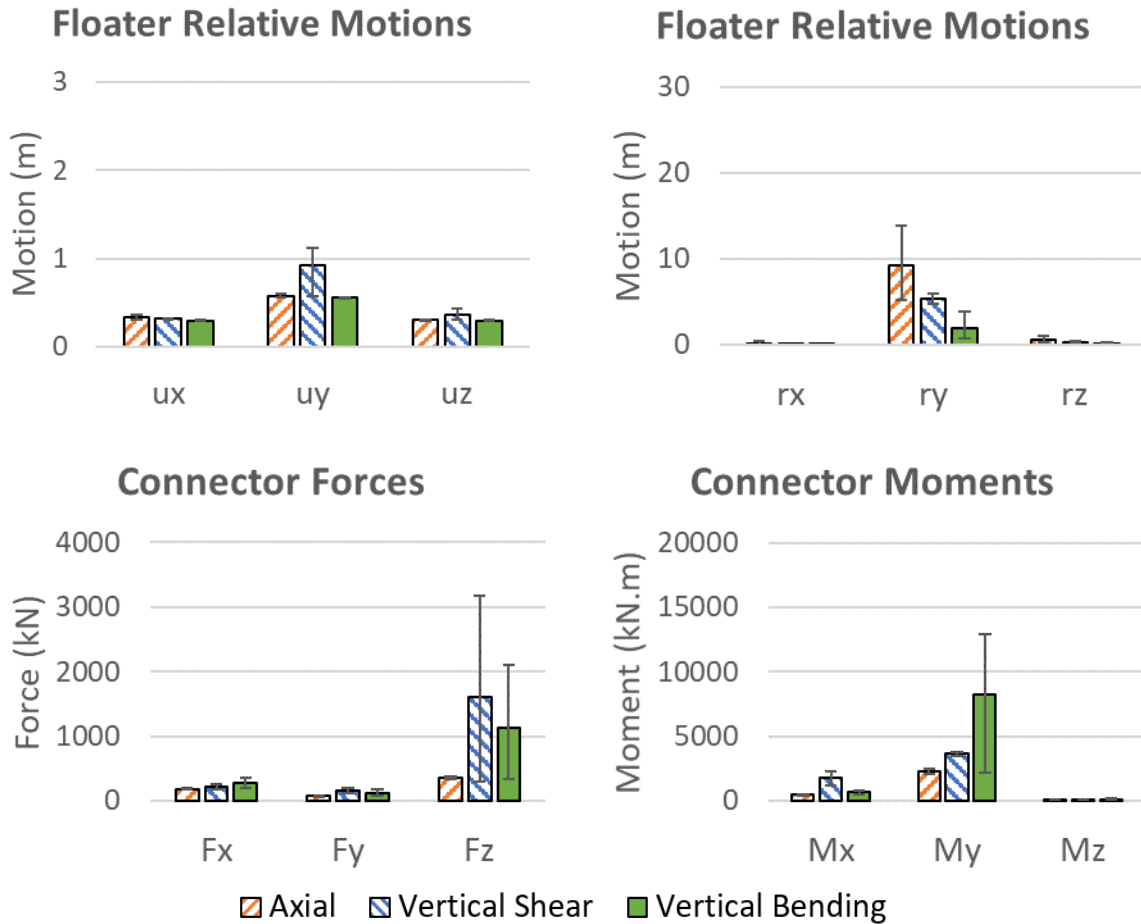


Figure 34, Wave heading **120 degrees** floater relative motions and connector forces and moments for varying individually connector stiffness for DOF (soft, medium, and stiff) in axial, vertical shear and vertical bending. Values are averaged for the three floaters and error bars show maximum and minimum values. For motions the least stiff connector is generally the maximum and most stiff is the minimum. For forces and moments, the maximum is generally the stiffest connector and minimum is the least stiff.

There is a clear relation between the connector stiffness and the floater motions and connector forces and moments. The results show that connector stiffness is a critical parameter for determine the VLFS response. This was expected because the connectors have more resistance to motion when the stiffness is greater. When there is more resistance, the connectors experience higher loads. The effect of stiffness is largest for vertical shear and bending. The stiffness in these DOFs are much lower than in the axial direction. There is also a coupling between these stiffnesses so that modifying one stiffness results in changes to the motions and connector loads in other DOF.

There is small variation in the maximum connector forces and moments for all 4 connectors for all wave headings. This means that in the three floater model the loads are reasonably well distributed over the structure. The connectors aft generally experienced smaller loads than those in the front. This is due to a screening effect from the forward floater which experiences the full wave forces and dissipates some energy away from the structure. The small variation in the forces and moments is probably because the structure not being so large compared to the waves.

6.1.4. Effect of Damping

The effect of damping was also investigated for the three floater model in irregular head waves. There is a noticeable reduction in motions and connector forces and moments for SS-A (Figure 35) whereas, there is a very little effect when modifying damping for SS-C shown in Figure 36. The effectiveness of damping is larger in reducing the vertical shear forces and bending moments than for the axial forces. Even by applying a very low percentage of critical damping the bending moment (M_y) reduced by a considerable amount.

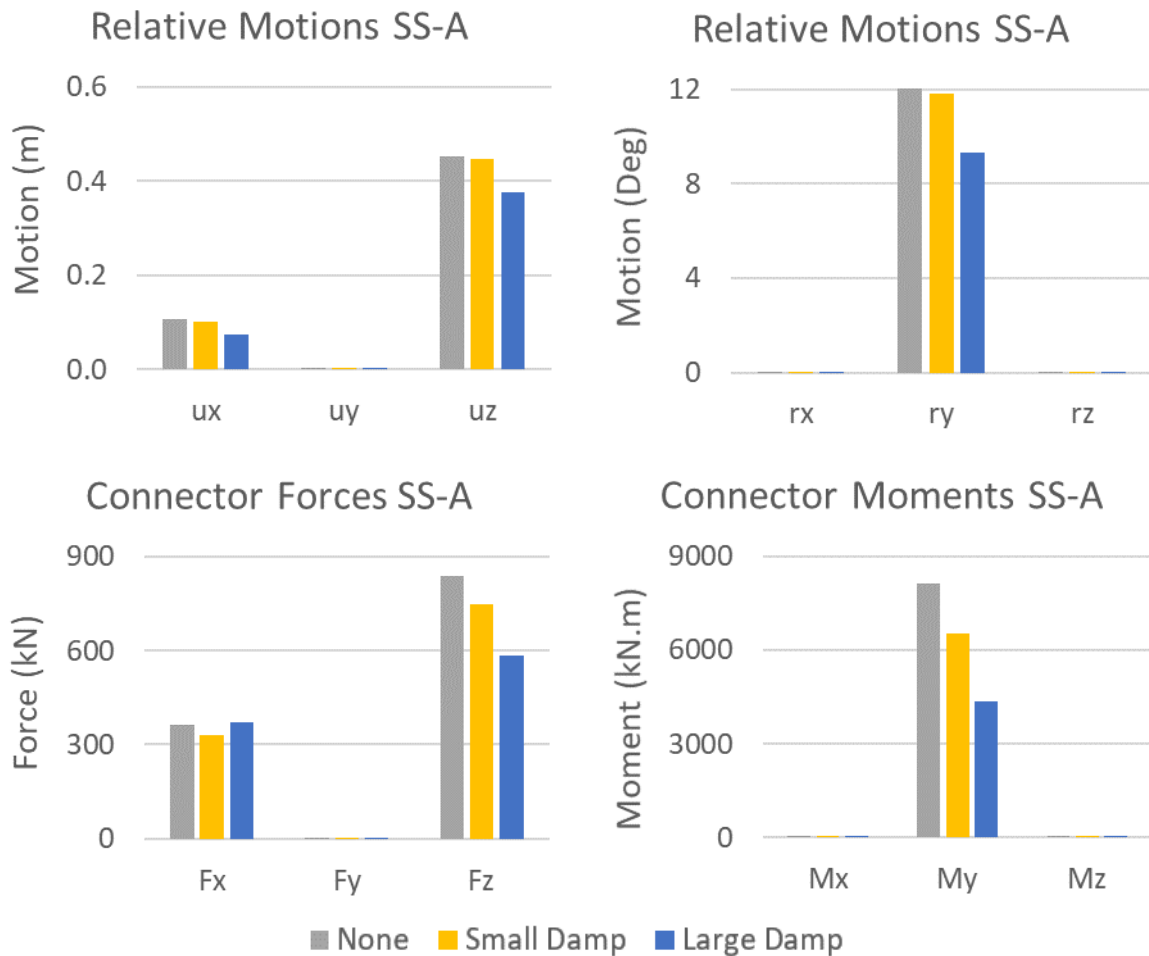


Figure 35, **Sea state A**, floater relative motions and connector forces and moments for no damping, lower damping ($1e3$ kg/s) and larger damping ($1e5$ kg/s). The results are an average of the three floaters in wave heading 180 degrees.

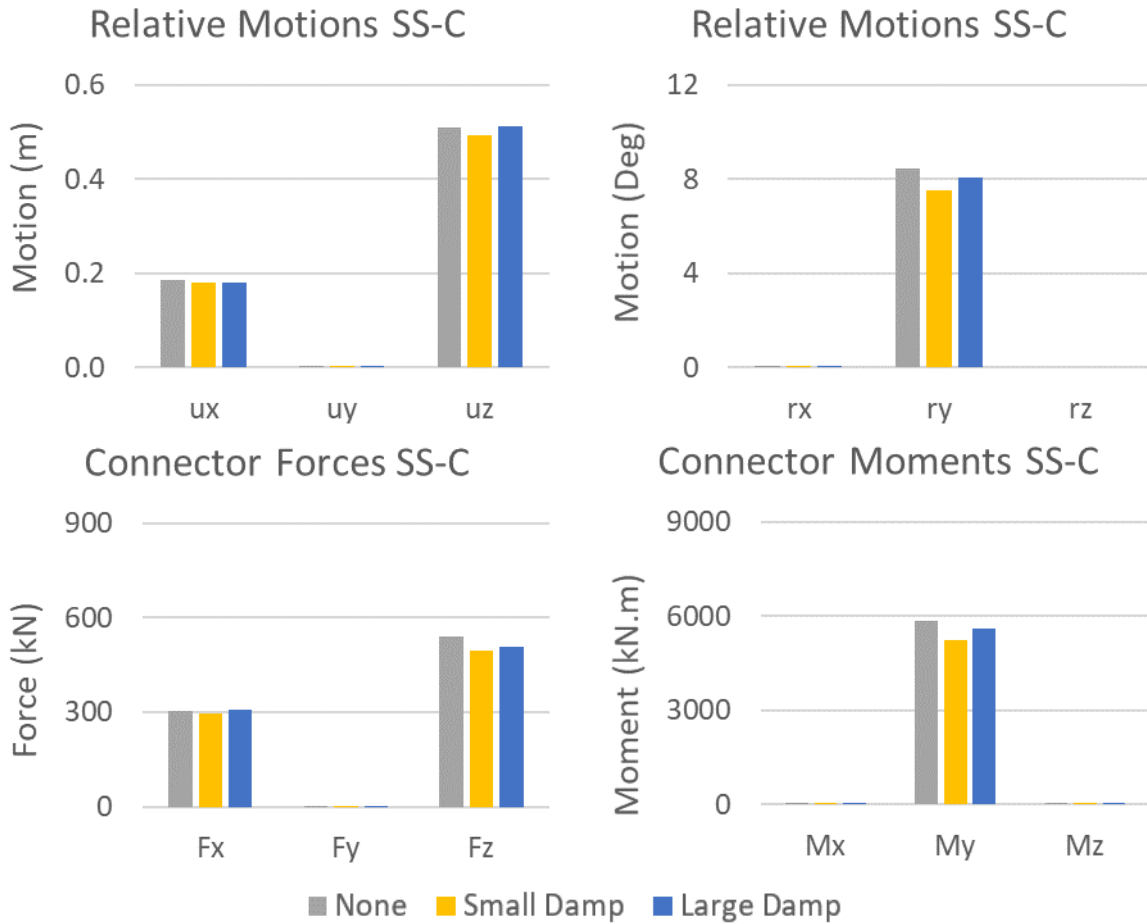


Figure 36, **Sea state C**, floater relative motions and connector forces and moments for no damping, lower damping (1e3 kg/s) and larger damping (1e5 kg/s). The results are an average of the three floaters in wave heading 180 degrees.

The resulting trend shows that damping reduces the motions and connector loads when the wave peak period of the sea state is close to the natural frequency of the structure. The effectiveness of damping diminishes away from the structures natural frequency as is shown for SS-C where the effects from damping are negligible. In SS-C there is less wave energy distributed close to the natural frequency of the structure while for SS-A there is much more. Since damping works to reduce the dynamic response the results are expected. The energy dispelled from the connector movement is dispelled into a fluid for both cases (i.e., Rayleigh damping). The ratio of Rayleigh damping to critical damping is estimated to be between 2-15% [75], [95].

6.1.5. Distribution of Loading

The distribution of the loading of the connectors on the serially connected structure is shown in this Section. The results are compared for the SS-A (Hs 3.5m, Tp 5.0 sec) in oblique and head seas. The maximum forces and moments are shown in Table 11. The normalized distribution of loads are presented for the oblique sea case in Figure 37 and the head sea case in Figure 38.

There is little variation in the connector loads across the structure. The oblique seas result in slight differences which is greatest for the vertical shear force which is 35-

40% less on one side of the structure. The forward connectors experience 10-20% lower vertical bending moment (M_y) loads compared to the aft connectors.

Table 11, Maximum connector loads for wave headings 150 and 180 degrees in SS-A (H_s 3.5m, T_p 5.0 sec).

Wave	Fx (kN)	Fy (kN)	Fz (kN)	Mx (kN.m)	My (kN.m)	Mz (kN.m)
150	304	112	527	1200	3286	114
180	304	1	505	0	4051	1

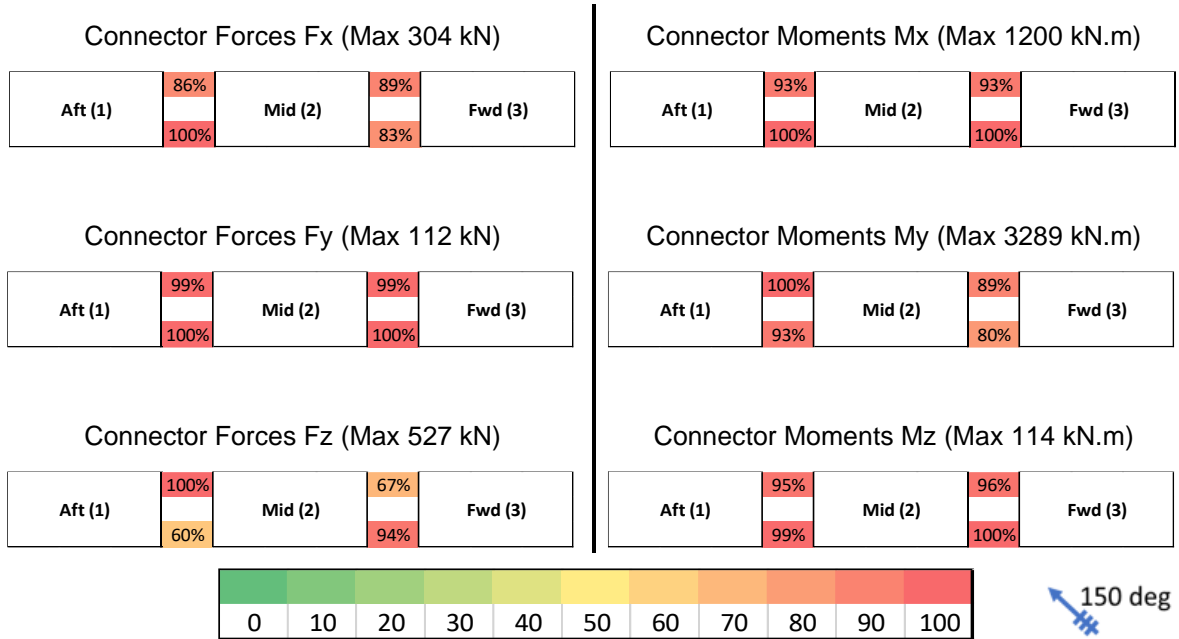


Figure 37, Distribution of connector forces and moments for SS-B for wave heading 150 degrees. Results relative to the maximum force or moment in the structure. Percentage of maximum load shown in color scale below. Arrow shows wave direction (bottom right).

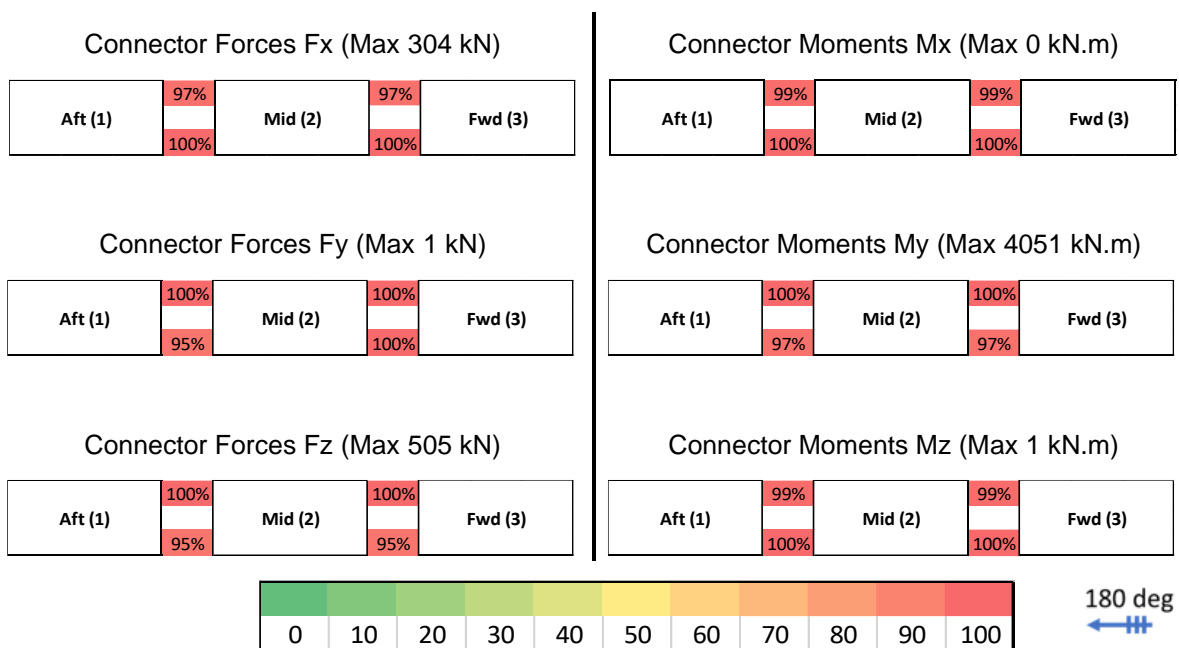


Figure 38, Distribution of connector forces and moments for SS-B for wave heading 180 degrees. Results relative to the maximum force or moment in the structure. Percentage of maximum load shown in color scale below. Arrow shows wave direction (bottom right).

6.1.6. Frequency Response Functions

The pitch frequency response function for the three floater model with nominal stiffness connectors is presented in Figure 39. The average motion is shown and the shaded areas represent the maximum and minimum values of the three floaters. The response function is obtained by calculating the maximum pitch motion in nine regular head wave frequencies. The peak motion at 1.2 rad/s signifies that this is a natural frequency and the structural response is excited at this frequency. The pitch motion for 1m waves is 1.5 degrees at this wave frequency.

The connector model VLFS has been compared with a case where there are three free floaters with no connections, and one continuous rigid structure which is equal in length to the three floater model and gaps. The result shows that the addition of connectors shifts the natural frequency of the structure and magnitude of the peak motion to somewhere in between the free and continuous case (1.67 rad/s and 0.92 rad/s respectively).

The variation for the motion response for the connector model is quite small for lower frequencies, within 5% at the peak but then deviates up to 34% at higher frequencies. However, the variation when the floaters are not connected is much smaller over the entire range of frequencies.

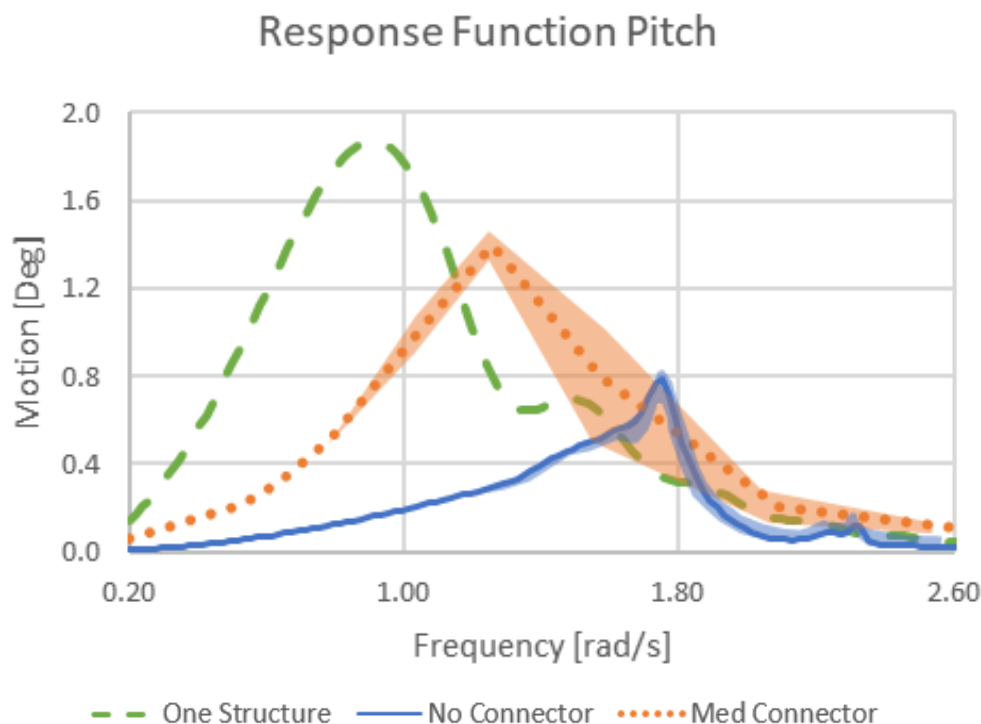


Figure 39, Pitch motion response calculated in regular 1m wave height head waves for the three floater model (average shown where applicable) with one continuous structure (dashed line), no connectors (solid line), and nominal stiffness connectors (dotted line). Shaded zones represent the minimum and maximum values.

The frequency response results give insight into why there is a large motion at sea states with lower significant wave heights. The resonant frequency of the structure is towards the lower frequency range while a free floating structure has a higher

frequency. The inputs to SS-A were chosen to match with the bending natural frequency from Figure 39. The response function explains why the response of SS-A is larger even if the significant wave height is much lower than the other two sea states. There is more wave energy directed at the same frequency as the natural frequency of the structure. The conditions of SS-A are taken from the wave scatter plot of the Hollandse Kust Noord site [94], meaning this structure experiences resonant motions and higher connector loads.

It is demonstrated in this thesis that the connector stiffness determines the natural excitation frequency of the entire structure. The peak motion shifts from a lower frequency to a higher frequency as the structure behaves more like independent floaters. This is due to the connectors influencing the floater motions because the individual (three) free floaters have higher natural frequencies. By separating the structure into multiple smaller floaters with connectors, the resonant frequency is shifted away from the wave spectral peaks of SS-C and SS-D (0.62- and 0.49 rad/s respectively) but also the magnitude of the peak is reduced for a structure that has the same surface area. Reducing the size of the floaters and making them more independent would reduce the motion response for the analysed sea location.

The pitch natural frequency of the three floater structure is approximately 1.2 rad/s. This compares with the analytical result presented in Section 4.1.4 where the natural frequency is calculated as 1.02 rad/s. The peak pitch motion is 18% higher in the numerical case compared to the semi-analytical prediction. The stiffness of the structure could be slightly higher in the numerical case because of the coupled heave and pitch DOF in the stiffness matrix. The higher stiffness would mean the numerical model has a higher natural frequency.

6.2. Case 2 – 3x3 Grid Model

There were two parametric studies performed on the 3x3 grid structure described in Chapter 5. The first assumes a fixed (nominal) connector stiffness and then analysing the response of the structure for wave headings of 180 degrees and 150 degrees in sea states A, B, C, and D. The second explores the effect of individually modifying the connector stiffness per DOF for a wave heading of 150 degrees and in sea states B and D. The full results are shown in Appendix A.

The floater motions are taken as relative to the adjacent floater in Y (red) or X (green) at the connector node as shown in Figure 40. The connector loads are similarly separated into a connector in the Y (red) and X (green) directions. The results are shown as significant value of the time-signal and then averaged for all floater relative motions or connector loads. Results are discussed in the following subsections.

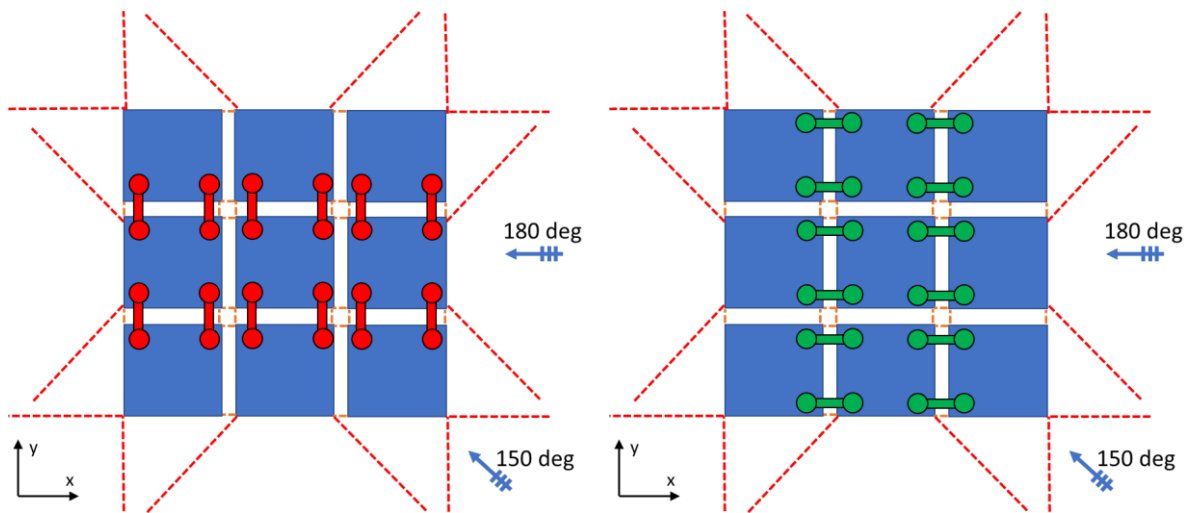


Figure 40, Grid model VLFS marking **Y** connectors (left) and **X** connectors (right). NOT TO SCALE.

6.2.1. Effect of Wave Heading

The results in Table 12 show the maximum values for both 150- and 180 degree wave headings in SS-B (Hs 4.5m, Tp 6.3 sec). The motions and connector loads are compared for all 6 DOFs and results show the maximum significant values from the entire structure. The pitch and surge motions are larger for head seas, but the motions in the other DOFs are greater for oblique seas. In many cases, the maximum motions for pitch and surge are also larger in oblique seas. There is a very large pitch motion (40- 55 degrees) which occurs when the floaters are bending out of phase in a hinged type of motion (shown in Figure 44). The roll and sway motion in the head sea case is caused by the coupling of the floaters.

There can be a large variability in the floater motions and connector loads across the grid structure. This is also shown in Table 12 when comparing the standard deviation of the results for the individual floaters or connectors in head and oblique seas. The variation becomes greater in SS-B which has a peak period close to the natural frequency in bending. The largest motions occur at the corner(s) of the structure which can be up to 60% greater than the averages. Meanwhile, the minimum motions or connector loads which occur at the centre of the structure are not more than 35% of the averaged value.

The floater motions in head and oblique seas are shown in Figure 44 and Figure 45. These also show the corner floaters experiencing larger motion than the centremost floater. The floaters experiment movement in three distinct rows for head seas (Figure 44) compared to oblique seas when the structure experiences vertical bending in multiple bending directions which causes large connector loads (Figure 45). The motion is greater at the corner because it is less constrained and the system is in resonance with the wave loading. The underprediction of both the hydrodynamic and connector damping might lead to exaggerated motions at resonance.

The maximum values of the averaged forces and moments are then shown in Table 13 for SS-B (Hs 4.5m, Tp 6.3 sec). The forces in the axial direction (F_x) and the vertical shear (F_z) are larger in oblique seas than head seas but then smaller in the other degrees of freedom. There is generally more variability in the forces and moments for

oblique seas as shown in Figure 16. This is because the wave load excites different mode shapes in oblique waves than in head seas. The connectors respond to the floater motions by restraining the larger motion of the outer floaters which causes high loads.

Table 12, Relative floater **motions** for head seas (180 deg) and oblique seas (150 deg) in all DOF. Results are maximums of significant values and standard deviation in SS-B (Hs 4.5m, Tp 6.3sec).

Wave Heading		Surge (m)	Sway (m)	Heave (m)	Roll (deg)	Pitch (deg)	Yaw (deg)
180 deg	Motion	2.8	2.5	1.4	3.9	55.8	1.0
	Std Dev	0.0	0.1	0.3	0.4	7.6	0.3
150 deg	Motion	2.3	4.0	2.6	13.0	42.4	1.6
	Std Dev	0.0	0.7	0.5	0.5	1.2	0.2

Table 13, **Forces and moments** for head seas (180 deg) and oblique seas (150 deg) in all DOF. Results are maximums of the significant values and standard deviations in SS-B (Hs 4.5m, Tp 6.3sec).

Wave Heading		Fx (kN)	Fy (kN)	Fz (kN)	Mx (kN.m)	My (kN.m)	Mz (kN.m)
180 deg	Max	1545	1083	2262	491	7280	597
	Std Dev	266	129	346	63	928	90
150 deg	Max	2738	571	3522	407	5640	474
	Std Dev	242	12	782	72	207	133

6.2.2. Effect of Sea State

The sea state is influential in the motion and connector response for the grid structure. Results are presented for head seas for the X-facing relative floater motions and connectors in Figure 41. The floater motions are large in surge (ux), heave (uz) and pitch (ry). The connector vertical shear force (Fz) and the vertical bending moments (My) are both large. There is a vertical bending natural frequency close to SS-B (Hs 4.5m, Tp 6.3sec) and the motions and connector responses are higher for this sea state even if the significant wave height might be lower (i.e., SS-C, and SS-D).

There is also a greater spread in the floater motions and connector loads at a sea state close to the structural natural frequency (SS-B). This is primarily caused by the floaters and connectors acting in resonance with the waves. Resonance can play an important role in the motion and connector response so the sea state is a critical parameter when considering the design of an OFPV system.

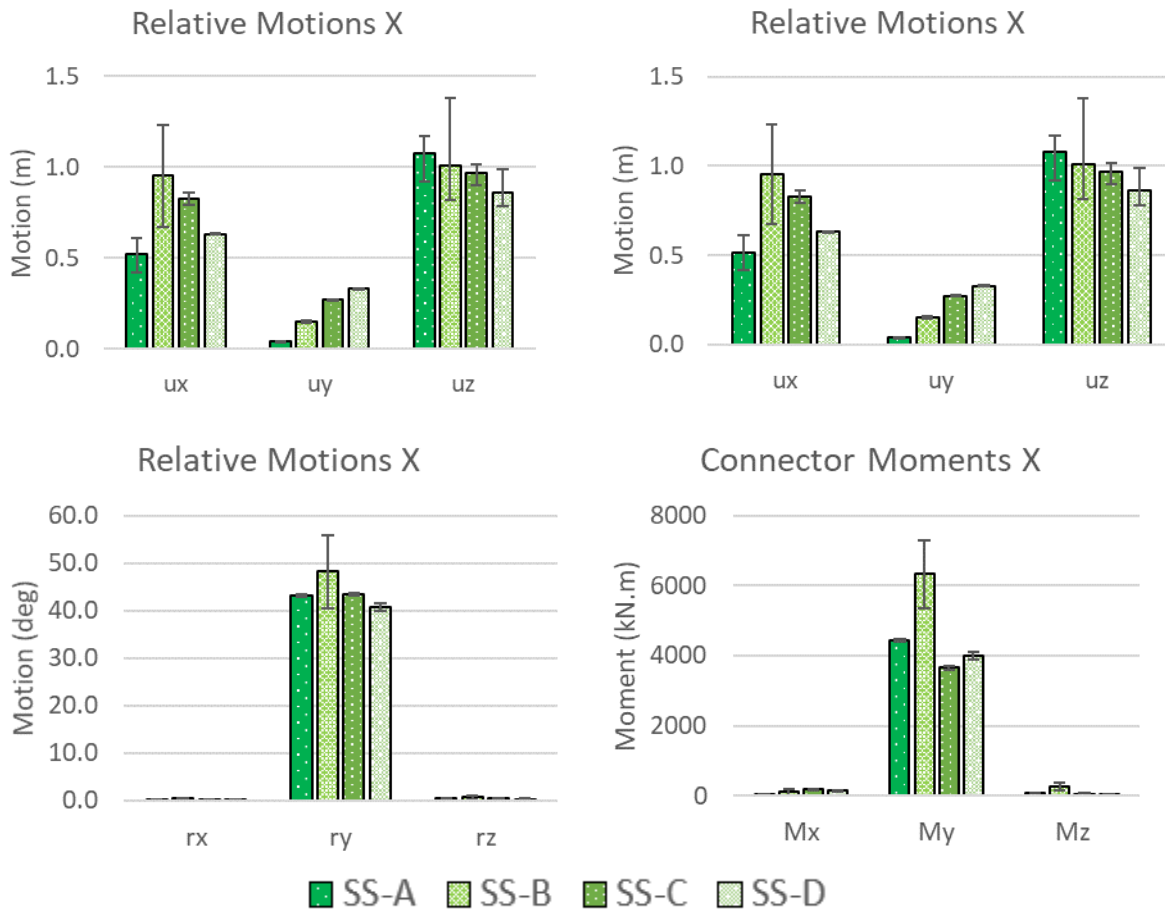


Figure 41, Relative motions in X (see Figure 40) and connector forces and moments with average of significant values. Results presented for SS-A, SS-B, SS-C, and SS-D with the wave heading 180 degrees. Error bars show the maximum and minimums.

6.2.3. Effect of Connector Stiffness

Another study was performed to determine the effect of connector stiffness on floater motions and connector loads in a grid structure. The stiffness is varied individually per DOF in vertical shear (translation) and vertical bending (hinge-type rotation). Table 14 and Table 15 show the relative motions and connector loads in SS-B (Hs 4.5m Tp 6.3sec) and the standard deviation of the soft, medium and stiff connector cases. The full results are shown in Appendix A. Modifying the stiffness per DOF allows the importance of each individual DOF to be identified more easily.

The case where the vertical stiffness is modified has a larger difference in the floater motions compared to changing the bending stiffness. The trend is the opposite when comparing for connector loads where the vertical bending has a much larger effect. There doesn't seem to be a large impact on the variation in the results (i.e., how different the floater motions or connector loads would be) as this is more affected by the value of the stiffness.

Table 14, Average of significant relative floater **motions** and standard deviations for three connector stiffness configurations when varying vertical bending and vertical shear stiffness individually. Results in all DOF for SS-B (Hs 4.5m, Tp 6.3sec).

Stiffness DOF Varied		Surge (m)	Sway (m)	Heave (m)	Roll (deg)	Pitch (deg)	Yaw (deg)
Vertical Bending	Average	4.3	4.0	2.2	15.1	44.0	1.5
	Std Dev	0.1	0.1	0.1	4.7	4.4	0.2
Vertical Shear	Average	4.5	4.2	2.1	12.5	40.1	1.3
	Std Dev	0.6	0.5	0.1	0.4	0.8	0.0

Table 15, Average of significant **forces and moments** and standard deviations for three connector stiffness configurations when varying vertical bending and vertical shear stiffness individually. Results in all DOF for SS-B (Hs 4.5m, Tp 6.3sec).

Stiffness DOF Varied		Fx (kN)	Fy (kN)	Fz (kN)	Mx (kN.m)	My (kN.m)	Mz (kN.m)
Vertical Bending	Average	3048	786	3240	359	6392	380
	Std Dev	853	330	834	88	2848	115
Vertical Shear	Average	2186	529	2515	297	5111	270
	Std Dev	122	35	75	101	442	10

6.2.4. Grid Distribution of Loading

The distribution of the loading on the connectors for the grid structure is discussed in this Section. The maximum connector forces and moments are initially presented in Table 16. Then, the connector forces and moments are shown on the grid model relative to the maximum load in SS-B (Hs 4.5m, Tp 6.3sec). The oblique sea case is shown in Figure 42 and the head sea case in Figure 43. A visual representation of the response is also shown in Figure 44 and Figure 45.

Table 16, Maximum connector loads for wave headings 150 and 180 degrees in SS-B (Hs 4.5m, Tp 6.3 sec).

Wave	Fx (kN)	Fy (kN)	Fz (kN)	Mx (kN.m)	My (kN.m)	Mz (kN.m)
150	2738	571	3522	407	5640	474
180	1554	1093	2268	494	7319	601

The forces and moments for both wave headings are greater in Fx, Fz, and My compared to the other DOFs. The force in the axial direction (Fx) is large due to the being the main translational restraint in the direction of the wave train. The vertical shear (Fz) force is usually large because it is coupled to the vertical bending moment (My). The force (Fy) becomes much greater for head seas because then there is an interaction between the outer and inner rows of floaters. In oblique seas the value of Fy is unevenly distributed across the structure because the floaters behave more individually compared to head seas where they move in rows.

In oblique seas the forces and moment distribution does not follow an obvious trend. The vertical moments (My) are much larger for the X-facing connectors compared to the Y-facing connectors. Conversely, the moments (Mz) are much higher for Y-facing connectors. For the other forces and moments, there is a more random distribution across the grid. The vertical forces (Fz) along the outer edge of the structure are generally (not always) greater than internal and at the side facing away from the incoming wave.

The distribution of connector forces and moments on the structure in head seas follows more of a consistent pattern. Generally the X-facing connectors have greater loads in F_x , F_z , and M_y while the Y-facing connectors have greater loads in F_y , M_x , and M_z . The loads are fairly symmetrical about the x-axis. For F_y , M_x , and M_z the connectors in the centre of the structure are much higher because they restrain rows of outer floaters which have greater motions. For the same reason but this time to restrain the translation in the axial direction, the outer connectors have higher axial forces (F_x). The force F_z is generally higher on one side of the floated compared to the other which is caused by uneven rotation (pitch or roll).

The vertical bending moment (M_y) is distributed evenly for both head and oblique seas. The X-facing connectors have much greater bending moments than the Y-facing connectors which makes sense considering they are perpendicular to the main direction of the wave train. The Y-facing connectors have a vertical bending moment approximately 80% lower than the X-facing connectors. In oblique seas, the connectors adjacent to the corner floater aft of the incoming waves (i.e., floater 1) experiences the maximum bending moment while the forward corner (i.e., floater 9) experiences the minimum.

The distribution of the connector loads is complex because of fluid structure interaction. The shielding that the nearby floaters might provide is negated by the dynamics of the connectors. The velocity potentials from the radiated and incident wave forces interact with the structure in such a way that causes resonance. The gaps between the floaters also increase the magnitude of the wave forces. These interacting excitation forces result in an uneven distribution of connector forces and moments across the structure. The bending moments (M_y) for the X-facing and Y-facing connectors might not be equal but bending across two axes causes some high loads that are undesirable.

When considering the design of connectors the distribution of loads can provide insights for raising or lowering stiffnesses across the structure or for certain DOFs. The moments M_x and M_y are the most obvious choice because there is a large variation in these moments and also a clear difference between the X- and Y-facing connectors. The X-facing connectors could reduce in stiffness k_y while increase in stiffness in k_x . This would result in a more even distribution of these moments. This is not as simple in other DOF but generally, the central floater stiffness could be decreased in k_y , k_z which would reduce these loads by providing more flexibility.

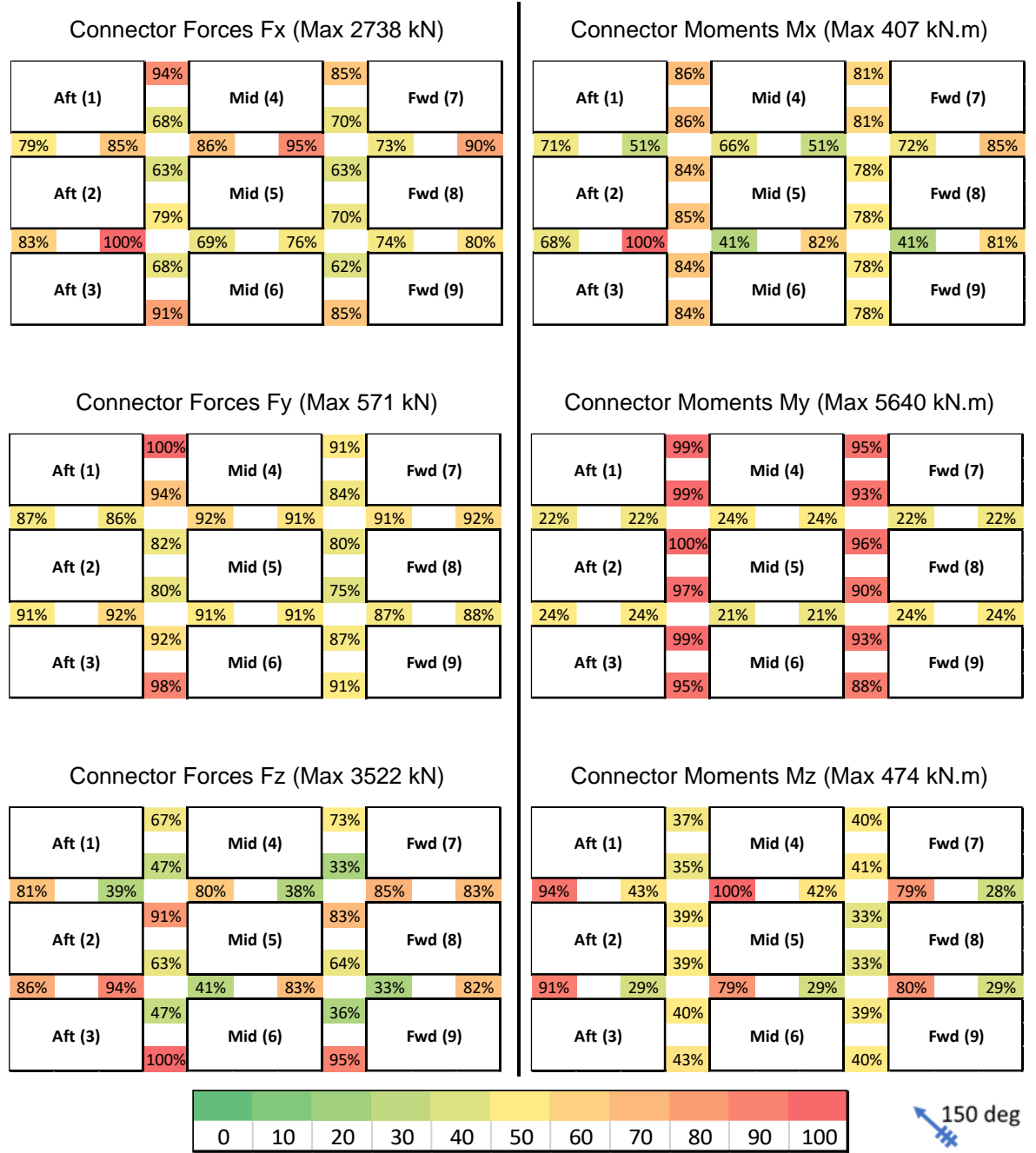


Figure 42, Distribution of connector forces and moments for SS-B for wave heading 150 degrees. Results relative to the maximum force or moment in the structure. Percentage of maximum load shown in color scale below. Arrow shows wave direction (bottom right).

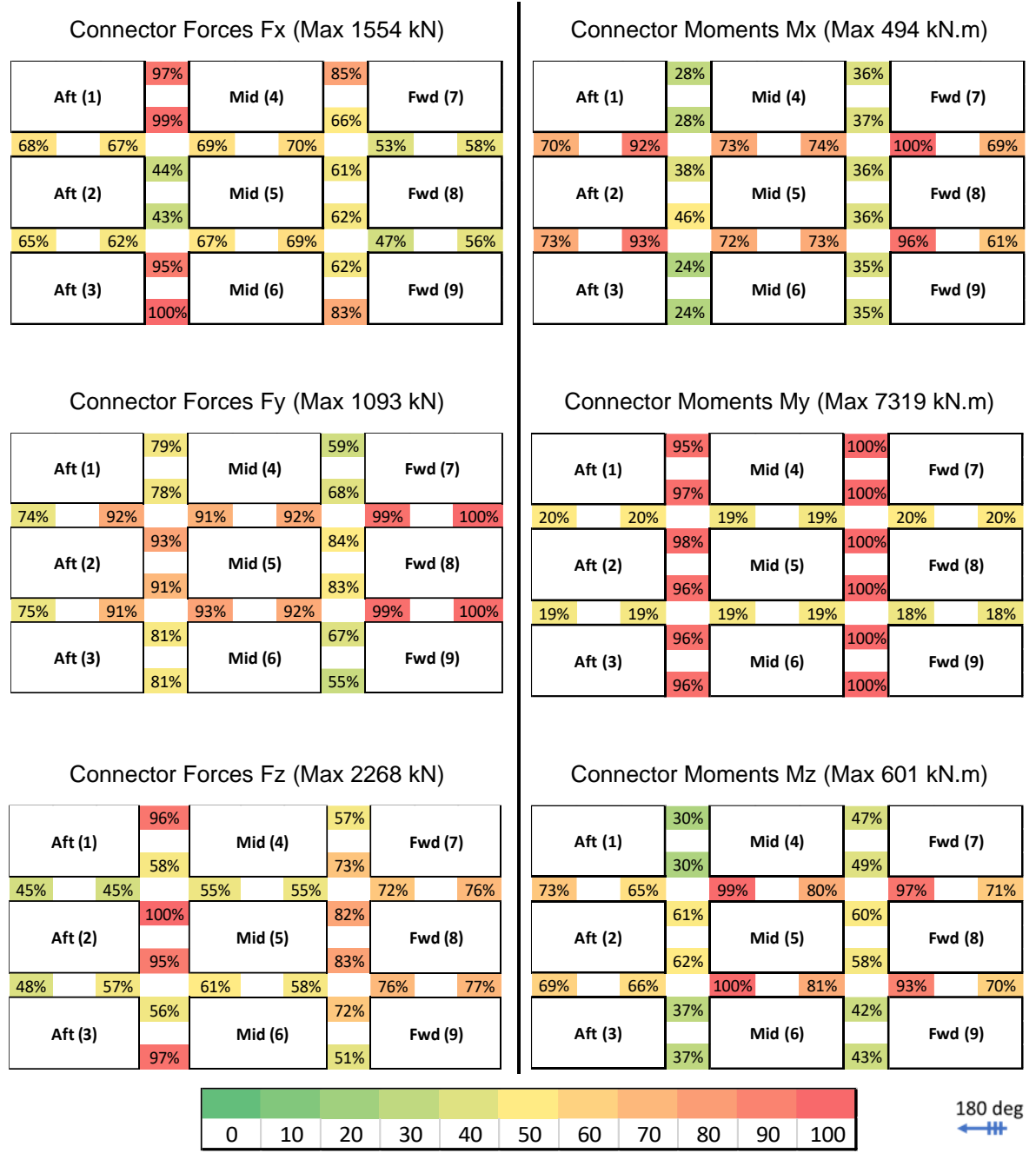


Figure 43, Distribution of connector forces and moments for SS-B for wave heading 180 degrees. Results relative to the maximum force or moment in the structure. Percentage of maximum load shown in color scale below. Arrow shows wave direction (bottom right).

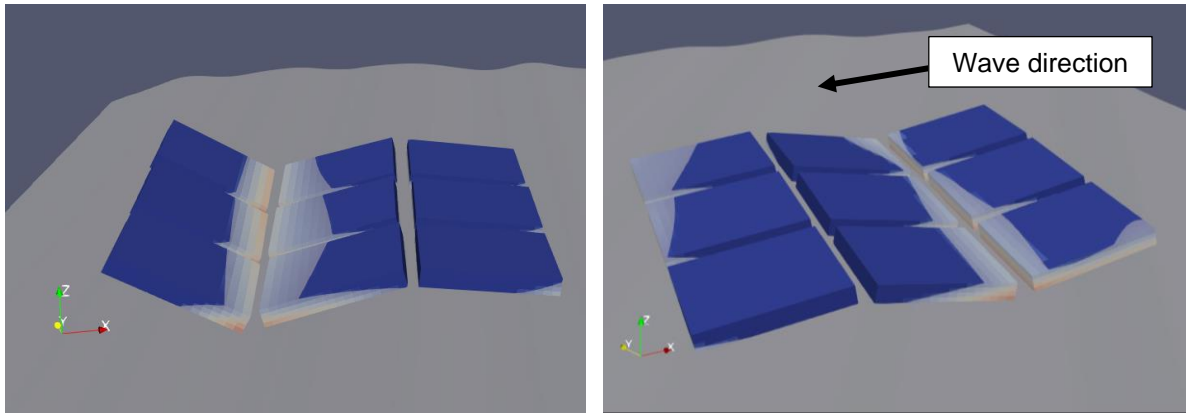


Figure 44, Motions in SS-C with wave heading 180 degrees. Grid model with med connector stiffness.

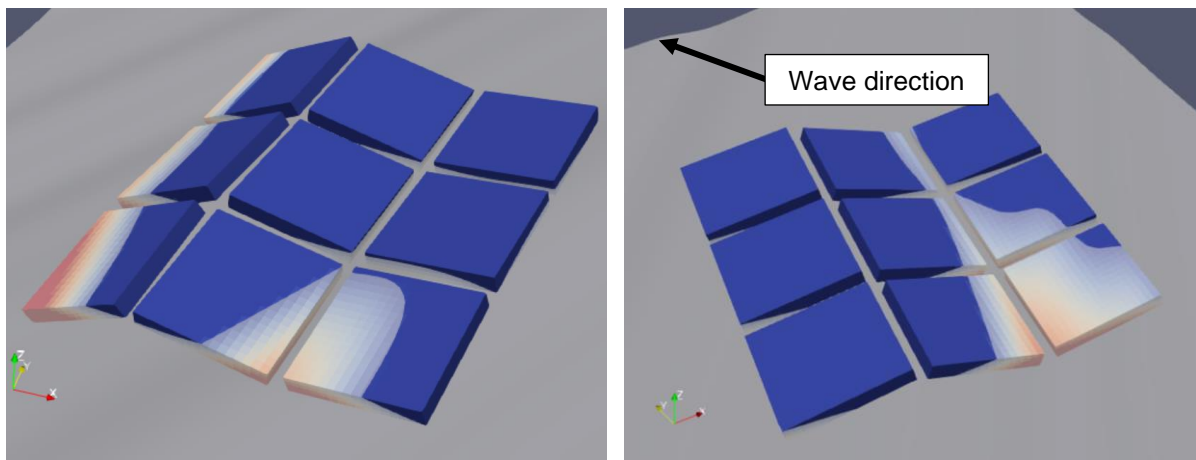


Figure 45, Motions in SS-C for wave heading 150 degrees. Grid model with med connector stiffness.

6.2.5. Grid Frequency Response Functions

Pitch frequency response functions for the grid structure are presented in Figure 46. The magnitude and natural frequencies of the grid shift when comparing a single rigid body, a grid of free floaters, and two cases of connectors (soft and stiff with the rod diameter equal to 180mm and 300mm respectively). The average motion is shown and the shaded areas represent the minimum and maximum of the individual floaters.

The results follow a similar trend to the three floater pitch response (Figure 39) where the single large floater has a higher motion and lower natural frequency. As the stiffness increases, the natural frequency reduces and the magnitude of motion increases. When the connector becomes stiffer the response is more similar to the single rigid floater rather than the case with soft connectors.

The variation in the results for individual floaters is smaller compared to when there are connectors. For the individual case, at the natural frequency there is a variability of 7% whereas the stiff and soft connector case this is 17% and 21% (respectively). There are also larger changes between the floaters when the motion is close to the natural frequency. Increasing the stiffness of connectors makes structure behave like a single structure which decreases the natural frequency. There is a fluid structure interaction which has a dynamic amplification at certain wave frequencies.

Response Function Pitch

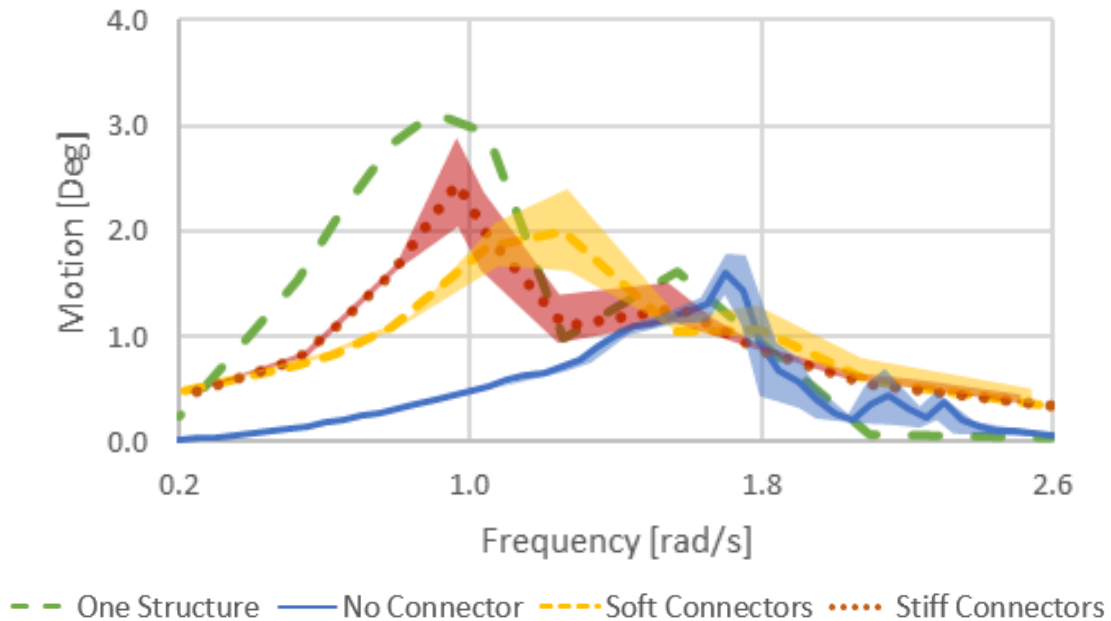


Figure 46, Pitch motion response calculated in regular 1m wave height head waves for the grid model (average shown where applicable) with one continuous structure (long dashed line), no connectors (solid line), soft connectors (short dashed line), and stiff connectors (dotted line). Shaded zones represent the minimum and maximum values.

The forces and moments of the connectors also have a frequency response which has been plotted in Figure 47 for the axial (F_x) and vertical shear (F_z) forces and vertical bending moment (M_y). The results are shown for head seas in 1m wave height regular waves. The stiff connector has a larger response at frequencies closer to resonance. The bending moment has a distinct resonant peak whereas the forces F_x and F_z both have more of a flattened peaks meaning that the response is inertia driven over more wave frequencies.

Similar to the pitch response plot, there is a shift to a higher resonant frequency when the stiffness of the connector decreases. However, the connector vertical bending response has a higher natural frequency than the pitch motion response. The difference in the location of the peak motion to the connector bending moment shows that the floater motion is only partially influenced by the connector natural frequency. The comparison of response plots show there is an interdependence between the connector stiffness and floater response and connector loads.

The connector frequency response is important because the connectors can experience their own resonance due to structural excitation. The connector forces and moments at resonance will be higher. The connectors have a higher natural frequency than the pitch bending frequency response. This is beneficial to the design because if the pitch motion and the connectors resonate at the same frequency this would cause even larger connector loads.



Figure 47, Frequency response functions for averaged F_x , F_z , M_y at the connector of the grid model. Results shown for soft (dashed line) and stiff (dotted line) connector stiffness. Shaded zones represent the minimum and maximum values.

6.3. Case 3 – 4x4 Grid Model

6.3.1. Grid Distribution of Loads

The third case investigated investigates the connector response on a 4x4 grid model. The distribution of forces and moments has been analyzed for SS-B (Hs 4.5m, T_p 6.3sec). The maximum force or moment is shown for head and oblique seas in Table 17. Normalized connector loads are shown for oblique seas in Figure 42 and head seas in Figure 43.

Table 17, Maximum connector loads for wave headings 150 and 180 degrees in SS-B (Hs 4.5m, T_p 6.3 sec).

Wave	F_x (kN)	F_y (kN)	F_z (kN)	M_x (kN.m)	M_y (kN.m)	M_z (kN.m)
150	479	151	3481	396	1302	46
180	238	35	2258	24	2359	16

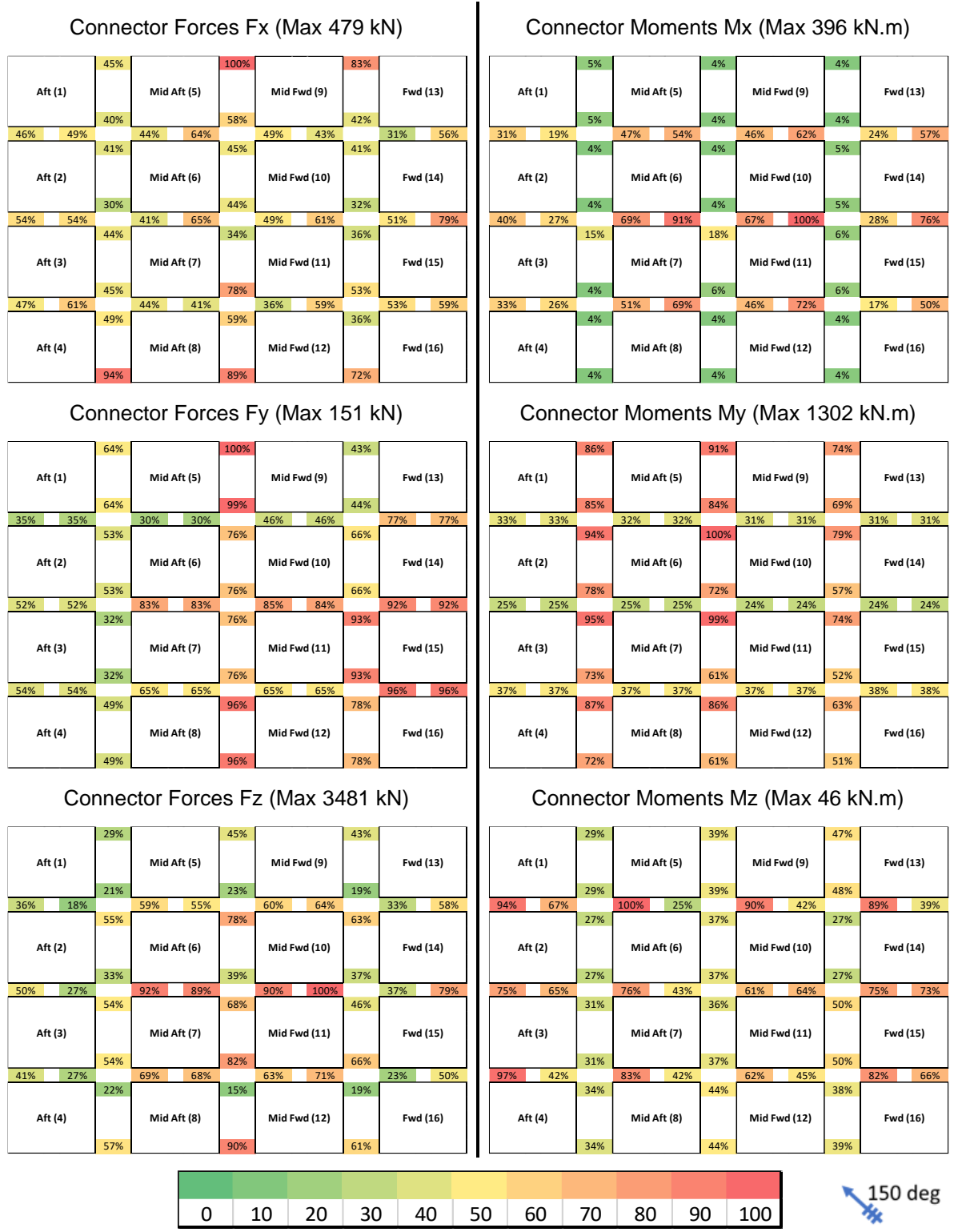


Figure 48, Distribution of connector forces and moments for SS-B for wave heading 150 degrees. Results relative to the maximum force or moment in the structure. Percentage of maximum load shown in color scale below. Arrow shows wave direction (bottom right).

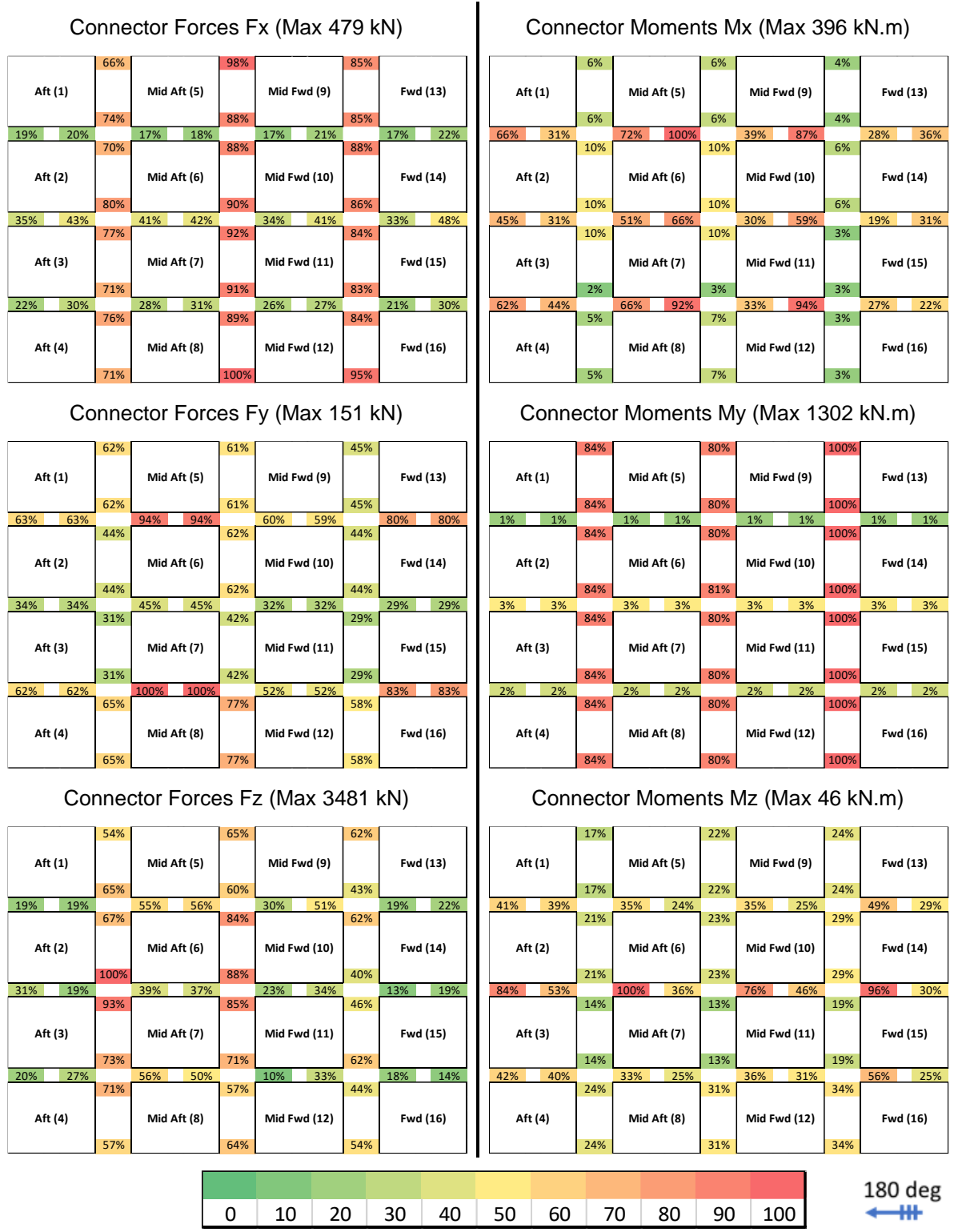


Figure 49, Distribution of connector forces and moments for SS-B for wave heading 180 degrees. Results relative to the maximum force or moment in the structure. Percentage of maximum load shown in color scale below. Arrow shows wave direction (bottom right).

The vertical shear force (F_z) and the bending moment (M_y) are both greater than other forces and moments. This differs from the 3x3 grid where the axial force (F_x) is much greater and comparable to F_z . When the grid size increases most of the connector loads decrease because the loads are more distributed through the structure. Additionally, there is more shielding from forward floaters which have larger motions as shown in Figure 50. The wavelength of a deep water wave with a period of 6.3 seconds is approximately 60m and the length of the grid is 66m. This explains the lower axial force for SS-B because the grid floats with the wave train.

The largest axial forces (F_x) are experienced at the sides of the structure in oblique seas. This occurs as the rigid floaters rotate in yaw but through symmetry the load is taken as axial force. In head seas the axial forces are more evenly distributed because the wave train is exactly perpendicular to the structure. There is a shielding effect from the forward floaters which generally experience larger forces than the aft floaters.

Similar to the 3x3 grid, F_z is greatest for the inner connectors which restrain the motion of the outer floaters compared to the inner floaters. The force distribution is varied for both the head and oblique sea cases. The larger F_z value at the aft side of the structure shows that the response is affected by dynamic amplification.

The distribution of moments in bending (M_y) is different to the 3x3 case because there is a shielding effect for the X-facing connectors. The aft connectors have 15-20% lower moments than the forward row in the head seas case. This shielding is less pronounced for the oblique seas. This is because in oblique loading other bending mode shapes become more significant to the response. For the 3x3 grid, the bending moments are all much more evenly distributed over the X- and Y-facing connectors showing that the interaction of the floaters and connectors is less than for the 4x4 grid.

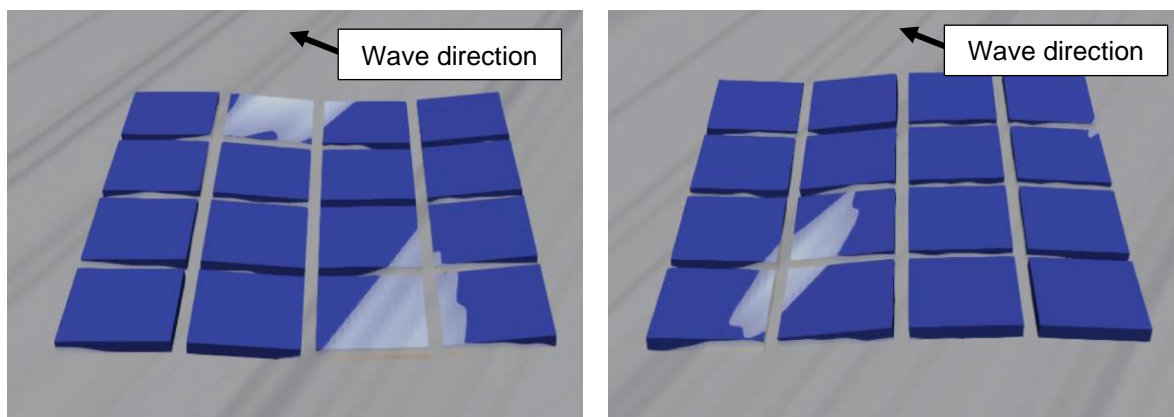


Figure 50, Grid model in oblique seas for SS-B (H_s 4.5m, T_p 6.3sec).

6.3.2. Grid Frequency Response Function

The frequency response in pitch is shown for SS-B (H_s 4.5, T_p 6.3) in Figure 51. There is a shift in the natural frequency towards the right compared to the 3x3 grid. The shaded area shows the minimum and maximum values. The maximum pitch motion occurs at approximately 1.3 rad/s with a magnitude of 2.5m for 1m regular waves. This frequency equals a wave period of 4.76 seconds which is similar to the wave peak period of SS-B showing that the floaters are in resonance. There are some floaters which experience quite a small motion even at the resonant frequency.

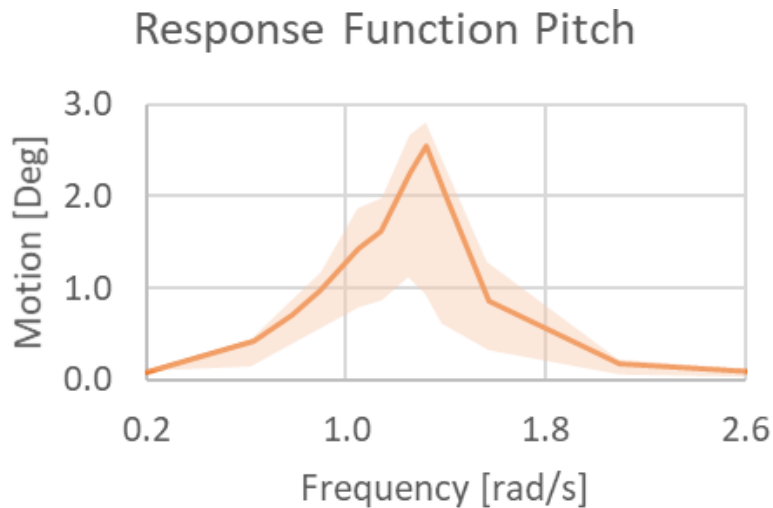


Figure 51, Frequency response function for vertical bending for medium stiffness connectors in SS-B (Hs 4.5m, Tp 6.3sec). Shaded zones represent the minimum and maximum values.

The connector frequency response functions are then shown for Fx, Fz and My in Figure 52. The response in Fx and Fz shows that there are two resonant peaks at approximately 1.1- and 1.3 rad/s. The maximum motion amplitude occurs at 1.3 rad/s for both DOFs. The response in My shows there is a single resonant peak at 1.3 rad/s. This frequency is the same as the resonant response in pitch motion from Figure 51.

The results of the connector frequency response functions show that the connectors are experiencing resonance at around the wave peak period of SS-B. This can explain why the connectors at the aft side of the structure still experience large loads even with the shielding effect of the other floaters.

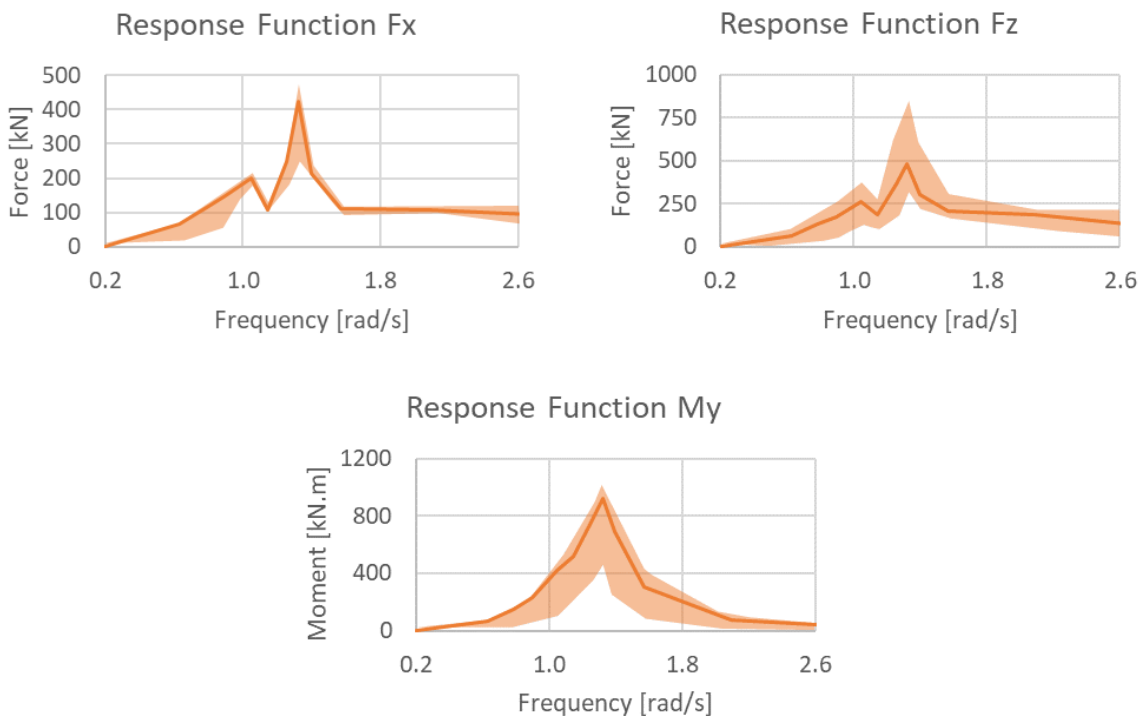


Figure 52, Frequency response functions for averaged Fx, Fz, My at the connector of the grid model with medium connector stiffness. Shaded zones show the minimum and maximum values.

6.4. Discussion of Assumptions

This Section discusses the implications of the assumptions made for the numerical model and how they might affect the results. The main assumptions that are discussed are use of potential flow, the deep water assumption, linearized connector stiffness, and number of connectors used in the model.

The hydrodynamic problem is solved using potential flow theory which ignores the viscous effects. This assumption could affect the results because the corners of a barge experience significant viscous damping due to the formation of vortices. The gap between the modules also can be affected by viscosity. These viscous effects are more prominent close to resonance. The motions are expected to be reduced compared to the results presented in this thesis. The use of damping models might provide more accuracy when predicting the magnitude of results but the trends are likely to be the same.

The deep water assumption means that the velocity potentials are able to disperse evenly away from the structure. It is likely that an OFPV might be deployed in shallow water. The Hollandse Kust Noord site has a water depth of 15-25m which is not deep [94]. In shallow water, the seabed causes the radiated waves to reflect back towards the floating body and affect the wave excitation forces on the structure. The added mass is usually reduced in shallow water because of the influence of the seabed and this can shift the natural frequency to higher than predicted. The viscosity from the sea-bed of underwater obstacles also effects the hydrodynamics. Finally, shallow water causes the waves to increase in height and velocity. Overall, these factors usually cause the structure to experience greater forces and motions.

The connector stiffness has been assumed to be linear which makes the computations simpler. However, there are cases where stiffness acts in only one direction which is the case with fenders. Alternatively, the connector might exhibit nonlinear stiffness properties such as for certain rubber or springs. These can be designed to become stiffer as the deformation or applied forces increase. The results of this Section show the potential for designing nonlinear or contact based connectors in areas of higher or lower loads. It is recommended that future work would investigate nonlinear connector stiffness or damping, or fenders which have stiffness in compression but not in tension. These cases would require the use of a time-domain analysis.

It has been assumed that there are only two connectors per side of the floaters. If more connectors would be used, then either the stiffness stays the same and then motions and loads will both decrease. The overall load transferred through the set of connectors will increase but the load for individual connectors decreases. The natural frequency will also increase as the structure would get stiffer. The other situation would be if the stiffness decreases but the number of connectors increases. This would result in the natural frequency being similar but then the connector loads would decrease while motions remain similar.

6.5. Practical OFPV Design

This Section discusses some practical design considerations that have arisen due to this thesis. The numerical model can be used to predict the motions of floaters and connector forces and moments. Therefore, design decisions for the OFPV structure can be made using this method, particularly for calculating motions and connector loads.

The results from this thesis are presented for a grid of 3x3 and 4x4 floaters but to be practical and cost effective the design of an OFPV should be much larger with a total footprint of roughly 200m² (or a grid of 15x15 floaters) [53]. The time domain approach is computationally expensive compared to a frequency domain analysis. However, the time domain is required to accurately predict the connector forces and moments in the OFPV because of the nonlinear behaviour due to large deformations and the multi-body interaction. These nonlinearities are captured by solving the Froude-Krylov and wave incident forces directly. Also, the nonlinear connector stiffness which is recommended for future implementation requires the time domain to solve.

The distribution of loads allows the designer to understand which connectors could become more or less stiff. The forward floaters experience the largest loads because there is a shielding effect for the larger (4x4) grid model. The central floaters experience the larger F_z forces while the connectors on the edge of the structure experience greater F_x forces. The connector stiffness in k_z can be reduced in the centre of the structure which would allow more floater movement but lower forces.

The trade-off between numerical accuracy and computational expense is a significant challenge when designing an OFPV. The results of this thesis show that the governing load would occur close to the natural excitation frequency of the structure. It is recommended that the maximum connector loads calculated at sea states with wave peak frequencies close to the natural frequency. In particular the natural frequency in bending appears to dominate the response. However, to obtain the ultimate predicted strength requires solving each possible sea state in a given wave scatter diagram.

A practical solution to reducing the time taken for running analyses for OFPV structures is to solve the boundary value problem to obtain the connector and floater response functions in the frequency domain. The high frequency responses which are required to calculate the impulse functions of the radiation potentials use a fine mesh. In the time domain, the mesh size doesn't need to be so fine so can become larger hence, speeding up the solve times. The time domain simulations are used to calculate the floater motions and connector loads at critical sea states. The calculations should also be performed in the time-domain to optimise the connector stiffness and damping.

7. Conclusions and Recommendations

7.1. Conclusions

This thesis expands on an existing numerical model that was developed by Tuitman [2]. The determination of connector responses in multi-body OFPV structures is the main contribution of this work. The hydrodynamic problem is solved in the frequency domain using a 3D-BEM to determine frequency dependent coefficients before converting to the time domain and solving a multi-body equation of motion. The floaters are connected using linear beam elements which are compliant in all degrees of freedom. After the model has been verified and validated, three case studies, a three floater serially connected structure, a 3x3 grid and 4x4 grid connected structure are used to explore the influence of various factors on the OFPV response. The research sub-questions from Chapter 1 are shown.

A. How does wave direction and frequency affect the connector response for grid-like VLFS?

The floater motions and connector loads are investigated for various wave directions and frequencies. The first case with the serially connected structure shows that the vertical bending motion (pitch) gives the largest motions and connector loads and is the governing load for design. When considering the 3x3 grid, the oblique seas generally give higher loading than head sea for all DOFs apart from in vertical bending. The distribution of forces and moments across the grid structures are much more varied than for the serially connected structure. This is more prominent for oblique seas than head seas and is caused by the larger motion of the corner or outermost floaters. The connectors can also be in resonance which causes high loading throughout the structure. It is also shown that the resonant frequencies of the connectors and floaters are not always the same in the same DOF.

B. What is the connector response in irregular waves?

C. How does connector compliance affect the motions of a grid-like VLFS and what are forces and moments at the connectors?

Both case studies are performed in irregular waves which are based on ocean conditions in the Hollandse Kust Noord site in The Netherlands. Two sea states (SS-C and SS-D) are predicted maximum expected values for 10- and 100 year waves. The other two sea states (SS-A and SS-B) are based on peak periods close to the bending natural frequency of the structures from Case 1 and Case 2 respectively. The sea state with a peak frequency close to the natural frequency of the structure causes larger motions and connector loads even if the wave height might be lower. Structural dynamics clearly plays an important role in the response of an OFPV. The forces are greater in the outermost connectors compared to those on the insider of the structure.

D. How does connector stiffness and damping affect its loads and the motions of the floaters?

The connector stiffness affects both the motion response and the connector response. As the connectors increase in stiffness, the floater motions become larger but the

connector forces and moments decrease. An increase in the connector stiffness decreases the magnitude of motion and the natural frequency of the structure so that it behaves more like a single continuous structure rather than individual (free) floaters. The connectors also have their own natural frequency and this shifts towards a lower frequency when the stiffness increases. Therefore, connector stiffness is an important parameter when designing an OFPV system because it influences the frequency response of the connectors and the floaters.

The effect of damping was investigated for the three floater OFPV using a linear spring mass damper model. The floater motions and the forces and moments in the connectors reduce because of damping but only close to the natural frequency of the structure where the inertia terms dominate the response. As the peak frequency of the sea state moves away from the natural frequency the damping has a negligible effect. Increasing damping reduces the floater motions and also the connector loads.

E. How does the distribution of connector forces and moments vary from a 3x3 to a 4x4 grid?

The 3x3 grid was expanded to a 4x4 grid with floaters and connector with the same properties. The results showed that the larger grid reduced the connector loads because the structure behaved more flexibly because of the compliance in the connectors. In the larger grid, the floaters are still bending in two directions but now there is more of a shielding effect from some floaters which reduces the loads. The 4x4 grid experiences much lower axial forces (F_x) relative to the other forces compared to the 3x3 grid but similar in the other DOFs.

7.2. Recommendations

This numerical method has been used to determine the structural response of a multibody VLFS in offshore conditions. There is a real lack of research in this area meanwhile, small pilot OFPV projects are being realized across the world. Over the course of this thesis there are lessons learnt which can be passed on to aid further research in this field.

The grid structure of an OFPV should have many smaller interconnected floaters with soft connectors. The smaller floaters are shown to have a higher natural frequency which shifts the resonant response away from the peak period of the sea states in consideration. Having softer connectors has the same effect because the grid structure starts behaving more like free floating modules rather than one large rigid structure.

There should be experimental work performed which serves to validate future numerical models. During this thesis validation has been conducted using an experimental test case of a serially connected structure and also comparing results with another numerical 3x3 grid model. However, future OFPV systems will almost certainly contain many more floating modules and experimentation will be crucial to validating the results. Additionally, the connector models need further validation especially in such a large interconnected structure.

This thesis has outlined that a time domain simulation takes significant time and that solving every case in a wave scatter diagram for a very large structure might be unrealistic. The results from the parametric studies already show that the response functions already give a lot of insight into the VLFS design. The natural frequencies should first be calculated and then results can be obtained for the most critical load-cases using the time domain simulation which is more accurate and sometimes necessary when calculating forces and moments. The connector stiffness should be included in the frequency solution so that mode shapes and connector response functions can be calculated more easily.

Further improvements to this method would be to introduce nonlinear stiffness to the connector model. This would require obtaining the nonlinear curves by experimentation. Alternatively, the fender type design has a stiffness in compression but not tension. These cases require the equation of motion to be solved in the time-domain to capture the displacement varying response. Additionally, it is recommended that further research is performed to improve the understanding of damping on grid connected OFPVs because this could result in a reduction of both the highest floater motions and connector loads.

The floaters are assumed to act like rigid bodies because the connector stiffness is significantly lower. In this regard some OFPV concepts exhibit high floater flexibility [11] while others assume high floater stiffness [86] so this is situation dependent. There should be a sensitivity study with flexible floater to determine up until which stiffness ratio with the connectors is the rigid body assumption still valid.

There should also be more research into the mooring design. The mooring arrangement has not been the focus of this thesis however, this will have a significant impact on the design loads and motions. The mooring stiffness has been assumed to be linear and no damping was applied. However, the actual mooring arrangement are likely to have nonlinear stiffness and some line damping. These influences on the OPFV responses should be further investigated.

A larger grid model should be investigated which has the same sized but more floaters (e.g., a grid size of 15x15). Both of the grid model test cases have demonstrated that the floater motions and connector loads can be obtained. Connector resonance was recorded for certain wave headings and sea states. Further expanding the grid will reveal additional mode shapes and potentially critical natural frequencies. The shape and design of the floater might also lead to some interesting results. This thesis has assumed a simple box shape but with companies like SolarDuck pursuing triangular shaped semi-submersible structures, these should be publicly investigated further.

Bibliography

- [1] Novacavi, "Prototype for an innovative floating solar power plant system," 2020. [Online]. Available: <https://www.novacavi.it/prototype-for-innovative-floating-solar-power-plant-system/>.
- [2] J. T. Tuitman, "Hydro-elastic response of ship structures to slamming induced whipping," [PhD Doctoral dissertation, Delft University of Technology], Delft, The Netherlands, 2010.
- [3] United Nations - Framework Convention on Climate Change, "Report of the Conference of the Parties serving as the meeting of the Parties to the Paris Agreement on its third session, held in Glasgow from 31 October to 13 November 2021," Glasgow, UK, 2022.
- [4] X. Che, D. Wang, M. Wang and Y. Xu, "Two-dimensional hydroelastic analysis of very large floating structures," *Journal of Marine Technology*, vol. 29, no. 1, pp. 13-24, 1992.
- [5] M. Lamas-Pardo, G. Iglesias and L. Carral, "A review of very large floating structures (VLFS) for coastal and offshore uses," *Journal of Ocean Engineering*, vol. 109, pp. 677-690, 2015.
- [6] C. M. Wang and Z. Y. Tay, "Very large floating structures: applications, research and development," in *The 12th East Asia-Pacific Conference on Structural Engineering and Construction*, Hong Kong, China, 2011.
- [7] M. Fousert, "Floating breakwater theoretical study of a dynamic wave attenuating system," [PhD Doctoral dissertation, Delft University of Technology], 2006.
- [8] A. Hikai and H. Omori, "On the prediction of the flow and water quality change due to a mega-float installation," in *22nd Meeting of the US-Japan Marine Facilities Panel*, Washington, USA, 1998.
- [9] F. Remy, M. B and A. Ledoux, "Experimental and numerical study of the wave response of a flexible barge," in *4th International Conference on Hydroelasticity in Marine Technology*, Wuxi, China, 2006.
- [10] C. Michailides, E. Loukogeorgaki and D. C. Angelides, "Response analysis and optimum configuration of a modular floating structure with flexible connectors," *Journal of Applied Ocean Research*, vol. 43, pp. 112-130, 2013.
- [11] S. Schreier and G. Jacobi, "Measuring hydroelastic deformation of very flexible floating structures," in *2nd World Conference on Floating Solutions*, Rotterdam, Netherlands, 2019.
- [12] H. R. Riggs and R. C. Ertekin, "Hydroelastic response of very large floating structures," in *International Conference on Offshore Mechanics and Arctic Engineering*, Stavanger, Norway, 1991.
- [13] J. N. Newman, "Wave effects on deformable bodies," *Journal of Applied Ocean Research*, vol. 16, pp. 47-59, 1994.
- [14] M. Kashiwagi, "A B-spline Galerkin scheme for calculating the hydroelastic response of a very large floating structure in waves," *Journal of Marine Science and Technology*, vol. 3, pp. 37-49, 1998.

- [15] R. E. D. Bishop and W. G. Price, "Hydroelasticity of ships," Cambridge University Press, 1979.
- [16] W. G. Price and Y. Wu, "Fluid structure interaction in multi-hull structures travelling in waves," in *International Symposium on the Practical Design of Ships*, Tokyo and Seoul, 1983.
- [17] R. E. D. Bishop, W. G. Price and Y. Wu, "A general linear hydroelastic theory of floating structures moving in a seaway," *Philosophical Transactions of the Royal Society of London*, vol. A316, pp. 375-426, 1986.
- [18] J. Ding, Y. Wu, Z. Xie, W. Yang, S. Wang, J. Yu and T. Yu, "Overview - Research on hydroelastic response of VLFS in complex environments," *Journal of Marine Structures*, vol. 78, pp. 328-340, 2021.
- [19] X. Che, R. H. Riggs and R. C. Ertekin, "Composite 2D-3D hydroelastic analysis method for floating structures," *Journal of Engineering Mechanics*, vol. 120, no. 7, pp. 1499-1520, 1994.
- [20] I. V. Struova, "Diffraction of shallow-water waves on a floating elastic platform," *Journal of Applied Mathematics and Mechanics*, vol. 64, pp. 1004-1012, 2000.
- [21] S. Wang, R. C. Ertekin, A. T. F. M. van Stiphou and P. G. P. Ferrier, "Hydroelastic response analysis of a box-like floating airport of a shallow draft," in *Offshore and Polar Engineering Conference*, The Hague, Netherlands, 1995.
- [22] W. Wei, S. Fu, T. Moan, C. Song and T. Ren, "A time-domain method for hydroelasticity of very large floating structures in inhomogeneous sea conditions," *Journal of Marine Structures*, vol. 57, pp. 180-192, 2018.
- [23] P. Mamidipudi and W. C. Webster, "The motions performance of a mat-like floating airport," in *Proceedings of the International Conference on Hydroelasticity in Marine Technology*, Trondheim, Norway, 1994.
- [24] M. Ohkusu and Y. Namba, "Hydroelastic analysis of a large floating structure," *Journal of Fluid and Structures*, vol. 19, pp. 543-555, 2004.
- [25] M. H. Meylan and V. A. Squire, "Response of circular ice floe to ocean waves," *Journal of Geophysical Research Atmospheres*, pp. 1-12, 1996.
- [26] R. Eatock Taylor and M. Ohkusu, "Green functions for hydroelastic analysis of vibrating free-free beams and plates," *Journal of Applied Ocean Research*, vol. 22, no. 5, pp. 295-314, 2000.
- [27] J. L. F. van Kessel, "Air-cushion supported mega-floaters," [PhD Doctoral dissertation, Delft University of Technology], Delft, The Netherlands, 2010.
- [28] D. Lu, S. Fu, X. Zhang, F. Guo and Y. Gao, "A method to estimate the hydroelastic behaviour of VLFS based on multi-rigid-body dynamics and beam bending," *Journal of Ship and Offshore Structures*, vol. 14, pp. 354-362, 2016.
- [29] X. Zhang and D. Lu, "An extension of a discrete-module-beam-bending-based hydroelasticity method for a flexible structure with complex geometric features," *Journal of Ocean Engineering*, vol. 163, pp. 22-28, 2018.
- [30] V. A. Squire, "Synergies between VLFS hydroelasticity and sea ice research," *Journal of Offshore and Polar Engineering*, vol. 18, no. 4, pp. 241-253, 2008.

- [31] M. H. Meylan, "The forced vibration of a thin plate floating on an infinite liquid," *Journal of Sound and Vibration*, vol. 205, no. 5, pp. 581-591, 1997.
- [32] M. H. Meylan, "The wave response of an ice floe of arbitrary geometry," *Journal of Geophysical Research Atmospheres*, vol. 107, no. C1, pp. 5.1-5.11, 2002.
- [33] E. Watanabe, T. Utsunomiya and S. Tanigaki, "A transient response analysis of a very large floating structure by finite element method," *Journal of Structural and Earthquake Engineering*, vol. 15, no. 2, pp. 155-163, 1998.
- [34] K. Kada, T. Fujita and K. Kitabayashi, "Stress analysis for structurally discontinuous parts in a mega-float structure," *Journal of Offshore and Polar Engineering*, vol. 12, no. 1, pp. 48-55, 2002.
- [35] M. Kashiwagi, "A time-domain mode-expansion method for calculating transient elastic responses of a pontoon-type VLFS," *Journal of Marine Science and Technology*, vol. 5, pp. 89-100, 2000.
- [36] W. J. Kim and R. C. Ertekin, "An eigenfunction-expansion method for predicting hydroelastic behavior of a shallow draft VLFS," in *2nd International Conference On Hydroelasticity in Marine Technology*, Fukuoka, Japan, 1998.
- [37] G. A. Athanassoulis and K. A. Belibassakis, "A consistent coupled-mode theory for the propagation of small amplitude water waves over variable bathymetry regions," *Journal of Fluid Mechanics*, vol. 389, pp. 275-301, 1999.
- [38] J. H. Kyoung, S. Y. Hong, B. W. Kim and S. K. Cho, "Hydroelastic response of a very large floating structure over a variable bottom topography," *Journal of Ocean Engineering*, vol. 32, pp. 2040-2052, 2005.
- [39] H. Abyn, J. Koto and A. Maimun, "Hydrodynamic interaction of floating structure in regular waves," *Jurnal Teknologi*, vol. 66, no. 2, pp. 91-96, 2014.
- [40] V. Kostikov, M. Hayatdavoodi and R. C. Ertekin, "Hydroelastic interaction of nonlinear waves with floating sheets," *Journal of Theoretical Computational Fluid Dynamics*, vol. 35, pp. 515-537, 2021.
- [41] M. Liu, R. Jin and Z. Cui, "Numerical modeling of fluid resonance in narrow gaps of fixed rectangular structures," *Advances in Mechanical Engineering*, vol. 11, no. 8, pp. 1-7, 2019.
- [42] K. Takagi and M. Nagayasu, "Hydroelastic behavior of a mat-type very large floating structure of arbitrary geometry," in *Proceedings of MTS/IEEE Conference and Exhibition Oceans*, Honolulu, USA, 2001.
- [43] T. Hamamoto and K. Fujita, "Wet-mode superposition for evaluating the hydroelastic response of floating structures with arbitrary shape," in *Proceedings of the 12th International Offshore and Polar Engineering Conference*, Kitakyshu, Japan, 2002.
- [44] K. Takagi, K. Shimada and T. Ikebuchi, "An anti-motion device for a very large floating structure," *Journal of Marine Structures*, vol. 13, pp. 421-436, 2000.
- [45] H. Ohta, T. Torii, N. Hayashi, E. Watanabe and T. Utsunomiya, "effect of attachment of a horizontal/vertical plate on the wave response of a VLFS," in *Proceedings of the 3rd International Workshop on VLFS*, Honolulu, USA, 1998.

- [46] Y. Cheng, G. J. Zhai and J. Ou, "Time-domain analysis and experimental analysis of hydroelastic response of a very large floating structure edged with a pair of submerged horizontal plates," *Journal of Marine Structures*, vol. 39, pp. 198-224, 2014.
- [47] T. I. Khabakhpasheva and A. A. Korobkin, "Hydroelastic behaviour of compound floating plate in waves," *Journal of Engineering Mathematics*, vol. 44, pp. 21-40, 2002.
- [48] B. W. Kim, J. H. Kyoung, S. Y. Hong and S. K. Cho, "Investigation of the effect of stiffness distribution and structure shape on hydroelastic responses of very large floating structures," in *Proceedings of the 15th International Offshore and Polar Engineering Conference*, Seoul, Korea, 2005.
- [49] T. Utsunomiya, E. Watanabe and R. Eatock Taylor, "Wave response analysis of a box-like VLFS close to a breakwater," in *International Conference on Offshore Mechanical and Arctic Engineering*, Lisbon, Portugal, 1998.
- [50] Z. Y. Tay, C. M. Wang and T. Utsunomiya, "Hydroelastic responses and interactions of floating fuel storage modules placed side-by-side with floating breakwaters," *Journal of Marine Structures*, vol. 22, pp. 633-658, 2009.
- [51] J. A. Pinkster, A. Fauzi, Y. Inoue and S. Tabeta, "The behaviour of large air cushion supported structures in waves," in *Proceedings of the 2nd International Conference on Hydroelasticity in Marine Technology*, Fukuoka, Japan, 1998.
- [52] R. P. Gao, C. M. Wang and C. G. Koh, "Reducing hydroelastic response of pontoon-type very large floating structures using flexible line connector and gill cells," *Journal of Engineering Structures*, vol. 52, pp. 372-383, 2013.
- [53] TNO, "Challenges and Potential For Offshore Solar," 2022.
- [54] N. Ren, C. Zhang, A. R. Magee, O. Hellan, J. Dai and K. K. Ang, "Hydrodynamic analysis of a modular multi-purpose floating structure system with different outermost connector types," *Journal of Ocean Engineering*, pp. 158-168, 2019.
- [55] J. Kerley, W. Eklund, R. Burkhardt and P. Rossoni, "Cable compliance, NASA technical paper 3216," NASA Goddard Space Flight Center, 1992.
- [56] M. S. Derstine and R. T. Brown, "A compliant connector concept for the mobile offshore base," *Journal of Marine Structures*, vol. 13, pp. 399-419, 2000.
- [57] H. Maeda, S. Maruyama and R. Inoue, "On the motions of a floating structure which consists of two or three blocks with rigid or pin joints," *Journal of Ocean Engineering*, vol. 17, pp. 91-98, 1979.
- [58] R. P. Gao, Z. Y. Tay, C. M. Wang and C. G. Koh, "Hydroelastic response of very large floating structures with a flexible line connection," *Journal of Ocean Engineering*, vol. 38, pp. 1957-1966, 2011.
- [59] R. C. Ertekin and H. R. Riggs, "Efficient methods for hydroelastic analysis of very large floating structures," *Journal of Ship Research*, vol. 37, no. 1, pp. 58-76, 1993.
- [60] Y. Wu, D. Wang, H. R. Riggs and R. C. Ertekin, "Composite singularity distribution method with application to hydroelasticity," *Journal of Marine Structures*, vol. 6, pp. 143-163, 1993.

- [61] H. R. Riggs, R. C. Ertekin and T. R. J. Mills, "A comparative study of RMFC and FEA models for the wave-induced response of a MOB," *Journal of Marine Structures*, vol. 13, pp. 217-232, 2000.
- [62] D. Xu, H. Zhang, S. Xia, C. Lu, E. Qi, C. Tian and Y. Wu, "Nonlinear dynamic characteristics of a multi-module floating airport with rigid-flexible connections," *Journal of Fluid Structures*, vol. 59, pp. 270-284, 2015.
- [63] Q. J. Shi, D. I. Xu, H. C. Zhang and Y. S. Wu, "Optimized stiffness combination of a flexible-base hinged connector for very large floating structures," *Journal of Marine Structures*, vol. 60, pp. 151-164, 2018.
- [64] J. Ding, C. Tian, Y. S. Wu, X. F. Wang, X. L. Liu and K. Zhang, "A simplified method to estimate the hydroelastic responses of VLFS in the inhomogeneous waves," *Journal of Ocean Engineering*, vol. 172, pp. 434-445, 2019.
- [65] R. Ding, D. L. Liu, H. C. Zhang, D. L. Xu, D. L. Shi, W. Y. Yang, W. P. Chen and Y. S. Wu, "Experimental investigation on characteristic change of a scale-extendable chain-type floating structure," *Journal of Ocean Engineering*, vol. 213, 2020.
- [66] J. N. Newman, "Wave effects on hinged bodies - Part I body motions, technical report," 1997a.
- [67] J. N. Newman, "Wave effects on hinged bodies - Part II hinge loads, technical report," 1997b.
- [68] J. N. Newman, "Wave effects on hinged bodies - Part III hinge loads vs. number of modules, technical report," 1998a.
- [69] H. Zhang, D. Xu, C. Lu, E. Qi, C. Tian and Y. Wu, "Connection effect on amplitude death stability of multi-module floating airport," *Journal of Ocean Engineering*, vol. 129, pp. 46-56, 2017.
- [70] Q. Shi, D. Xu, H. Zhang, H. Zhao, J. Ding and Y. Wu, "A face-contact connector for modularized floating structures," *Journal of Marine Structures*, vol. 82, 2022.
- [71] G. Rognaaas, J. Xu, S. Lindseth and F. Rosendahl, "Mobile offshore base concepts - Concrete hull and steel topsides," *Journal of Marine Structures*, vol. 14, pp. 5-23, 2001.
- [72] H. C. Zhang, D. L. Xu, S. Y. Xia, C. Lu, E. R. Qi, C. Tian and Y. S. Wu, "Nonlinear network modeling of multi-module floating structures with arbitrary flexible connections," *Journal of Fluids and Structures*, vol. 59, pp. 270-284, 2015.
- [73] H. R. Riggs and R. C. Ertekin, "Characteristics of the wave response of mobile offshore bases," in *18th International Conference on Offshore Mechanics and Artic Engineering*, St Johns, USA, 1999.
- [74] A. Karperaki, K. A. Belibassakis and P. Theodosios, "Time-domain, shallow-water hydroelastic analysis of VLFS elastically connected to the seabed," *Journal of Marine Structures*, vol. 48, 2016.
- [75] Y. Wang, S. Xu, X. Wang, L. Wang and L. Yang, "Effects of connector stiffness and damping on motion response of a multi-module VLFS," in *28th International Ocean and Polar Engineering Conference*, Sapporo, Japan, 2018.

- [76] J. N. Newman, "Wave effects on hinged bodies - Part IV vertical bending modes, technical report," 1998b.
- [77] B. W. Kim, S. Y. Hong, J. H. Kyoung and S. K. Cho, "Evaluation of bending moments and shear forces at unit connections of very large floating structures using hydroelastic and rigid body analysis," *Journal of Ocean Engineering*, vol. 34, pp. 1668-1679, 2007.
- [78] E. Loukogeorgaki, E. N. Lentsiou, M. Aksel and O. Yagci, "Experimental investigation of the hydroelastic and the structural response of a moored pontoon-type modular floating breakwater with flexible connectors," *Journal of Coastal Engineering*, vol. 121, pp. 240-254, 2017.
- [79] Q. Shi, H. Zhang and D. Xu, "Design of a flexible-base hinged connector for very large floating structures," in *Proceedings of the ASME 37th International Conference on Ocean, Offshore, and Arctic Engineering*, Madrid, Spain, 2018.
- [80] Y. Lu, H. Zhang, Y. Chen, Q. Shi and Y. Zhou, "A new type of connection with optimum stiffness configuration for very large floating platforms," *Journal of Engineering for the Maritime Environment*, pp. 1-15, 2021.
- [81] E. Loukogeorgaki, C. Michailides and D. C. Angelides, "Hydroelastic analysis of a flexible mat-shaped floating breakwater under oblique wave action," *Journal of Fluids and Structures*, vol. 31, pp. 103-124, 2012.
- [82] S. Fu, T. Moan, X. Chen and W. Cui, "Hydroelastic analysis of flexible floating interconnected structures," *Journal of Ocean Engineering*, vol. 34, pp. 1516-1531, 2007.
- [83] M. K. Ochi and S. B. Malakar, "Design forces for connecting elemental units of very large floating structure," University of Florida Coastal and Oceanographic Engineering Program, Florida, USA, 1993.
- [84] C. Michailides, E. Loukogeorgaki and D. C. Angelides, "Influence of connectors stiffness on the performance of flexible floating breakwaters," in *Proceedings of the 19th International Offshore and Polar Engineering Conference*, Osaka, Japan, 2009.
- [85] H. Zhao, D. Xu, H. Zhang, S. Xia, Q. Shi, R. Ding and Y. Wu, "An optimization method for stiffness configuration of flexible connectors for multi-modular floating systems," *Journal of Ocean Engineering*, vol. 181, pp. 134-144, 2019.
- [86] SolarDuck, "SolarDuck," 2021. [Online]. Available: <https://solarduck.tech/>.
- [87] "Fastener Engineering," [Online]. Available: <https://fastenerengineering.com/>. [Accessed January 2022].
- [88] B. J. Lazan, *Damping of materials and members in structural mechanics*, Oxford: Oxford Pergamon Press, 1968.
- [89] J. Woodhouse, "Linear damping models for structural vibration," *Journal of Sound and Vibration*, vol. 215, no. 3, pp. 547-569, 1998.
- [90] V. Bertram, *Practical Ship Hydromechanics*, Oxford: Butterworth-Heimann, 2012.
- [91] W. E. Cummins, "The Impulse Response Function and Ship Motions," Hydromechanics Laboratory Research and Development Report, 1962.

- [92] L. Eca and M. Hoekstra, "A procedure for the estimation of the numerical uncertainty of CFD calculations based on grid refinement studies," *Journal of Computational Physics*, vol. 262, pp. 104-130, 2014.
- [93] DNV, "DNV-RP-C205 - Environmental Conditions and Environmental Loads," 2014.
- [94] Fugro and Deltares, "Hollandse Kust (noord) Field Measurement Campaign," 2017.
- [95] I. Chowdhury and S. Dasgupta, "Computation of Rayleigh damping coefficients for large systems," *Journal of Geotechnical Engineering*, vol. 43, pp. 6855-6868, 2003.

Appendix A – Grid Model Results

The complete results of Case 2 for the 3x3 grid VLFS are presented in this Appendix. The first parametric study is presented first and shows the results for various sea states and wave headings of 150- and 180 degrees. Meanwhile, the second part shows the influence of individually varying the connector stiffness in heave and pitch for SS-B and SS-D with a wave heading of 150 degrees.

The results are presented by separating the floaters or connectors that are side by side (Y) and those forward and aft (X). This separation shown in Figure 53 is used to get a better impression of the distribution of floater motions or connector loads across the structure.

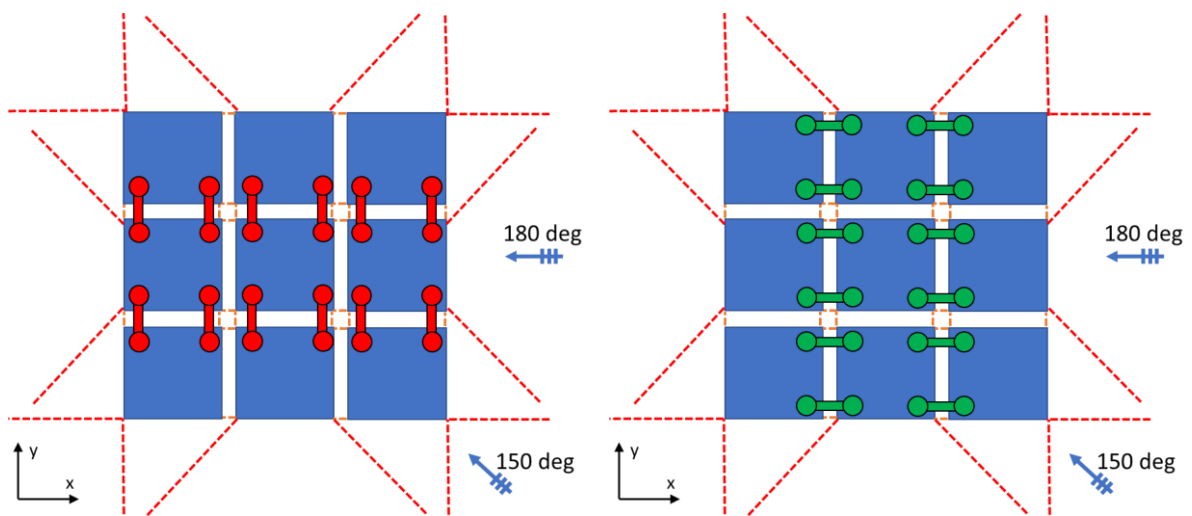


Figure 53, Grid model VLFS marking Y connectors (left) and X connectors (right). NOT TO SCALE.

Sea State and Wave Heading

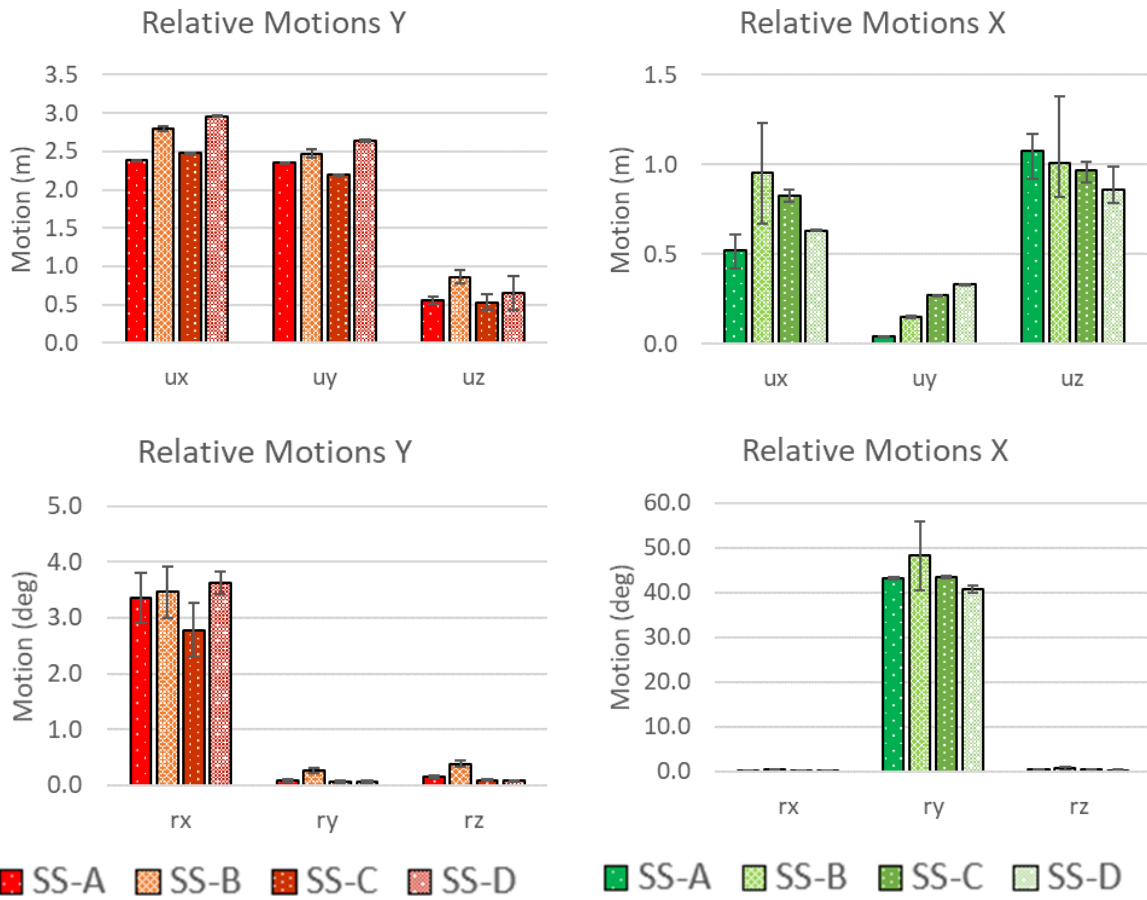
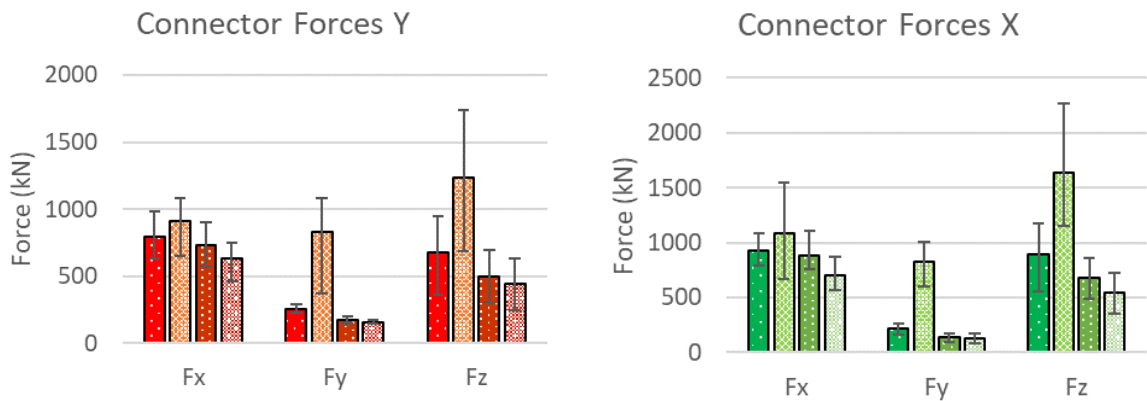


Figure 54, Significant motions relative to Y (left side) or X (right side) adjacent floaters. Wave heading is **180 degrees** and sea states A, B, C, and D are shown. Averaged values are shown for the X or Y relative floaters (see Figure 57) and error bars show the maximum and minimum relative motion.



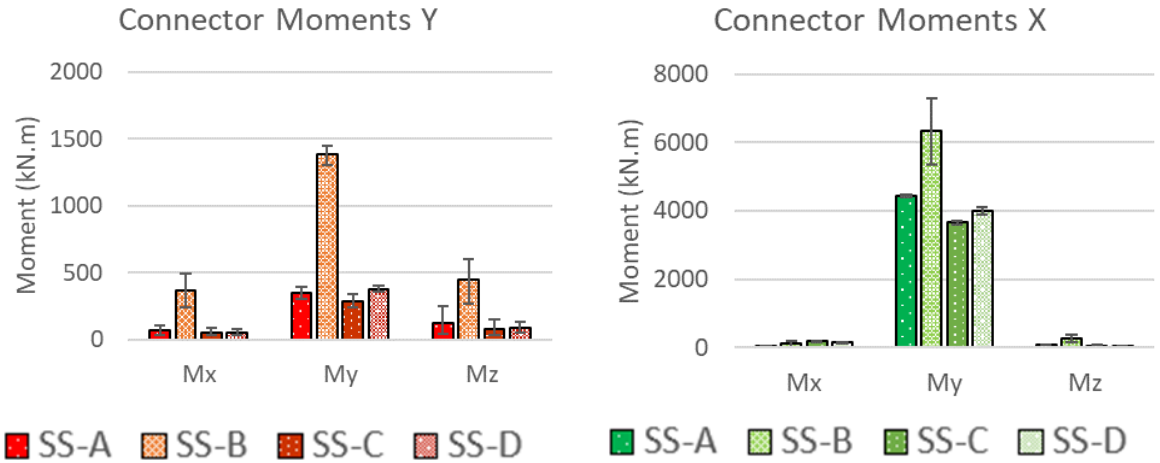


Figure 55, Significant connector forces or moments relative to Y (left side) or X (right side) adjacent floaters. Wave heading is **180 degrees** and sea states A, B, C, and D are shown. Averaged values are shown for the X or Y relative connectors (see Figure 57) and error bars show the maximum and minimum individual force or moment.

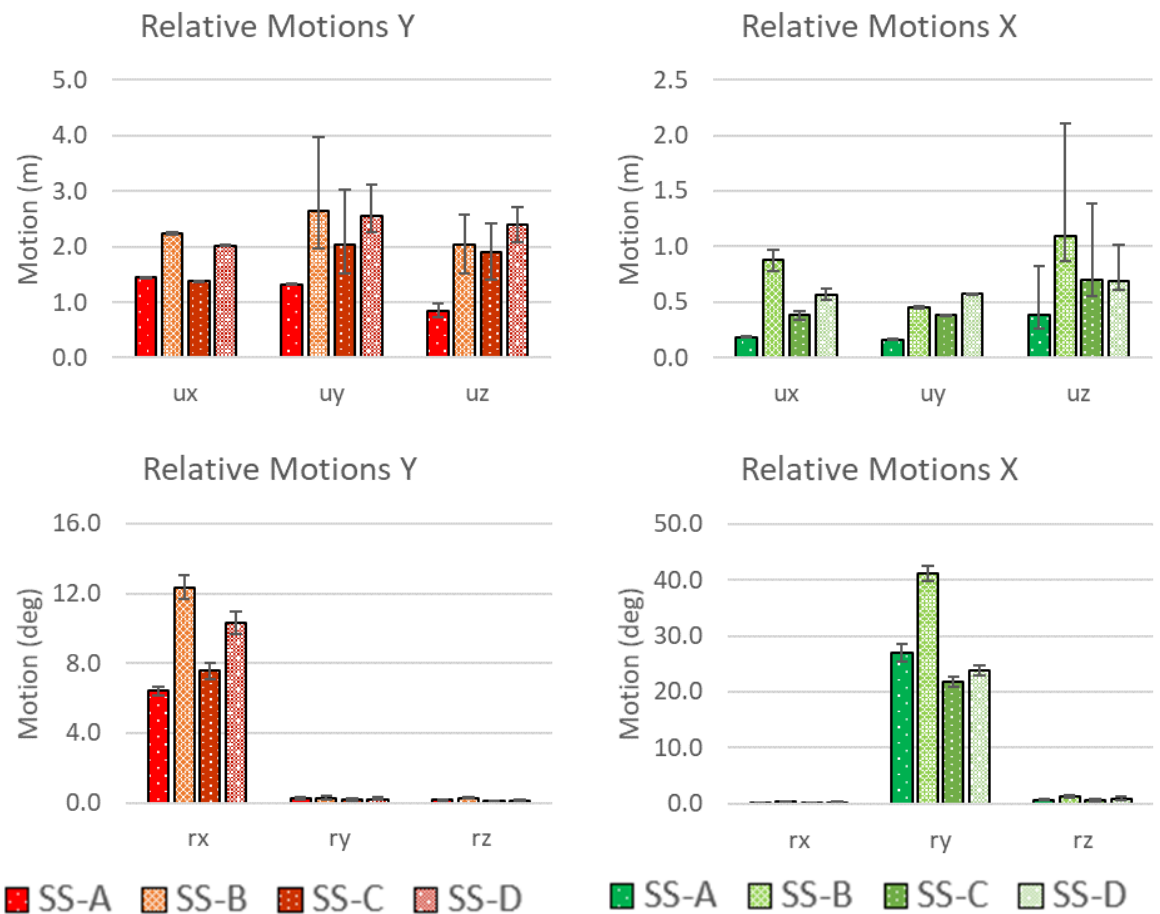


Figure 56, Significant motions relative to Y (left side) or X (right side) adjacent floaters. Wave heading is **150 degrees** and sea states A, B, C, and D are shown. Averaged values are shown for the X or Y relative floaters (see Figure 57) and error bars show the maximum and minimum relative motion.

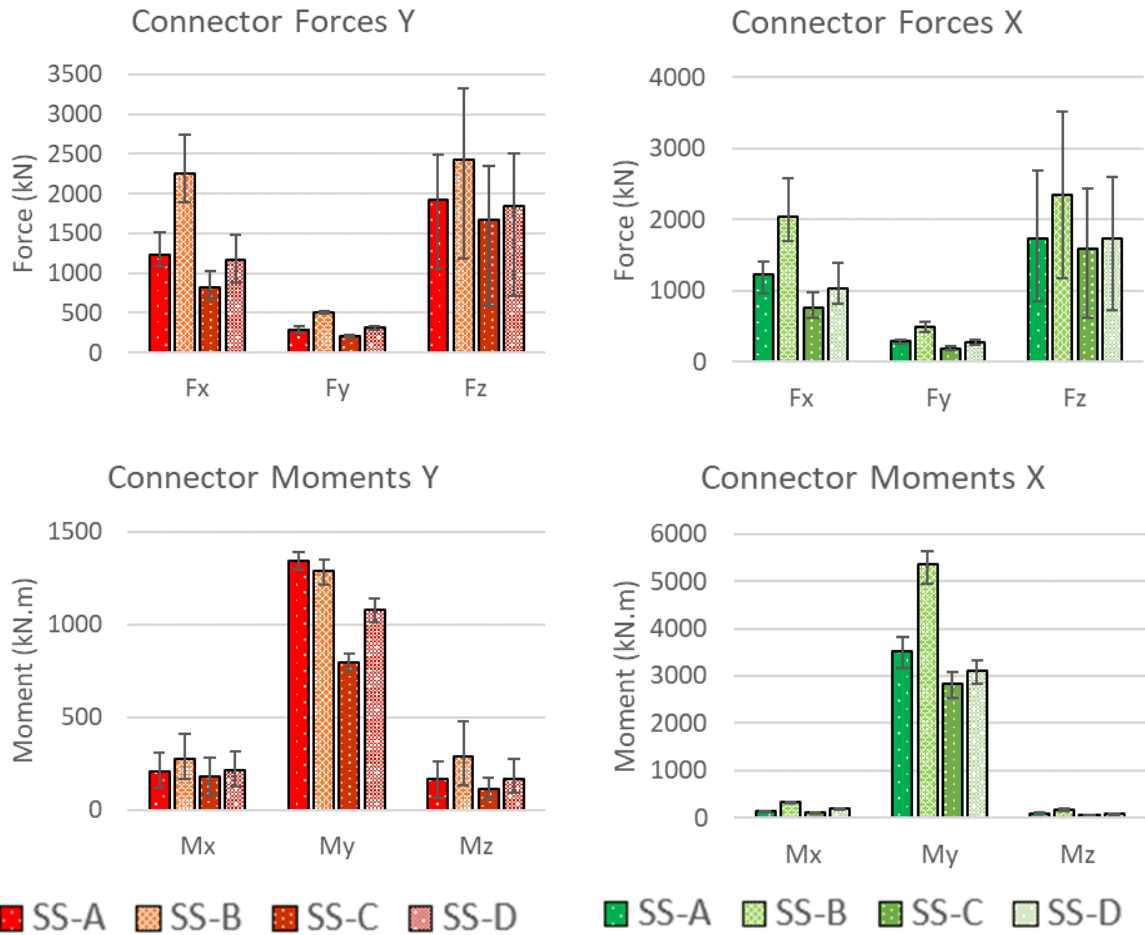


Figure 57, Significant connector forces or moments relative to Y (left side) or X (right side) adjacent floaters. Wave heading is **150 degrees** and sea states A, B, C, and D are shown. Averaged values are shown for the X or Y relative connectors (see Figure 57) and error bars show the maximum and minimum individual force or moment.

Varying Stiffness in Heave and Pitch

This Section presents the results of the parametric study on modifying the connector stiffness individually in either heave or pitch. The wave heading of 150 degrees is presented for SS-B (Hs 4.5m, Tp 6.3sec) and SS-D (Hs 7.6m, Tp 11.8sec).

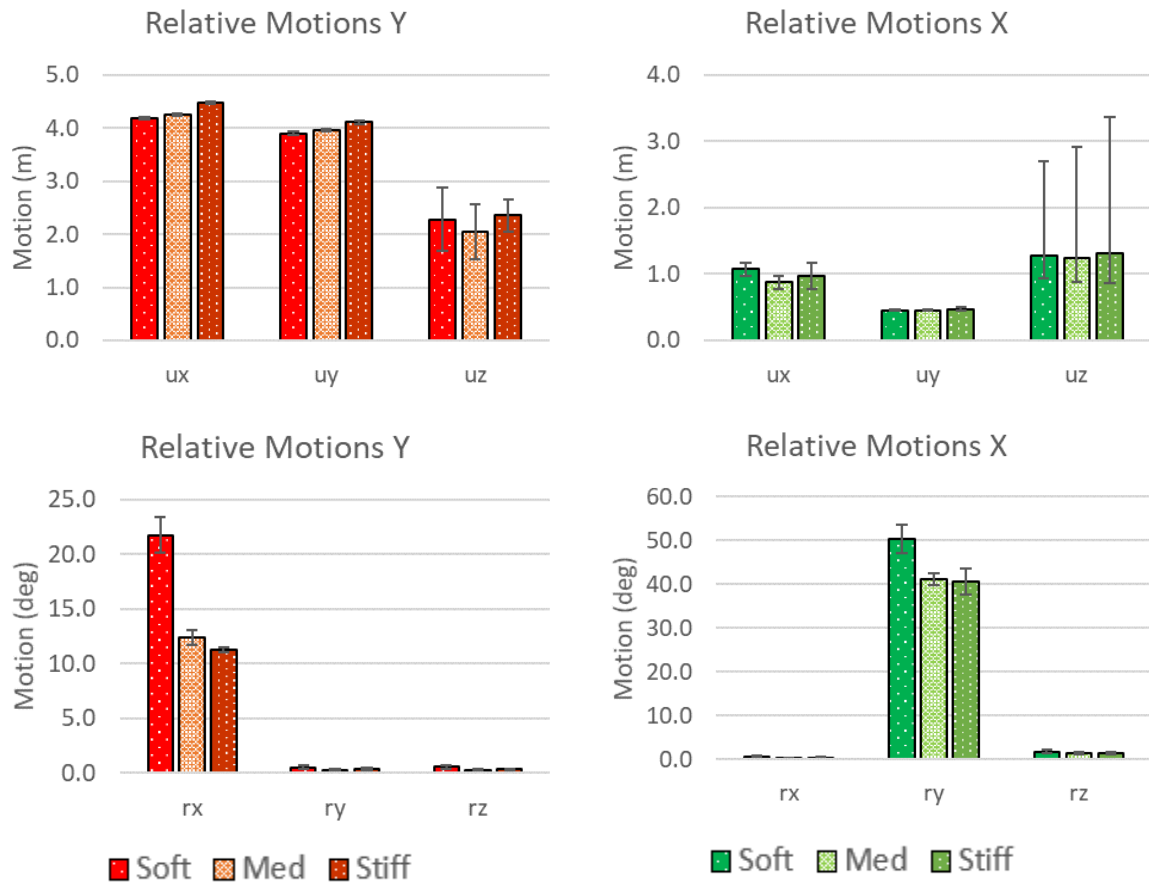
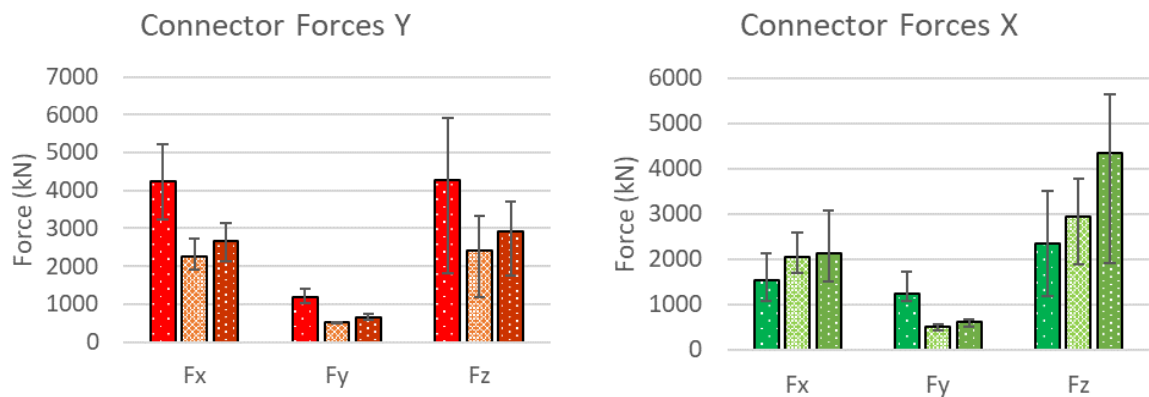


Figure 58, Significant motions relative to Y (left side) or X (right side) adjacent floaters when modifying only **pitch stiffness**. Wave heading is **150 degrees** in **sea state B** (Hs 4.5, Tp 6.3sec). Results presented for soft, medium and stiff connectors. Averaged values are shown for the X or Y relative connectors (see Figure 57) and error bars show the maximum and minimum relative motion.



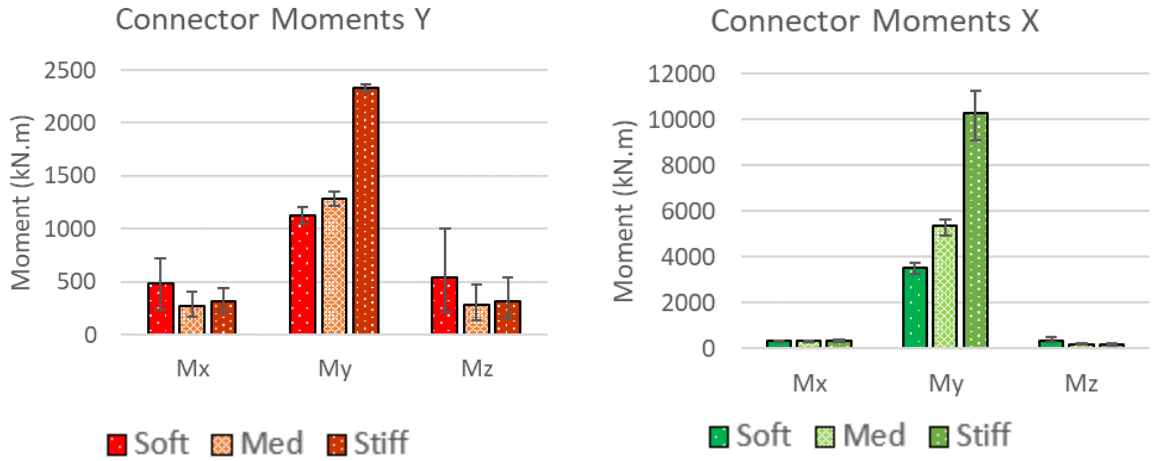


Figure 59, Significant connector forces and moments relative to Y (left side) or X (right side) adjacent floaters when modifying only **pitch stiffness**. Wave heading is **150 degrees** in **sea state B** (Hs 4.5, Tp 6.3sec). Results presented for soft, medium and stiff connectors. Averaged values are shown for the X or Y relative connectors (see Figure 57) and error bars show the maximum and minimum forces or moments.

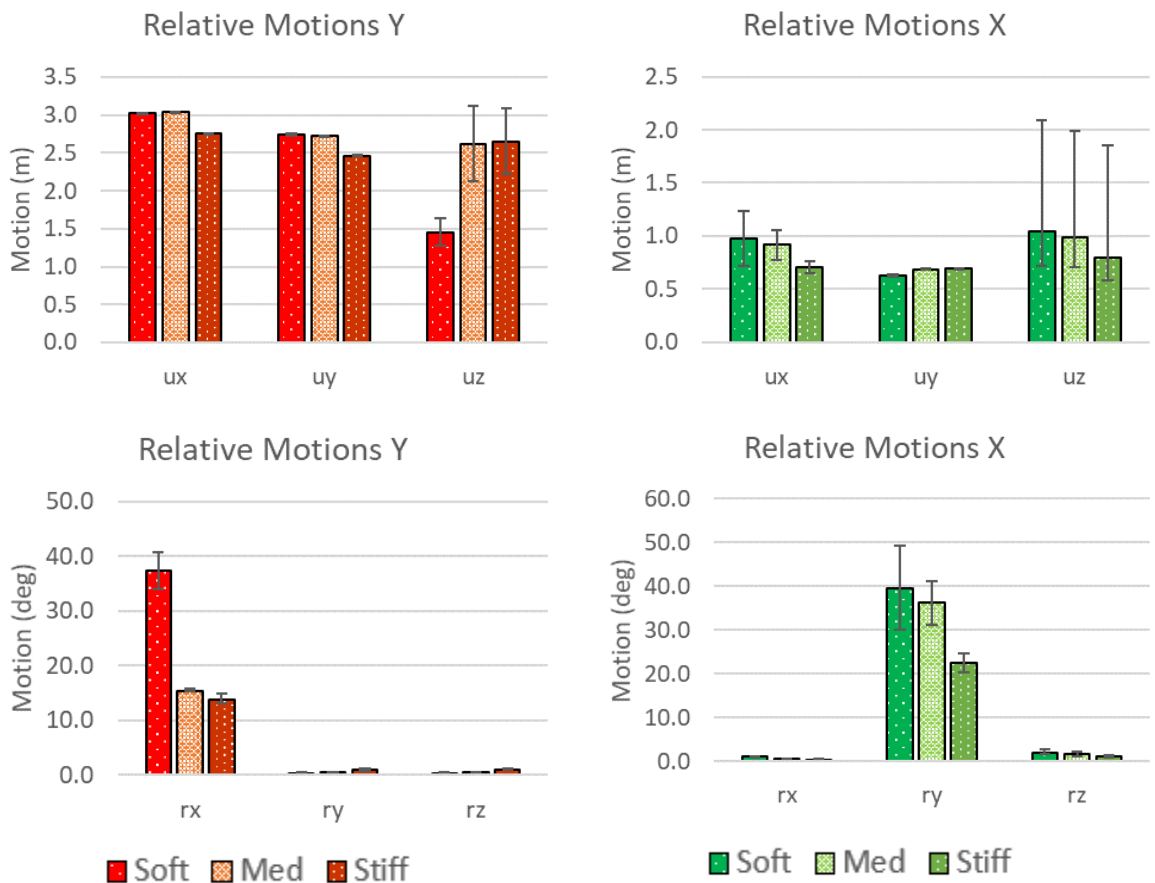


Figure 60, Significant motions relative to Y (left side) or X (right side) adjacent floaters when modifying only **pitch stiffness**. Wave heading is **150 degrees** in **sea state D** (Hs 7.6, Tp 11.8sec). Results presented for soft, medium and stiff connectors. Averaged values are shown for the X or Y relative connectors (see Figure 57) and error bars show the maximum and minimum relative motion.

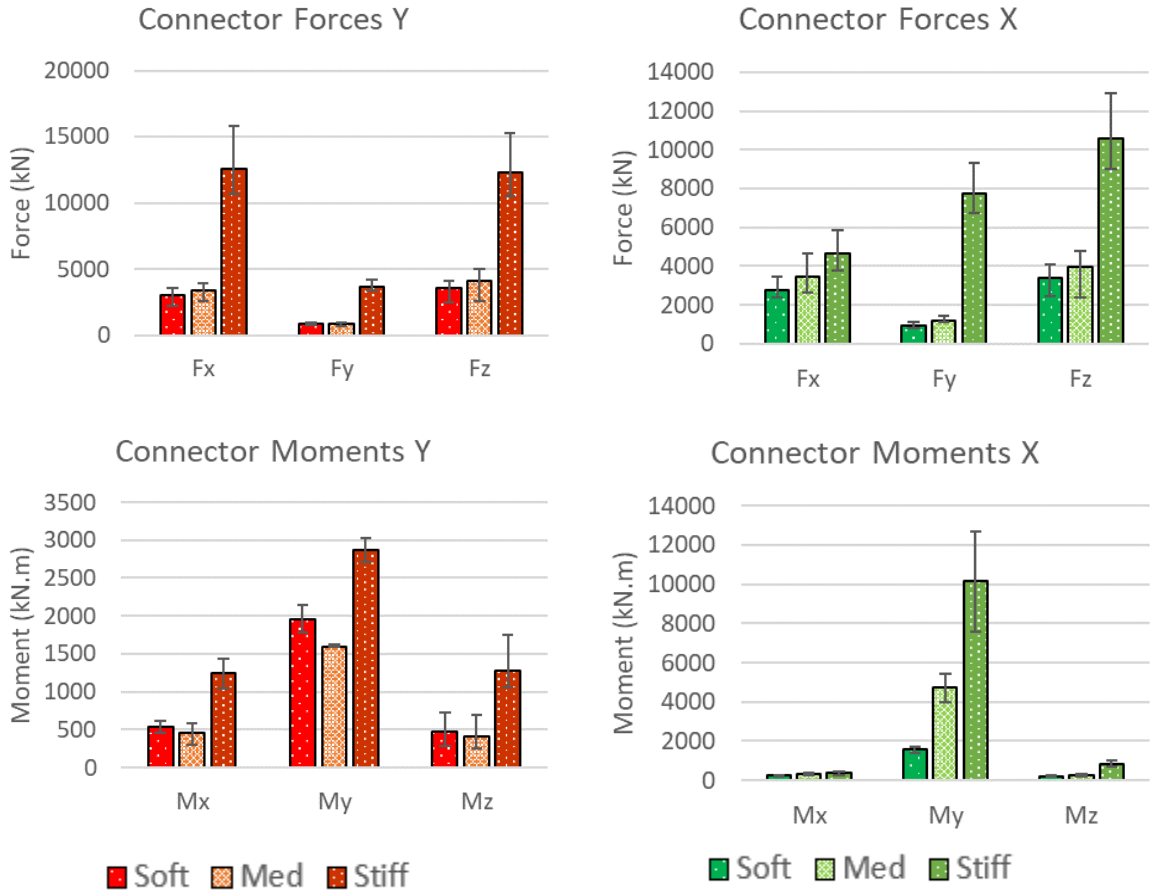
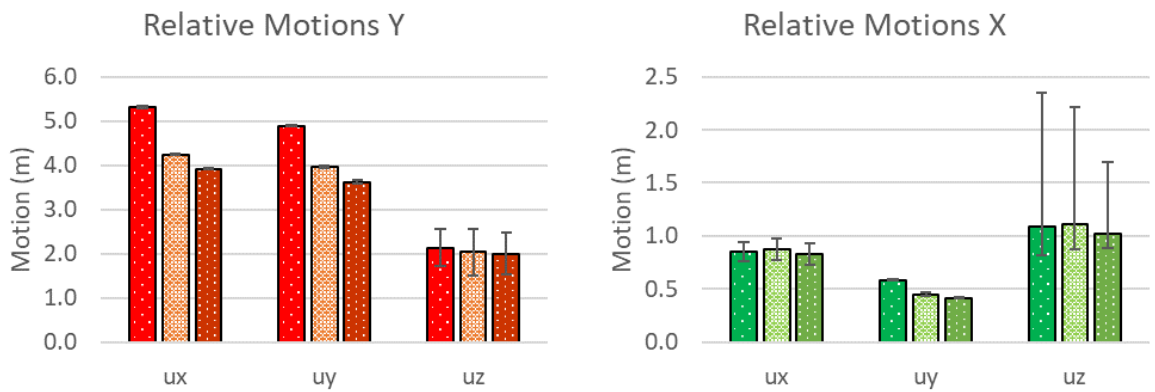


Figure 61, Significant connector forces and moments relative to Y (left side) or X (right side) adjacent floaters when modifying only **pitch stiffness**. Wave heading is **150 degrees in sea state D** (Hs 7.6, Tp 11.8sec). Results presented for soft, medium and stiff connectors. Averaged values are shown for the X or Y relative connectors (see Figure 57) and error bars show the maximum and minimum forces or moments.



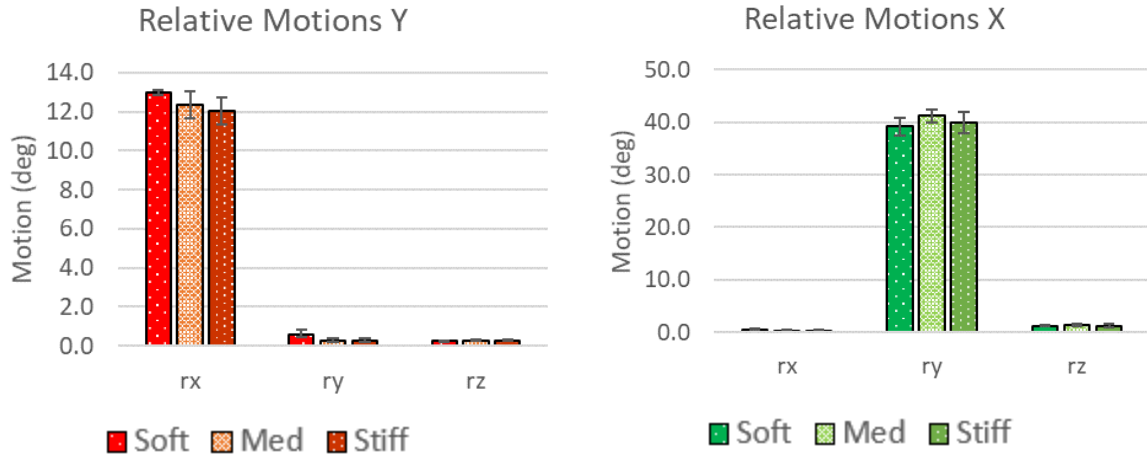


Figure 62, Significant motions relative to Y (left side) or X (right side) adjacent floaters when modifying only **heave stiffness**. Wave heading is **150 degrees** in **sea state B** (Hs 4.5, Tp 6.3sec). Results presented for soft, medium and stiff connectors. Averaged values are shown for the X or Y relative connectors (see Figure 57) and error bars show the maximum and minimum relative motion.

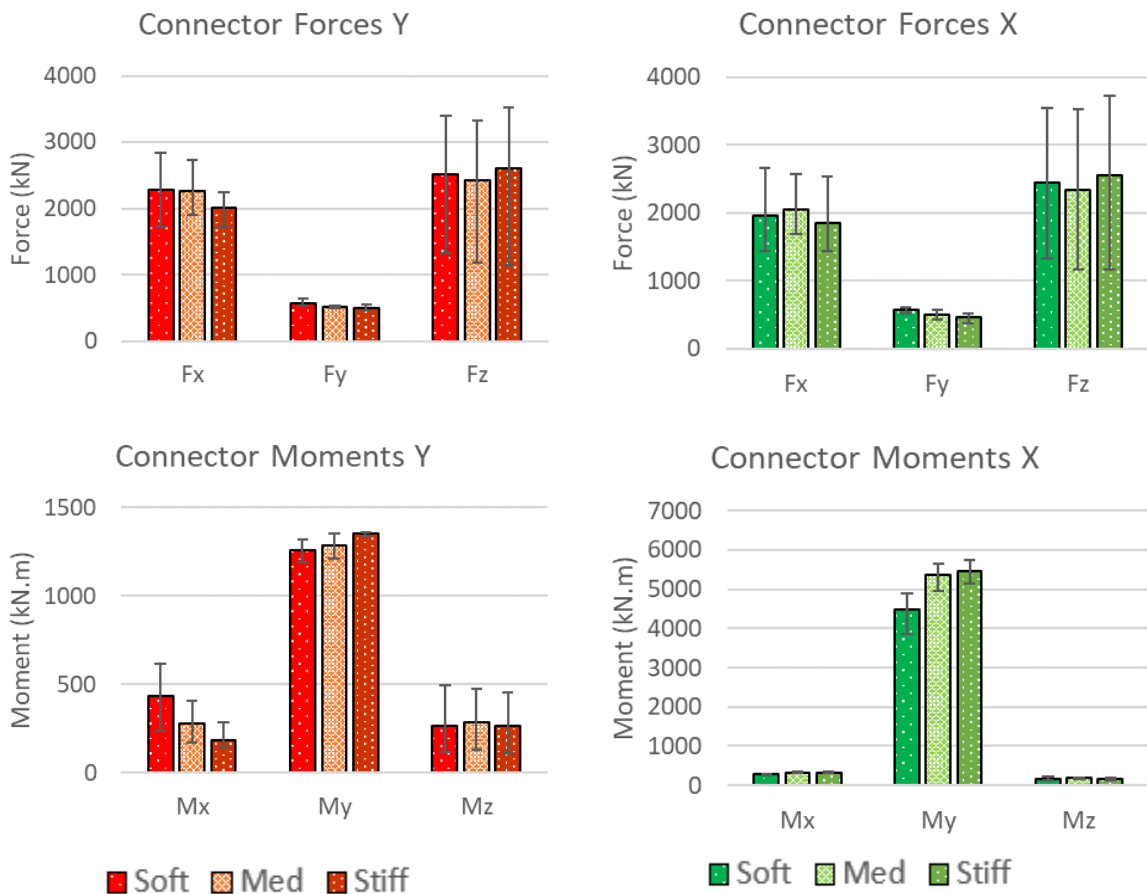


Figure 63, Significant connector forces and moments relative to Y (left side) or X (right side) adjacent floaters when modifying only **heave stiffness**. Wave heading is **150 degrees** in **sea state B** (Hs 4.5, Tp 6.3sec). Results presented for soft, medium and stiff connectors. Averaged values are shown for the X or Y relative connectors (see Figure 57) and error bars show the maximum and minimum forces or moments.

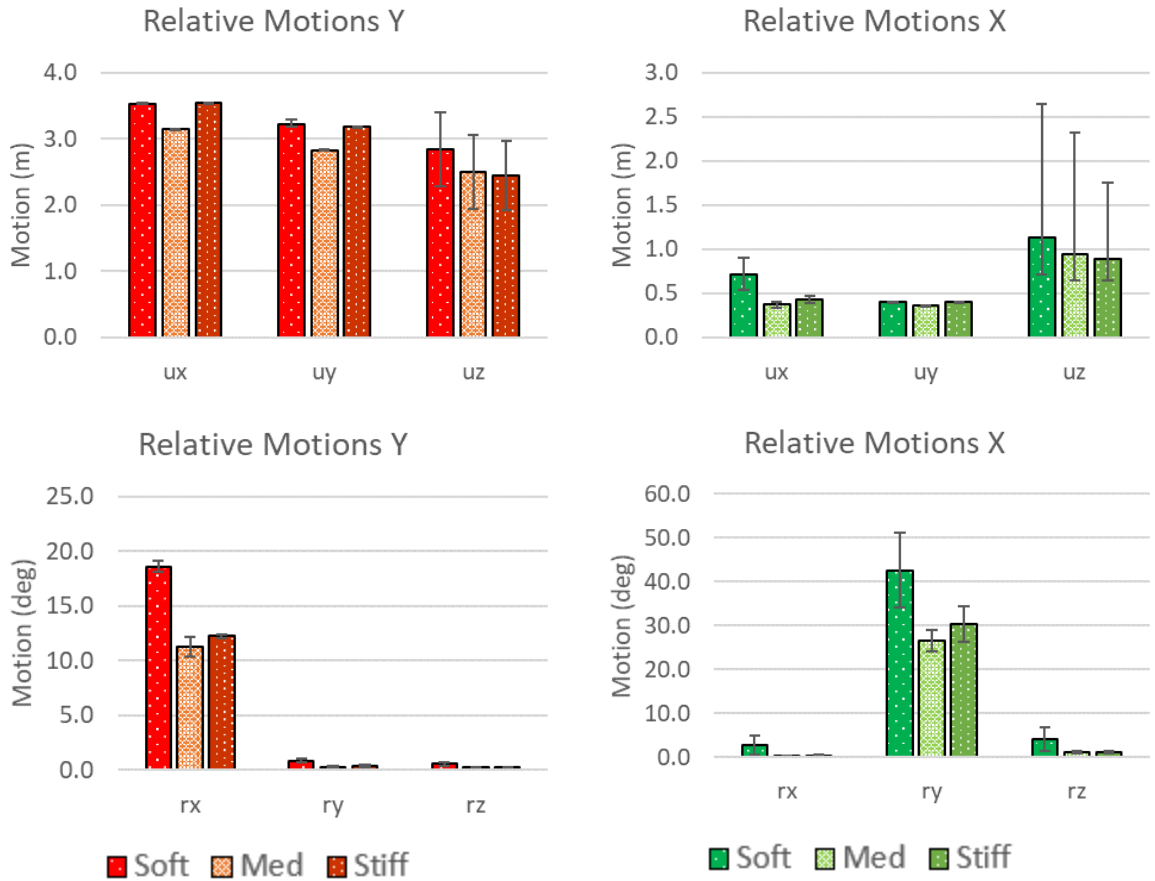
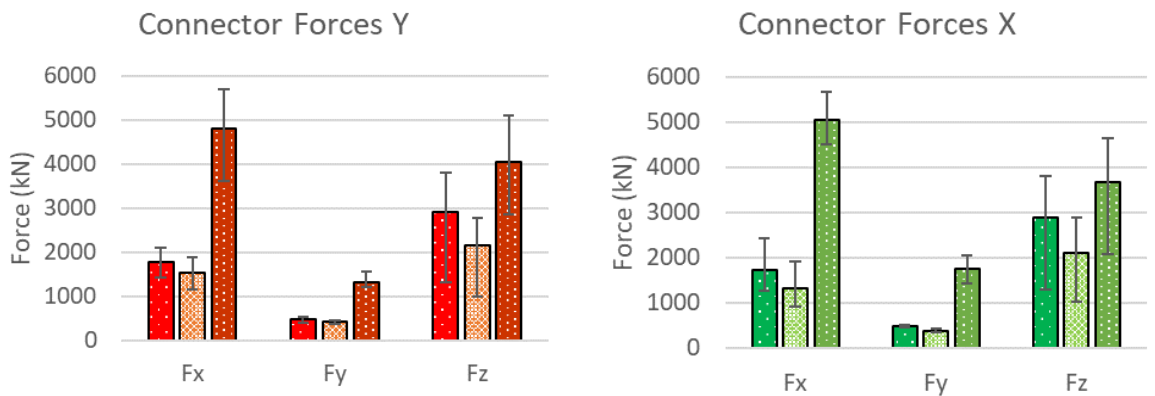


Figure 64, Significant motions relative to Y (left side) or X (right side) adjacent floaters when modifying only **heave stiffness**. Wave heading is **150 degrees** in **sea state D** (Hs 7.6, Tp 11.8sec). Results presented for soft, medium and stiff connectors. Averaged values are shown for the X or Y relative connectors (see Figure 57) and error bars show the maximum and minimum relative motion.



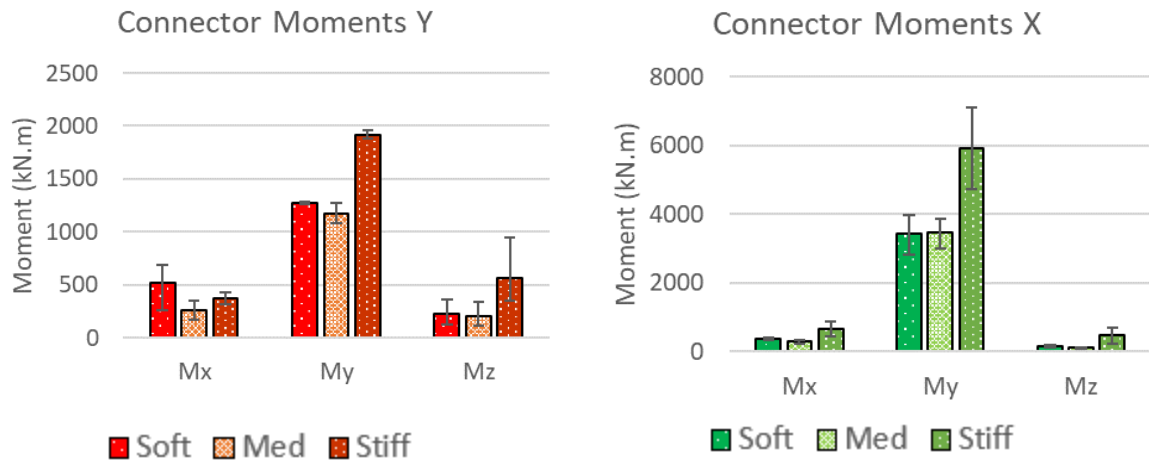


Figure 65, Significant connector forces and moments relative to Y (left side) or X (right side) adjacent floaters when modifying only **heave stiffness**. Wave heading is **150 degrees** in **sea state D** (H_s 7.6, T_p 11.8sec). Results presented for soft, medium and stiff connectors. Averaged values are shown for the X or Y relative connectors (see Figure 57) and error bars show the maximum and minimum forces or moments.